Enhanced two-photon absorption of organic chromophores: theoretical and experimental assessments

Francesca Terenziani, Claudine Katan, Ekaterina Badaeva, Sergei Tretiak, Mireille Blanchard-Desce

Enhanced two-photon absorption of organic chromophores: theoretical and experimental assessments[**]

By *Francesca Terenziani*[3], *Claudine Katan*[1*], *Ekaterina Badaeva*[4], *Sergei Tretiak*[2*] and *Mireille Blanchard-Desce*[1]

[*] Corresponding Author(s)

Dr. C. Katan, Dr. M. Blanchard-Desce

[1] Université de Rennes 1

CNRS

Chimie et Photonique Moléculaire (CPM)

Campus de Beaulieu case 1003, 35042 Rennes (France)

E-mail: claudine.katan@univ-rennes1.fr

E-mail: mireille.blanchard-desce@univ-rennes1.fr

Dr. S. Tretiak

[2] Theoretical Division, Center for Nonlinear Studies (CNLS)

and Center for Integrated Nanotechnologies (CINT)

Los Alamos National Laboratory, Los Alamos, NM 87545 (USA)

E-mail: serg@lanl.gov

Dr. F. Terenziani

[3] Dipartimento di Chimica GIAF, Parma University and INSTM UdR-Parma

Parco Area delle Scienze 17/a, 43100 Parma (Italy)

E-mail: francesca.terenziani@unipr.it

E. Badaeva

[4] Department of Chemistry, University of Washington

Seattle, WA 98195-1700 (USA)

E-mail: ebadaeva@u.washington.edu

Keywords: Two-photon absorption (TPA), Nonlinear Optics, Chromophores, time-

dependent Density Functional theory (TD-DFT)

[**] We wish to thank Dr. Olivier Mongin and Dr. Martinus Werts for stimulating discussions. MBD and ST gratefully acknowledge CNRS for an invited research associate position for ST. This work was performed in part at the US Department of Energy, Center for Integrated Nanotechnologies (CINT), at Los Alamos National Laboratory (LANL) (Contract DE-AC52-06NA25396). We also acknowledge support of Center for Nonlinear Studies (CNLS) at LANL. FT acknowledges MIUR for funding through PRIN2006. A portion of the calculations was funded by the "Centre Informatique National de l'Enseignement Supérieur" (CINES-France).

Abstract: Functional organic materials with enhanced two-photon absorption (TPA) lead to new technologies in the fields of chemistry, biology, and photonics. In this article we review experimental and theoretical methodologies allowing detailed investigation and analysis of TPA properties of organic chromophores. This includes femtosecond two-photon excited fluorescence (TPEF) experimental setups and quantum-chemical methodologies based on time-dependent density functional theory (TD-DFT). We thoroughly analyze physical phenomena and trends leading to large TPA responses of a few series of model chromophores focusing on the effects of symmetric and asymmetric donor/acceptor substitution and branching.

Contents

1 Introduction

Two-photon absorption (TPA) is defined as the electronic excitation of a molecule induced by a simultaneous absorption of pair of photons of the same or different energy. This phenomenon was first predicted by M. Göppert-Mayer in 1931[1] who calculated the transition probability for a two-quantum absorption process. Observation of TPA was possible only thirty years later with the advent of lasers. The first experimental evidence was performed by W. Kaiser and C.G.B. Garret[2] by illuminating a crystal of CaF_2 containing Eu^{2+} ions with a ruby laser beam. The recent emergence of technologies that can exploit TPA has attracted significant interest in the fields of chemistry, biology, and photonics. This, in turn, inspired a broad quest in functional chromophores with enhanced TPA properties.[3–6]

TPA is a third-order nonlinear optical process. The energy absorbed through a two-photon process is quadratically proportional to the intensity of the incident light. This provides improved spatial selectivity in three dimensions down to one wavelength resolution. Moreover, TPA can be induced at a frequency of half the actual energy gap which stretches the accessible range of conventional lasers (longer wavelengths at 700-1300 nm) and ensures deep penetration into scattering media. These distinct properties enable a large variety of improved and novel technological capabilities[7–9] such as spectroscopy,[10,11] fabrication of optoelectronic logical circuits,[12] microfabrication,[13–16] high-resolution fluorescence microscopy and characterization,[9,17–24] three-dimensional optical data storage,[14,25–32] optical power limiting,[33–38] upconversion lasing,[39–42] non-destructive imaging of biological tissues,[3,9,43–46] photodynamic therapy,[47–52] and new nanobiophotonics applications.[53,54] For example, optical limiting has benefited from the advent of multiphoton absorption in particular in the visible region aiming at eye protection[55–58] whereas only scarce effort has been dedicated to the protection of near-infrared (NIR) detectors. TPA applications have also gained widespread popularity in the biology community. For instance, photodynamic therapy is a relatively new approach for targeted cellular apoptosis in biological tissues, with current applications in the treatment of tumors, cancers, blood purification and blindness.[47,59–61] This therapy involves a selective uptake and retention of a photosensitizer by the target area (e.g., tumor) followed by irradiation with light of a particular wavelength. This is intended to induce tumor apop-

tosis, presumably through the formation of free radicals and singlet oxygen. A number of photosensitizers that utilize one-photon absorbing mechanism have been described in the literature. Even though TPA based approaches hold a considerable advantage over conventional one-photon absorption (OPA) technique due to spatial resolution and deep penetration of long wavelength irradiation into tissues, few organic photosensitizers based on a TPA mechanism have been suggested.[53,62–67] Among the other applications in the field of biology, the technique of two-photon laser scanning fluorescence microscopy[9,17–19,68] is well-spread. For example, it enables in vivo imaging of calcium dynamics[20,69,70] or intracellular zinc.[71,72] Carrying out two-photon instead of conventional one-photon excitation offers number of advantages. These include highly spatially confined excitation, three dimensional resolution, increased penetration depth in tissues, in particular thanks to reduced scattering losses, and reduced photodamage owing to excitation in the visible red-NIR region (typically 700-1200nm) as well as improved signal-to-noise ratio due to reduced background fluorescence. The fast development of two-photon laser scanning fluorescence microscopy has triggered the design of novel fluorophores order of magnitudes more efficient than endogenous fluorophores[44,73,74] such as amino acids, flavins, etc.
Within this context, an increasing effort has been devoted over the past decade to the design of chromophores with large TPA responses and properties suitable for specific applications. Thereby, attention has progressively moved from the well-known push-pull dipolar molecular structures[34,41,75–88] to quadrupoles[3,33,36,57,58,63,76,78,81,85,86,89–107] and, more recently, toward complex molecular architectures. Quadrupoles have been found to be more efficient than dipoles in terms of TPA, in particular for multiphoton-based optical-limiting applications.[33,36,57] In turn, exploitation of intermolecular interactions through branching strategies and the supramolecular approaches offers even more possibilities to tune or enhance TPA properties. This has already been demonstrated for branched chromophores built from the gathering of either dipolar[108–123] or quadrupolar[97,102,124–126] sub-chromophores via common conjugated core moieties and multichromophore structures in which subchromophores interact only via electrostatic interactions.[127] Alternative routes such as those based on porphyrins,[128–136] oligomers and polymers[103,137–139] have been explored as well. The level of complexity has been increased even further by studying dendritic species such as conjugated dendrimers,[115,118,140–142] multichromophoric dendrimers[143] and nanodots.[144,145] For example, the latter represent a promising non-toxic

alternative to quantum dots[19] for (bio)imaging purposes.

The mentioned above molecular engineering effort has benefited considerably from the various theoretical approaches through their ability to contribute to our understanding of structure-property relationships.[146–149] Since only a few electronic transitions often predominate in the nonlinear resonant spectra of organic molecules, effective few-state models have become very popular for rational molecular design of NLO-phores.[90, 103, 127, 150–160] For branched structures, the Frenkel exciton model has been shown to provide a valuable qualitative tool to connect the photophysical properties of branched chromophores to those of their corresponding monomeric counterpart.[113, 120, 161–163] Theoretical limits for TPA activities have also been explored as well.[164]

Beyond understanding the underlying structure-property relations, computer design of nonlinear chromophores should allow accurate prediction of stable conformal structures of complex molecules, their fluorescent properties and nonlinear optical responses. In principle, wave-function based correlated *ab initio* methods (e.g., equations of motion with coupled-cluster approach (EOM-CC)[165]) can provide an accurate description of the electronic spectra.[166] However, these techniques are frequently computationally intractable, when applied to the molecules of practical interest. Semiempirical methods are numerically feasible, however, they are able to reproduce only certain quantities assumed by underlying parameterization of the Hamiltonian model.[167–169] The nonlinear spectra are typically dominated by higher excitation levels involving significant electronic correlations. Consequently, semiempirical models have somewhat limited quantitative performance for nonlinear optical responses, while providing an excellent qualitative insight into the nature of physical phenomena involved.[89, 94]

Adiabatic time-dependent density functional theory (TD-DFT)[170, 171] in the Kohn-Sham (KS) form is currently the method of choice for calculating the excited-state structure of large molecular systems.[172–178] Recently TD-DFT extensions for the calculations of molecular nonlinear optical properties have been suggested based on the residues of the quadratic response functions for TPA,[179, 180] and on the quasi-particle formalism of the TD-KS equations for arbitrary frequency-dependent nonlinear optical polarizabilities.[181, 182] Subsequently, the former approach was used for detailed studies of nonlinear polarizabilities in small organic molecules[183–191] and the latter method was applied to calculate OPA and TPA responses of several families of donor/acceptor sub-

stituted conjugated organic chromophores[192–197] and various substituted branched structures.[102,120,121,126] These studies have shown the excellent performance of TD-DFT based on hybrid functionals for molecular nonlinear responses.

This article overviews experimental and theoretical methodologies used for determination and analysis of TPA properties. We investigate in detail synthetic strategies that have been suggested recently to enhance TPA properties. This includes the effect of symmetric and asymmetric donor/acceptor substitution and branching. Both experimental and theoretical data are used to get an extensive comprehension of the physics underlying the two-photon process and its amplitude, as well as to suggest an exploratory root for novel molecular engineering for further enhancement of TPA.

The paper is organized as follows. In section 2 we define the TPA cross section by relating the microscopic hyperpolarizability to the macroscopic response. In particular, attention is paid to different conventions used in the literature when deducing expressions for the response. In section 3 we summarize the main theoretical and computational models used for calculation of the nonlinear responses and describe how to account for solvation and local-field effects. Section 4 deals with the principal experimental techniques and challenges for measurement of the TPA cross section. A variety of representative chromophores are investigated in section 5, both experimentally and theoretically, allowing for rationalization of different structural effects on the TPA cross section and for a test of different theoretical approaches. Finally, main conclusions are drawn in section 6.

2 Definitions of TPA response

2.1 From time domain response function to susceptibilities

Definition of NLO quantities is a subject to a lot of confusion given the different conventions and systems of physical units that can be used. Among the main sources of havoc are numerical factors arising from the choice for the definition of macroscopic susceptibilities, microscopic hyperpolarizabilities and the field, incorrect permutation symmetry and inconsistent units. This is particularly critical in the comparison between experimental and theoretical values. This subsection aims to clarify the derivation of the expressions defining the TPA cross section. We choose the cgs system of physical units, unless explicitly stated otherwise, and use bold typeface for vector and tensor quantities. The reader

should reckon that tensorial products are implicit and not marked by any special symbol. In optics, one is concerned with the interaction of light with matter. A light wave consists of electric and magnetic fields but for the process of interest here, the effect of magnetic field can be neglected. Interaction of the incoming light with the sample induces a macroscopic polarization $\mathbf{P}(\mathbf{r},t)$. For the sake of clarity, the spatial dependence is disregarded and we focus on the local response where the polarization at a point of the nonlinear medium is determined by the field $\mathbf{E}(\mathbf{r},t)$. The different nonlinear properties can be addressed by expanding the macroscopic polarization into a power series of the applied electric field:

$$\mathbf{P}(t) = \mathbf{P}^{(0)}(t) + \mathbf{P}^{(1)}(t) + \mathbf{P}^{(2)}(t) + \mathbf{P}^{(3)}(t) + \cdots \tag{1}$$

The first term is independent of the field and corresponds to the permanent polarization. $\mathbf{P}^{(1)}(t)$ is linear in the field, $\mathbf{P}^{(2)}(t)$ has quadratic dependence and so forth.

The explicit relation between polarization and electric field, can be expressed within different approaches: time-domain response functions, frequency domain response function or a hybrid between the two.[198,199] Here we start with the time domain approach and rapidly switch to the frequency domain that allows to define optical susceptibilities. Considering the principle of time invariance, the nth order polarization $\mathbf{P}^{(n)}(t)$ reads:[198]

$$\mathbf{P}^{(n)}(t) = \int_{-\infty}^{\infty} dt_1 \cdots \int_{-\infty}^{\infty} dt_n \mathbf{R}^{(n)}(t_1,\ldots,t_n)\mathbf{E}(t-t_1)\cdots\mathbf{E}(t-t_n). \tag{2}$$

This expression implies a definition of the time-domain response functions $\mathbf{R}^{(n)}$ within a perturbative expansion. Alternatives are discussed later.

To switch between time- and frequency- domains we introduce the Fourier transform defined for an arbitrary function $\mathbf{F}$ as

$$\mathbf{F}(\omega) = \frac{1}{2\pi}\int_{-\infty}^{\infty} d\tau \mathbf{F}(\tau)\exp(i\omega\tau), \tag{3}$$

$$\mathbf{F}(t) = \int_{-\infty}^{\infty} d\omega \mathbf{F}(\omega)\exp(-i\omega t). \tag{4}$$

The Fourier transform of the electric field allows to represent the susceptibility tensors as

$$\mathbf{P}^{(n)}(t) = \int_{-\infty}^{\infty} d\omega_1 \cdots \int_{-\infty}^{\infty} d\omega_n \boldsymbol{\chi}^{(n)}(-\omega_\sigma;\omega_1,\ldots,\omega_n)\mathbf{E}(\omega_1)\cdots\mathbf{E}(\omega_n)\exp(-i\omega_\sigma t), \tag{5}$$

and

$$\boldsymbol{\chi}^{(n)}(-\omega_\sigma;\omega_1,\ldots,\omega_n) = \int_{-\infty}^{\infty} d\tau_1 \cdots \int_{-\infty}^{\infty} d\tau_n \mathbf{R}^{(n)}(\tau_1,\ldots,\tau_n)\exp(i\sum_{j=1}^{n}\omega_j\tau_j), \tag{6}$$

where $\omega_\sigma = \omega_1 + \omega_2 + \cdots + \omega_n$. The nth order susceptibility is a tensor of rank $n+1$. For example, $\boldsymbol{\chi}^{(1)}(-\omega_\sigma, \omega)$ is a 3×3 matrix of components $\chi^{(1)}_{I,J}(-\omega_\sigma, \omega)$ where the subscripts take the values X, Y, and Z which label the cartesian laboratory coordinate axes. The polarization $\mathbf{P}(t)$ can be expanded in the frequency domain as well, $\mathbf{P}(\omega) = \sum_{n=0}^{\infty} \mathbf{P}^{(n)}(\omega)$. After applying the Fourier transform (Eq. (5)), the frequency domain analogue of Eq. (2) is given by:

$$\mathbf{P}^{(n)}(\omega) = \int_{-\infty}^{\infty} d\omega_1 \cdots \int_{-\infty}^{\infty} d\omega_n \boldsymbol{\chi}^{(n)}(-\omega_\sigma; \omega_1, \ldots, \omega_n)\mathbf{E}(\omega_1) \cdots \mathbf{E}(\omega_n)\delta(\omega - \omega_\sigma). \tag{7}$$

where $\delta(\omega - \omega_\sigma)$ is Dirac's delta function.

2.2 Polarization induced by a monochromatic wave

Let us consider the simple case of an applied field consisting of a single monochromatic wave that is specific to degenerate TPA. We express the incoming electric field of frequency ω' and amplitude $\mathbf{E}_{\omega'}$ as

$$\mathbf{E}(t) = \frac{1}{2}[\mathbf{E}_{\omega'} \exp(-i\omega' t) + \mathbf{E}_{-\omega'} \exp(i\omega' t)]. \tag{8}$$

Here $\mathbf{E}(t)$ are taken to be real ($\mathbf{E}_{\omega'} = \mathbf{E}^{\star}_{-\omega'}$). The frequency-domain equivalent of $\mathbf{E}(t)$ is given by

$$\mathbf{E}(\omega) = \frac{1}{2}[\mathbf{E}_{\omega'}\delta(\omega - \omega') + \mathbf{E}_{-\omega'}\delta(\omega + \omega')]. \tag{9}$$

The induced macroscopic polarization can then similarly be expressed as a superposition of monochromatic components in time- and frequency- domains as

$$\mathbf{P}^{(n)}(t) = \frac{1}{2}\sum_{\omega}[\mathbf{P}^{(n)}_{\omega} \exp(-i\omega t) + \mathbf{P}^{(n)}_{-\omega} \exp(i\omega t)], \tag{10}$$

$$\mathbf{P}^{(n)}(\omega) = \frac{1}{2}\sum_{\omega"}[\mathbf{P}^{(n)}_{\omega"}\delta(\omega - \omega") + \mathbf{P}^{(n)}_{-\omega"}\delta(\omega + \omega")]. \tag{11}$$

Insertion of Eq. (9) into Eq. (7) leads to

$$\mathbf{P}^{(n)}_{\omega_\sigma} = K(-\omega_\sigma; \omega_1, \ldots, \omega_n)\boldsymbol{\chi}^{(n)}(-\omega_\sigma; \omega_1, \ldots, \omega_n)\mathbf{E}_{\omega_1} \cdots \mathbf{E}_{\omega_n}. \tag{12}$$

Here we have introduced the numerical factor K, first defined by Orr and Ward:[200] $K(-\omega_\sigma; \omega_1, \ldots, \omega_n) = 2^{l+m-n}D$, where $l = 1$ if $\omega_\sigma \neq 0$ and $l = 0$ otherwise; m is the number of non zero frequencies among $\omega_1, \ldots, \omega_n$ and n the order of nonlinearity. D is the number of distinguishable arrangements (distinct permutations) of the set of field

frequency labels. This factor arises from the fact that a summation has to be performed over all of the distinct arrangements of $\omega_1, \ldots, \omega_n$. In fact, this expression is also valid for an applied field consisting of a superposition of monochromatic waves. In the case of a single monochromatic wave of frequency ω, the ω_i's are either equal to ω or $-\omega$ and it should be stressed that frequencies ω and $-\omega$ must be considered as distinguishable when performing the count of distinct permutations.[201] The 2^{l+m-n} pre-factor in the quantity K arises from the factors $\frac{1}{2}$ of Eqs. (8) and (10). It is important to notice that this pre-factor does not show up once spectroscopic observables such as intensities or cross sections are considered as it is only related to the convention chosen to express the electric field. However, sometimes part or all of the contributions arising from this K factor are included into the definition of the susceptibilities, which is one of the reasons of confusion existing in the literature.[202] Another reason originates from the expansion of polarization into a power series of the electric field. Here, we choose a perturbative expansion while Taylor series would have been an alternative choice. Within Taylor series, a factor $\frac{1}{n!}$ should be added in front of the K factor in Eq. (12). This means that the n-th order susceptibilities $\boldsymbol{\chi}^{(n)}$ defined within a Taylor expansion are $n!$ larger than those derived within a perturbative expansion.

The specific case of degenerate TPA ($\omega_\sigma = \omega$) corresponds to the third-order polarization derived from Eq. (12):

$$\mathbf{P}^{(3)}_{\omega_\sigma} = 3\left(\frac{1}{2}\right)^2 \boldsymbol{\chi}^{(3)}(-\omega_\sigma; \omega, \omega, -\omega)\mathbf{E}_\omega \mathbf{E}_\omega \mathbf{E}_{-\omega}. \tag{13}$$

After introducing the spatial dependence, Eq. (13) becomes

$$(P^{(3)}_{\omega_\sigma})_I = 3\left(\frac{1}{2}\right)^2 \sum_{J,K,L} \chi^{(3)}_{IJKL}(-\omega_\sigma; \omega, \omega, -\omega)(E_\omega)_J (E_\omega)_K (E_{-\omega})_L, \tag{14}$$

where the subscripts I, J, K, L run over the spatial coordinates X, Y and Z. The principles of time invariance and causality implies intrinsic permutation symmetry. Consequently, if any of the subscripts $\{J, K, L\}$ are permuted, then the susceptibility remains unchanged if at the same time the corresponding set of frequencies $\{\omega, \omega, -\omega\}$ are also permuted. Moreover, the nonlinear susceptibilities also reflect the structural symmetry of the medium that allows to reduce the number of independent and non-zero components needed to describe the material.[199]

2.3 Definition of the two-photon absorption cross section

The energy exchange between the light wave and the medium per unit time and volume is given by[203]

$$\frac{dW}{dt} = \langle \mathbf{E} \cdot \frac{d\mathbf{P}}{dt} \rangle, \tag{15}$$

where the brackets on the r.h.s. indicate that time average over cycles of the electric field has to be performed. Given Eq. (13), and combining Eqs. (8), (10), and (15) we obtain

$$\frac{dW}{dt} = \frac{3}{8}\omega \, \mathcal{I}m\Big(\boldsymbol{\chi}^{(3)}(-\omega;\omega,\omega,-\omega) \; \mathbf{E}_\omega \mathbf{E}_\omega^\star \mathbf{E}_\omega \mathbf{E}_\omega^\star\Big) \, . \tag{16}$$

Considering an incoming field to be linearly polarized along the x-axis and given that its optical intensity is expressed by:[204]

$$I = \frac{nc(E_\omega)_X (E_\omega^\star)_X}{8\pi}, \tag{17}$$

where n is the index of refraction of the medium and c the speed of light in vacuum, the energy absorbed through two-photon processes is, therefore,

$$\frac{dW}{dt} = \frac{24\pi^2\omega}{n^2c^2} \; I^2 \, \mathcal{I}m\Big(\chi^{(3)}_{XXXX}(-\omega_\sigma;\omega,\omega,-\omega)\Big) \, . \tag{18}$$

The TPA activity is usually quantified through the so called two-photon absorption cross section $\sigma_2(\omega)$ defined by the rate equation

$$\frac{dn_p}{dt} = \sigma_2(\omega) N F^2, \tag{19}$$

where $\frac{dn_p}{dt}$ is the number of photons absorbed per unit time through a TPA process, N is the density of absorbing species and $F = \frac{I}{\hbar\omega}$ being the photon flux. Since $dW = dn_p \hbar\omega$,

$$\sigma_2(\omega) = \frac{24\pi^2\hbar\omega^2}{n^2c^2N} \; \mathcal{I}m\{\chi^{(3)}_{XXXX}(-\omega_\sigma;\omega,\omega,-\omega)\}. \tag{20}$$

For hyperpolarizabilities defined within a Taylor series expansion, the numerical factor 24 should be replaced by 4. Here one can notice another source of differences in numerical factors. In fact, in a few studies[205] $\sigma_2(\omega)$ is defined starting from the number of two-photon transitions in Eq. (19), instead of the number of photons. This leads to cross sections values being two times smaller than those derived with the definition used in this review. The definition we adopt here is, however, the most widely used and accepted.

2.4 From macroscopic susceptibilities to microscopic polarizabilities

In the previous subsections, $\sigma_2(\omega)$ has been related to the third-order susceptibility tensor which is a macroscopic quantity. When the sample of interest consists of an assembly of microscopic units such as molecules, it is convenient to relate the TPA cross section to the relevant quantity at the microscopic level, i.e., the second hyperpolarizability $\boldsymbol{\gamma}$. This is especially useful for estimating the TPA cross section from quantum chemical approaches and hence comparing them to experimental values. The definition of microscopic quantities follows along the same lines as those used in subsections 2.1 and 2.2 where the macroscopic polarization should be replaced by the (induced) molecular dipole moment, the external macroscopic field should be replaced by the local field acting on the microscopic species in the material, and the susceptibility tensors $\boldsymbol{\chi}^{(1)}$, $\boldsymbol{\chi}^{(2)}$, $\boldsymbol{\chi}^{(3)}$, ... should be replaced respectively by the (hyper)polarizabilities $\boldsymbol{\alpha}$, $\boldsymbol{\beta}$, $\boldsymbol{\gamma}$, ... of the species of interest. Here, a new source of discrepancies in numerical factors arises, because the same expansion (i.e., perturbative vs. Taylor) into a power series of the field is not used consistently for both macroscopic polarization and molecular dipole moment. This shows up as an additional $n!$ factor between the nth order macroscopic vs. microscopic quantities.[206] Here we proceed with perturbative expansions.

Derivation of the rigorous relation between macroscopic and microscopic quantities is not a simple problem. It can be artificially split in three steps: (*i*) definition of the local field experienced by the molecule of interest, (*ii*) mutual influence between the molecule of interest and its environment, and (*iii*) transformation from the molecular coordinate system to the laboratory coordinate system. For the sake of clarity, we focus on the case, where a material of interest is a mixture of chromophores (solute) dissolved in a solvent. Typically, the distribution of solute molecules in solution can be considered as isotropic. Hence, the transformation from the molecular coordinate system to the laboratory coordinate system involves an average over all possible orientations, involving direction cosines between the laboratory axes $\{X, Y, Z\}$ and the molecular axes $\{x, y, z\}$. Considering Eq. (20), such transformation is given by[207]

$$\langle\gamma\rangle_{XXXX} = \frac{1}{5}\sum_i \gamma_{iiii} + \frac{1}{15}\sum_{i\neq j}(\gamma_{iijj} + \gamma_{ijij} + \gamma_{ijji}), \tag{21}$$

where the subscripts i and j run over the solute molecular axes x, y, and z.

Different approaches exist for the treatment of the mutual influence between the solute molecule and the solvent. The solvent is generally approximated by a homogeneous dielectric medium characterized by its frequency-dependent dielectric constant ϵ_ω. The mutual influence can be either split into different contributions or taken into account self-consistently. For example, the latter has been proposed within the framework of the Polarizable Continuum Model (PCM) .[184,206,208–210] This approach focuses on the solute molecule or a small cluster of the solute with a few solvent molecules and represents the influence of the rest of the solvent by an effective continuum surrounding them. Alternatively, Conductor-like Screening Model (COSMO) developed by Andreas Klamt,[211,212] calculates the dielectric screening charges and energies on a van-der-Waals-like molecular surface in the approximation of a conductor screening, and allows for the direct determination of the surface charges within the self-consistent field procedure using only the electrostatic potentials.

In Ref.,[213] R. Wortmann and D. M. Bishop treat static and frequency dependent contributions to the interaction between solute and solvent in two different steps. The static contribution accounts for all solute-solvent interactions that are present in the absence of any externally applied field. Consequently, one has to consider the microscopic unit under investigation in the presence of solvent and derive so-called *solute polarizabilities*. The solute polarizabilities (e.g., $\boldsymbol{\alpha}^{sol}(-\omega;\omega)$, $\boldsymbol{\gamma}^{sol}(-\omega;\omega,\omega,-\omega)$) are typically obtained using electronic structure calculations performed with a continuum dielectric approach for the solvent after geometry optimization of the solute molecule in the presence of the solvent.[206] These polarizabilities account for the static reaction field resulting from the solute-solvent interactions. Based on the solute polarizabilities, the expansion of the induced microscopic polarization (or dipole moment) is further defined using the local fields effectively experienced by the solute molecule. For example, an expansion of the induced dipole moment amplitude $\mathbf{p}_\omega$ at frequency ω into a power series of the local-field amplitudes $\mathbf{E}^{loc}_\omega$ at the same frequency is given by

$$\mathbf{p}_\omega = \boldsymbol{\alpha}^{sol}(-\omega;\omega)\ \mathbf{E}^{loc}_\omega + \boldsymbol{\gamma}^{sol}(-\omega;\omega,\omega,-\omega)\ \mathbf{E}^{loc}_\omega\mathbf{E}^{loc}_\omega\mathbf{E}^{loc}_{-\omega} + \cdots \tag{22}$$

where the first hyperpolarizability $\boldsymbol{\beta}^{sol}$ does not appear as there is no static applied field. Effects of the corrections to the field(s) acting on the solute molecules are introduced separately, leading to the definition of so-called *effective polarizabilities*, which are directly

related to the macroscopic susceptibilities. This second step is based on the correct definition of local fields to avoid any double counting. Here we proceed with the approach presented in Ref.,[213] based on the Onsager's model[214] to derive the relation between the applied field amplitude $\mathbf{E}_\omega$ and the corresponding local-field amplitude $\mathbf{E}_\omega^{loc}$. According to this model, the solute is approximated as a point electric dipole located in a spherical or ellipsoidal cavity in the solvent, considered as a dielectric continuum. The local field acting on the solute is described by two contributions:

$$\mathbf{E}_\omega^{loc} = \mathbf{E}_\omega^C + \mathbf{E}_\omega^R, \tag{23}$$

where $\mathbf{E}_\omega^C$ and $\mathbf{E}_\omega^R$ correspond to the cavity and reaction fields, respectively. Within the dipole approximation, the cavity field is related to the macroscopic (applied) field as

$$\mathbf{E}_\omega^C = \mathbf{f}_\omega^C \mathbf{E}_\omega, \tag{24}$$

where $\mathbf{f}_\omega^C$ is a tensor of rank 2, whose components are known as cavity field factors at frequency ω. The induced dipole moment $\mathbf{p}_\omega$ at frequency ω of the solute molecule creates a reaction field according to

$$\mathbf{E}_\omega^R = \mathbf{f}_\omega^R \mathbf{p}_\omega, \tag{25}$$

where $\mathbf{f}_\omega^R$ is the reaction-field tensor of rank 2 at frequency ω. The local field then reads:

$$\mathbf{E}_\omega^{loc} = \mathbf{f}_\omega^C \mathbf{E}_\omega + \mathbf{f}_\omega^R \mathbf{p}_\omega \tag{26}$$

The effective solute polarizabilities are defined as the successive derivatives of the microscopic polarization with respect to the external field. For example, the effective third-order polarizability relevant to the TPA process is

$$\gamma_{ijkl}^{eff} = \frac{1}{6} \lim_{|E_\omega| \to 0} \frac{\partial^3 (p_\omega)_i}{\partial (E_\omega)_j \partial (E_\omega)_k \partial (E_\omega)_l}, \tag{27}$$

where the numerical factor $\frac{1}{6}$ appears due to perturbative expansion (22). By choosing a reference frame where $\boldsymbol{\alpha}^{sol}$ is a diagonal tensor, the relation between $\boldsymbol{\gamma}^{eff}$ and $\boldsymbol{\gamma}^{sol}$ has a quite simple form, obtained by substituting Eq. (26) into Eq. (22) and applying definition (27):

$$\begin{aligned} \gamma_{ijkl}^{eff}(-\omega;\omega,\omega,-\omega) &= (F_\omega^R)_{ii}(F_\omega^R)_{jj}(f_\omega^C)_{jj}(F_\omega^R)_{kk}(f_\omega^C)_{kk}(F_\omega^R)_{ll}(f_\omega^C)_{ll}\ \gamma_{ijkl}^{sol}(-\omega;\omega,\omega,-\omega) \\ &= (F_\omega^R)_{ii}(\mathcal{L}_\omega)_{jj}(\mathcal{L}_\omega)_{kk}(\mathcal{L}_\omega)_{ll}\ \gamma_{ijkl}^{sol}(-\omega;\omega,\omega,-\omega), \end{aligned} \tag{28}$$

where

$$(F^R_\omega)_{ii} = [1 - \alpha^{sol}_{ii}(-\omega;\omega)(f^R_\omega)_{ii}]^{-1}, \tag{29}$$

are the components of the reaction field factor (tensor of rank 2), and

$$(\mathcal{L}_\omega)_{ii} = (F^R_\omega)_{ii}(f^C_\omega)_{ii}. \tag{30}$$

For a spherical cavity, the tensorial components of $\mathbf{f}^C_\omega$ and $\mathbf{f}^R_\omega$ are given by:[215]

$$(f^C_\omega)_{ij} = \frac{3\epsilon_\omega}{2\epsilon_\omega + 1}\delta_{ij}, \tag{31}$$

$$(f^R_\omega)_{ij} = \frac{2(\epsilon_\omega - 1)}{a^3(2\epsilon_\omega + 1)}\delta_{ij}, \tag{32}$$

where a is the cavity radius and δ_{ij} is the Kronecker's delta. For an ellipsoidal cavity we have[215]

$$(f^C_\omega)_{ij} = \frac{\epsilon_\omega}{\epsilon_\omega - \kappa_i(\epsilon_\omega - 1)}\delta_{ij}, \tag{33}$$

$$(f^R_\omega)_{ij} = \frac{3\kappa_i(1-\kappa_i)(\epsilon_\omega - 1)}{a_x a_y a_z[\epsilon_\omega - \kappa_i(\epsilon_\omega - 1)]}\delta_{ij}, \tag{34}$$

where a_x, a_y, a_z are the ellipsoidal semi-axes and κ_i are the depolarization factors

$$\kappa_i = \int_0^\infty \frac{a_x a_y a_z}{2(s + a_i^2)\sqrt{(s + a_x^2)(s + a_y^2)(s + a_z^2)}}\mathrm{d}s. \tag{35}$$

In the case of a spherical cavity, the linear polarizability in Eq. (29) can be derived using the Clausius-Mosotti equation, assuming that $\boldsymbol{\alpha}^{sol}$ solely depends on the solvent properties. As a result, $(\mathcal{L}_\omega)_{ii}$ in Eq. (30) becomes the Lorentz local-field factor:

$$L = \frac{\epsilon_\omega + 2}{3}. \tag{36}$$

However, this assumption means that the solute molecule has the same polarizability as the solvent. This is only true for pure liquids and is not applicable for solute molecules with high (hyper)polarizability values dispersed in common solvents or matrices.[216] This is also the reason why, as discussed in Ref.,[213] Eq. (28) does not allow to recover the commonly used Lorentz correction, which would link $\boldsymbol{\gamma}^{eff}$ to $\boldsymbol{\gamma}^{sol}$ through L^4. Indeed, Eq. (28) has been derived by imposing from the beginning distinct polarizations for solute and solvent, so that the Lorentz limit cannot be recovered by simply acting on the final expression. We emphasize that the assumption of having the same polarizabilities for

solute and solvent (both linear and nonlinear) should be imposed in order to find the Lorentz limit.

The macroscopic susceptibility is directly connected to the microscopic effective polarizability. In the case of the TPA process we have

$$\chi^{(3)}_{XXXX}(-\omega;\omega,\omega,-\omega) = N\langle\boldsymbol{\gamma}^{eff}(-\omega;\omega,\omega,-\omega)\rangle_{XXXX}, \tag{37}$$

where the brackets indicate the orientational average as described by Eq. (21). Evaluation of the macroscopic susceptibility thus requires calculation of the microscopic solute hyperpolarizability tensor, determination of the local-field factor tensors, and orientational averaging of the emerging product. The general result for the TPA cross section is the following:

$$\begin{aligned}\sigma_2(\omega) &= \frac{24\pi^2\hbar\omega^2}{n^2c^2}\,\mathcal{I}m\langle\boldsymbol{\gamma}^{eff}\rangle_{XXXX} \\ &= \frac{24\pi^2\hbar\omega^2}{n^2c^2}\,\mathcal{I}m\Bigg[\frac{1}{5}\sum_i (F^R_\omega)^4_{ii}(f^C_\omega)^3_{ii}\,\gamma^{sol}_{iiii} + \\ &\qquad \frac{1}{15}\sum_{i\neq j}(F^R_\omega)^2_{ii}(f^C_\omega)_{ii}(F^R_\omega)^2_{jj}(f^C_\omega)_{jj}\left(\gamma^{sol}_{iijj}+\gamma^{sol}_{ijij}+\gamma^{sol}_{ijji}\right)\Bigg].\end{aligned} \tag{38}$$

In the c.g.s. system, the TPA cross section has the following units: cm^4 s photon^{-1}. Practical units commonly adopted are the Göppert-Mayer (GM), defined as: 1 GM = 10^{-50} cm^4 s photon^{-1}.

Hereafter, the conventions introduced in this section are systematically and consistently adopted.

3 Theoretical approaches

Over the last decades, various theoretical approaches have been implemented to interpret experimental measurements of NLO properties. They have shown to be very useful to understand structure-property relations and to provide valuable tools for rational molecular engeeniring towards improved targets. Among the different approaches, *ab-initio* methods coupled with finite field techniques are widely used to calculate off-resonant NLO responses.[217] A more general approach, covering the entire frequency range, is the time dependent perturbation theory. In practice, this is essentially a sum-over-states (SOS) method which involves calculating both ground and excited-states wavefunctions and the

transition dipole moments between them.[200,202,217,218] Within this frame, the first-order frequency-dependent polarizability reads:[200]

$$\alpha_{ij}(-\omega;\omega) = \frac{1}{\hbar}\sum_{m\neq g}\left[\frac{\langle g|\mu_i|m\rangle\langle m|\mu_j|g\rangle}{(\Omega_{mg}-\omega)} + \frac{\langle g|\mu_j|m\rangle\langle m|\mu_i|g\rangle}{(\Omega^*_{mg}+\omega)}\right] \tag{39}$$

and the third-order frequency-dependent polarizability is given by:[200]

$$\begin{aligned}
&\gamma_{ijkl}(-\omega_\sigma;\omega_1,\omega_2,\omega_3) = \frac{1}{6\hbar^3}\mathcal{P}(j,k,l;\omega_1,\omega_2,\omega_3)\\
&\times\Bigg\{\sum_{m\neq g}\sum_{n\neq g}\sum_{p\neq g}\Bigg[\frac{\langle g|\mu_i|m\rangle\langle m|\bar{\mu}_l|n\rangle\langle n|\bar{\mu}_k|p\rangle\langle p|\mu_j|g\rangle}{(\Omega_{mg}-\omega_\sigma)(\Omega_{ng}-\omega_1-\omega_2)(\Omega_{pg}-\omega_1)}\\
&+\frac{\langle g|\mu_l|m\rangle\langle m|\bar{\mu}_i|n\rangle\langle n|\bar{\mu}_k|p\rangle\langle p|\mu_j|g\rangle}{(\Omega^*_{mg}+\omega_3)(\Omega_{ng}-\omega_1-\omega_2)(\Omega_{pg}-\omega_1)}\\
&+\frac{\langle g|\mu_j|m\rangle\langle m|\bar{\mu}_k|n\rangle\langle n|\bar{\mu}_i|p\rangle\langle p|\mu_l|g\rangle}{(\Omega^*_{mg}+\omega_1)(\Omega^*_{ng}+\omega_1+\omega_2)(\Omega_{pg}-\omega_3)}\\
&+\frac{\langle g|\mu_j|m\rangle\langle m|\bar{\mu}_k|n\rangle\langle n|\bar{\mu}_l|p\rangle\langle p|\mu_i|g\rangle}{(\Omega^*_{mg}+\omega_1)(\Omega^*_{ng}+\omega_1+\omega_2)(\Omega^*_{pg}+\omega_\sigma)}\Bigg]\\
&-\sum_{m\neq g}\sum_{n\neq g}\Bigg[\frac{\langle g|\mu_i|m\rangle\langle m|\mu_l|g\rangle\langle g|\mu_k|n\rangle\langle n|\mu_j|g\rangle}{(\Omega_{mg}-\omega_\sigma)(\Omega_{mg}-\omega_3)(\Omega_{ng}-\omega_1)}\\
&+\frac{\langle g|\mu_i|m\rangle\langle m|\mu_l|g\rangle\langle g|\mu_k|n\rangle\langle n|\mu_j|g\rangle}{(\Omega_{mg}-\omega_3)(\Omega^*_{ng}+\omega_2)(\Omega_{ng}-\omega_1)}\\
&+\frac{\langle g|\mu_l|m\rangle\langle m|\mu_i|g\rangle\langle g|\mu_j|n\rangle\langle n|\mu_k|g\rangle}{(\Omega^*_{mg}+\omega_\sigma)(\Omega^*_{mg}+\omega_3)(\Omega^*_{ng}+\omega_1)}\\
&+\frac{\langle g|\mu_l|m\rangle\langle m|\mu_i|g\rangle\langle g|\mu_j|n\rangle\langle n|\mu_k|g\rangle}{(\Omega^*_{mg}+\omega_3)(\Omega_{ng}-\omega_2)(\Omega^*_{ng}+\omega_1)}\Bigg]\Bigg\}.
\end{aligned} \tag{40}$$

Here $\mathcal{P}(j,k,l;\omega_1,\omega_2,\omega_3)$ is a permutation operator, $\omega_1,\omega_2,\omega_3$ denote the frequencies of radiation fields and $\omega_\sigma = \omega_1+\omega_2+\omega_3$; m, n and p denote excited states and g denotes the ground state. $\langle g|\mu_i|m\rangle$ is i-th component of transition dipole moment between ground and m-th excited state and $\langle m|\bar{\mu}_j|n\rangle = \langle m|\mu_j|n\rangle - \langle g|\mu_j|g\rangle\delta_{nm}$. $\Omega_{mg} = \omega_{mg} - i\Gamma_{mg}$, where ω_{mg} is the transition energy between m and g states and Γ_{mg} is the broadening factor of excited state m.

Such expressions allow for both simple modeling through approximate few-state models (subsection 3.1) and high-level quantum mechanical calculations (subsection 3.3 and 3.4). For multichromophoric systems, the increased complexity can be addressed through either the well-known excitonic model (subsection 3.2) or semi-empirical models for interacting chromophores,[127,219] depending on the nature and the strength of interchromophore interactions.

3.1 Effective 2/3-state models

Organic conjugated chromophores typically show only a few resonances in the UV-visible region of their linear absorption spectra. For example, many conjugated oligomers and donor-acceptor substituted compounds have only one major low energy broad peak (band-gap transition) in their optical absorption. This means that only a few excited states are optically active, which attributes to their strong transition dipole moments appearing due to delocalized π-electronic system. This picture, however, does not hold for other optical materials, such as semiconductor quantum dots, where broad multi-peak spectra are common.[220] Similarly, nonlinear resonant spectra of organic chromophores are frequently dominated by only a few electronic transitions, in our case, TPA bands. These observations give rise to approximate few-state models for description of observed spectra. These models can be derived under certain assumptions from the complete SOS expressions, providing expansions of molecular polarizabilities into dipolar contributions arising from the different many-body excited states. Particularly, such reduced models work well for compounds of well defined charge symmetry.

Here we consider typical quasi-one-dimensional examples. The simplest case is given by dipolar chromophores, with a donor-π-acceptor structure. The two-level approximation is a standard approach for these dipolar (push-pull) chromophores, based on the fact that such molecules resonate between two basis forms, the neutral and the zwitterionic structures. Being the ground and the first excited state well separated from the higher lying states, only one excited state mainly contributes to all responses, and can conveniently be accounted for in the SOS expressions for α, β, and γ. Moreover, the dipolar contribution along the molecular axis z is dominant for dipolar molecules, so that the tensorial component γ_{zzzz} is the only one needed. Consequently, the imaginary part of the second hyperpolarizability for the two-photon process (inh the gas phase), calculated at the maximum ($\omega = \omega_{eg}/2$, $\hbar\omega_{eg}$ being the excited-state transition energy), is:

$$\mathcal{I}m\{\gamma_{zzzz}(\omega_{eg}/2)\} = \frac{8}{3}\frac{\mu_{ge}^2(\mu_{ee}-\mu_{gg})^2}{\hbar^3\omega_{eg}^2\Gamma}. \tag{41}$$

Here μ_{gg}, μ_{ee}, and μ_{ge} are ground state, excited state, and transition dipole moments, respectively, and Γ is an average linewidth broadening parameter. Since the orientationally averaged second hyperpolarizability is given in this case by $\langle\gamma\rangle = \gamma_{zzzz}/5$, the TPA cross

section at the maximum adopts the following expression:

$$\sigma_2^{2state}(\omega_{eg}/2) = \frac{16\pi^2\mu_{ge}^2(\mu_{ee}-\mu_{gg})^2}{5\hbar^2c^2\Gamma}. \quad (42)$$

Thus, σ_2 is proportional to the product of the squared transition dipole moment and the squared difference between excited-state and ground-state dipole moments. In a two-state model, all molecular properties can be expressed as functions of a single electronic variable. Parameter MIX, as defined in Ref.,[150] is proportional to $(\mu_{ee}-\mu_{gg})$. It vanishes in the case of equal contributions of the two limiting resonance forms. Similar parameter ρ (proportional to μ_{gg}), as defined in Ref.,[151] describes the weight of the zwitterionic resonating structure in the ground state. The highest TPA cross section is thus expected for chromophores having MIX$\sim \pm 0.6$ or, analogously, $\rho \sim 0.2$ or 0.8. The simplified expression in Eq. (42) has been successfully used to evaluate the TPA peak cross section of dipolar compounds using computed dipole moments and transition energies.[123] Another semiempirical approach was developed to account for vibrational contributions. The resulting two-level model has proved to be adequate to describe the linear and nonlinear absorption of push-pull chromophores.[127,153,221]

Molecules with quadrupolar symmetry described by donor-π-acceptor-π-donor or acceptor-π-donor-π-acceptor structures, provide another simple case allowing for a reduced description. For this class of chromophores, a three-state model can be adopted, which is based on the neutral and two zwitterionic (degenerate) states.[154,155] The inversion symmetry imposes that the lower energy excited state (e) is one-photon allowed, whereas the higher-energy one (e') is accessible through two-photon absorption. Again, the diagonal γ_{zzzz} component along the principal molecular axis provides the major contribution to the two-photon process. Its imaginary part (relevant to the the gas phase), calculated at the maximum ($\omega = \omega_{e'g}/2$), reads:

$$\mathcal{I}m\{\gamma_{zzzz}(\omega_{e'g}/2)\} = \frac{2}{3}\frac{\mu_{ge}^2\mu_{ee'}^2}{\hbar^3(\omega_{eg}-\omega_{e'g}/2)^2\Gamma}. \quad (43)$$

Using the orientationally averaged $\langle\gamma\rangle = \gamma_{zzzz}/5$, we arrive to the following expression for the TPA cross section at the maximum:

$$\sigma_2^{3state}(\omega_{e'g}/2) = \frac{4\pi^2\omega_{e'g}^2}{5\hbar^2c^2}\frac{\mu_{ge}^2\mu_{ee'}^2}{(\omega_{eg}-\omega_{e'g}/2)^2\Gamma}, \quad (44)$$

where $\hbar(\omega_{eg}-\omega_{e'g}/2)$ is the so-called detuning energy, i.e., the energy difference between the incident photon and the one-photon resonance. The reliability of a three-state model

for quadrupolar chromophores with enhanced TPA response has been widely tested and accepted (e.g.,[90,157,158]). Similar to the two-state case, MIX[155] or ρ[158] parameter can be chosen to describe molecular properties in the framework of the three-state model. The highest TPA cross section for quadrupolar chromophores can be attained for MIX = 0 (or $\rho = 0.5$).[155] This corresponds to a ground state described by an equal mixing of the neutral and the symmetric zwitterionic resonance forms. If this is the case, both numerator and denominator in Eq. (44) are maximized. The detuning term in the denominator is a key parameter in order to explain the high TPA cross sections of quadrupolar dyes, which are usually higher than that of dipolar molecules.

If one-photon resonance ω_{eg} is close to the exciting photon energy $\omega_{e'g}/2$, the TPA probability is strongly increased, because of the supplementary resonant denominator.[89,90,113,156] However, a perfect resonance or a small detuning may not allow for determination of the TPA cross section because of the concomitant one-photon absorption, as discussed in section 4. Consequently, optimized quadrupolar chromophores for TPA applications need to be designed by compromising between the maximal intrinsic response (high transition dipole moments and small detuning) and experimentally accessible response. Finite detuning must be chosen with respect to the sharpness of the absorption edge, in order to simultaneously maintain high cross sections and the specific features of TPA.[103]

3.2 Frenkel exciton model

Many chromophores of choice for TPA applications have (multi)branched structures, where a central electron donor (or acceptor) core is connected to electron acceptor (or donor) groups by two or more conjugated branches, to give rise to quadrupolar, octupolar and in general multipolar structures. Such a modular strategy based on the gathering of dipolar modules provides an additional *synthetic freedom* to tune the nonlinear response even further. To connect the photophysical properties of multibranched chromophores to those of their single-branch (dipolar) counterparts, the Frenkel exciton model has been proposed and adopted,[113,120] offering a reduced description compared to 'supramolecular' approaches.

The Frenkel exciton model describes the limit of tightly bound and localized excitons as opposed to the Wannier limit of diffuse delocalized excitons.[220,222] The former usually applies to clusters of weakly interacting molecules such as organic molecular crystals

or aggregates.[223] It assumes that all intermolecular interactions are driven by electrostatic forces (Förster limit[224]), while short-range interactions resulting from the direct wavefunction overlaps among neighboring chromophores are negligible. Consequently, if intermolecular couplings are small compared to the relevant transition energies, the problem can be treated perturbatively, so that the zero-order wavefunction basis for the aggregate is the direct product of the local wavefunctions relevant to each molecular site. Let us consider a single excitation on each molecular site, so that each molecule can either be in the ground state, $|g_i\rangle$, or in the excited state, $|e_i\rangle$. The reduced Frenkel exciton Hamiltonian is then given by:[225]

$$H = \sum_i \hbar\omega_i b_i^\dagger b_i + \sum_{i \neq j} V_{ij}(b_i^\dagger b_j + b_j b_i^\dagger). \tag{45}$$

Here indices i and j run over the molecular sites, and $b_i^\dagger$ (b_i) are creation (annihilation) operators of a local excitation on the i-th site. The first term in Eq. (45) characterizes the total excitation energy of the aggregate, which, to zero-order, is additive with respect to the local excitations of individual chromophores. Here $\hbar\omega_i$ is the transition energy on the i-th site. Even for an ensemble of the same chromophores, ω_i may not be identical for each site: $\omega_i = \omega_0 + \delta_i$, where ω_0 is the transition energy in vacuum, and δ_i is a diagonal disorder term accounting for effects caused by solvent, molecular vibrations, temperature fluctuations, etc.[226–232] The second term in Eq. (45) describes the effect of intermolecular interactions, where V_{ij} is the matrix element describing coupling between sites i and j (hopping integral). Notably, $||V_{ij}|| \ll ||\omega_i||$. Since the electrostatic forces decrease quickly with the intermolecular distance, often only the nearest-neighbor exciton hopping is retained. Similar to ω_i, a decomposition $V_{ij} = J_{ij} + \Delta_{ij}$ may be useful to account for disorder effects by an off-diagonal term Δ_{ij}. A competition between coupling and disorder terms define exciton delocalization properties. When disorder prevails ($||V_{ij}|| \ll ||\delta_i||$), the excited states remain localized on individual chromophores.[229,230,233] In the opposite limit ($||V_{ij}|| \gg ||\delta_i||$), the excited states of the aggregate form quantum-mechanical superposition of local excitations resulting in delocalized excitonic states.[233–235] In the discussion below we focus on the latter regime.

Describing multipolar branched molecular systems (quadrupolar and octupolar chromophores) as interacting submolecular dipolar entities, is a first approximation: indeed other communication channels may exist between the branches, other than simple elec-

trostatic interactions, which can not be accounted for in the exciton model. In the simple dipolar approximation for electrostatic forces, V_{ij} measures the interaction between the transition dipole moments on the i-th and j-th branches, hence depending on the reciprocal orientation and distance. In the case of dipolar branches the approximation of two-level molecules is reasonable (Fig. 1). When branches do not interact, single excitations on the distinct branches are degenerate. However, when interaction is allowed, diagonalization of the Hamiltonian (45) results in a splitting of the initially degenerate single excitations. For a dimeric chromophore made of two identical subchromophores ($V_{12} = V$), the two one-exciton transitions are separated by $2V$. Here, the lower and higher-energy states are one-photon and two-photon allowed, respectively. For a trimeric chromophore made of three identical dipolar units with C_3 symmetry ($V_{12} = V_{13} = V_{23} = V$), a twofold degenerate first excited state is obtained, which is mostly one-photon allowed, while the higher-energy one-exciton state is two-photon allowed (Fig. 1). In both cases, the description of branched molecules through the Frenkel exciton model qualitatively corresponds to predictions based on charge resonance few-states models.

In general, when applied to (multi)branched structures, the Frenkel exciton model provides a reasonable qualitative agreement with experimental observation. However, when applied to homologous series comprised by dipoles, quadrupoles and octupoles, experimental trends not always are correctly reproduced, depending on the nature of the coupling between branches. In particular, it has been demonstrated that this model cannot quantitatively reproduce such trends when coherent interactions between branches are important.[120]

3.3 Overview of quantum-chemical approaches

First-principle calculations of molecular electronic spectra require extensive numerical effort and, therefore, exact treatment becomes impractical even for fairly small molecules. Correct description of excited states involved in NLO responses frequently requires inclusion of the higher-order electronic correlations. This makes their computing a much more complicated procedure compared to analogous ground-state calculations. For molecules of practical interest it becomes necessary to make various approximations to the underlying many-electron wavefunction. Restricting the size of active space in configuration interaction (CI) to a few orbitals (like in CASSCF), limiting the order of substitutions

to singles (CIS) and doubles (CISD), their combination (MRDCI) and/or simplifications in model Hamiltonians (AM1 or INDO/S) are typical examples of such approximations.[185,218,236–241] In spite of overall good performances, these calculations may undercorrelate the excited state wavefunctions (e.g., CIS) or over-correlate the ground-state wavefunctions (e.g., MDRCI/INDO),[89,90,237] and do not guarantee size-consistency.[242]

In a contrast to CI-based methods, adiabatic time-dependent density functional theory (TD-DFT)[170,171] in the Kohn-Sham (KS) form has rapidly emerged as an accurate and efficient method for studying the optical response of molecules. Excellent results have been obtained for organic molecules, organometallic compounds, inorganic finite clusters and infinite crystals (e.g., see[172–176,243–246]). Recently TD-DFT extensions for the calculations of molecular nonlinear optical properties were suggested and closed expressions for frequency-dependent optical polarizabilities up to the third order in the driving field were derived within adiabatic TD-DFT approximation.[179–182] TD-DFT was shown to give a better agreement with experiment than both semiempirical and low-level *ab initio* calculations for two-photon absorption (TPA) calculations in large conjugated organic chromophores[102,120,126,192–196] and small molecules.[183–188] In particular, a benchmark study of TPA and one-photon absorption (OPA) resonant frequencies calculated with TD-DFT (B3LYP/6-31G) against experimental data in a series of 16 substituted molecules found that both TPA and OPA transition energies are predicted with about 0.15 eV average accuracy.[192]

Search for the methods which can provide reliable qualitative and quantitative information about linear and NLO responses is still an active field. Some of the more recent contributions to the benchmark studies calibrating performances of higher (Coupled cluster, CCSD or CC3) and lower-order (CIS/MRD-CI) *ab-initio* methods with TD-DFT and RPA, and also semiempirical methods have been recently made by several groups.[238,239,247] Overall performance of TD-DFT methods is found to be good when combined with proper functionals and basis sets. The results are expected to improve with development of newer more accurate density functionals, while preserving overall computational complexity.

3.4 TD-DFT formalism for frequency-dependent polarizabilities

Computation of nonlinear polarizabilities with SOS approach[200] requires ground- and excited-state energies, state dipoles, and transition dipoles (see Eq. (40)). However, the manifold of contributing states and transition dipole moments between the excited states are not available from the linear response theory[171] (we refer to a detailed discussion in[182]). Alternative expressions for the frequency-dependent polarizabilities have been recently derived specifically for time dependent Hartree-Fock (TD-HF) and TD-DFT approaches.[182,248] These equations require only quantities that can be obtained from the linear response theory and the corresponding functional derivatives in the TD-DFT method. The first-order optical polarizability $\alpha_{ij}(-\omega;\omega)$ can be calculated using the following expression:[182]

$$\alpha_{ij}((-\omega;\omega) = \frac{1}{\hbar}\sum_{\nu=-M,\ldots,M}\frac{S_\nu \mu^{(i)}_{-\nu}\mu^{(j)}_{\nu}}{\Omega_\nu - \omega}. \tag{46}$$

The third-order polarizability can be calculated using 8 term expression symmetrized with respect to ω_1, ω_2, and ω_3 permutations:[182]

$$\gamma_{ijkl}(-\omega;\omega_1=\omega,\omega_2=\omega,\omega_3=-\omega) = \frac{1}{6\hbar^3}\sum_{\omega_1,\omega_2,\omega_3}^{perm}\left(\gamma^{(I)}_{ijkl}+\gamma^{(II)}_{ijkl}+\ldots\gamma^{(VIII)}_{ijkl}\right), \tag{47}$$

where

$$\gamma^{(I)}_{ijkl} = \sum_{\alpha\beta\gamma}\frac{\mu^{(j)}_{-\alpha\beta}\mu^{(k)}_{-\beta\gamma}\mu^{(i)}_{\alpha}\mu^{(l)}_{-\gamma}S_\alpha S_\beta S_\gamma}{(\Omega_\alpha-\omega_1-\omega_2-\omega_3)(\Omega_\beta-\omega_2-\omega_3)(\Omega_\gamma-\omega_3)}, \tag{48}$$

$$\gamma^{(II)}_{ijkl} = \sum_{\alpha\beta\gamma\delta}\frac{-\mu^{(j)}_{-\alpha\beta}V_{-\beta\gamma\delta}\mu^{(i)}_{\alpha}\mu^{(k)}_{-\gamma}\mu^{(l)}_{-\delta}S_\alpha S_\beta S_\gamma S_\delta}{(\Omega_\alpha-\omega_1-\omega_2-\omega_3)(\Omega_\beta-\omega_2-\omega_3)(\Omega_\gamma-\omega_2)(\Omega_\delta-\omega_3)}, \tag{49}$$

$$\gamma^{(III)}_{ijkl} = \sum_{\alpha\beta\gamma}\frac{\mu^{(j)}_{-\alpha\beta\gamma}\mu^{(i)}_{\alpha}\mu^{(k)}_{-\beta}\mu^{(l)}_{-\gamma}S_\alpha S_\beta S_\gamma}{(\Omega_\alpha-\omega_1-\omega_2-\omega_3)(\Omega_\beta-\omega_2-\omega_3)(\Omega_\gamma-\omega_3)}, \tag{50}$$

$$\gamma^{(IV)}_{ijkl} = \sum_{\alpha\beta\gamma\delta}\frac{-2V_{-\alpha\beta\gamma}\mu^{(k)}_{-\gamma\delta}\mu^{(i)}_{\alpha}\mu^{(j)}_{-\beta}\mu^{(l)}_{-\delta}S_\alpha S_\beta S_\gamma S_\delta}{(\Omega_\alpha-\omega_1-\omega_2-\omega_3)(\Omega_\beta-\omega_1)(\Omega_\gamma-\omega_2-\omega_3)(\Omega_\delta-\omega_3)}, \tag{51}$$

$$\gamma^{(V)}_{ijkl} = \sum_{\alpha\beta\gamma\delta\eta}\frac{2V_{-\alpha\beta\gamma}V_{-\gamma\delta\eta}\mu^{(i)}_{\alpha}\mu^{(j)}_{-\beta}\mu^{(k)}_{-\delta}\mu^{(l)}_{-\eta}S_\alpha S_\beta S_\gamma S_\delta S_\eta}{(\Omega_\alpha-\omega_1-\omega_2-\omega_3)(\Omega_\beta-\omega_1)(\Omega_\gamma-\omega_2-\omega_3)(\Omega_\delta-\omega_2)(\Omega_\eta-\omega_3)}, \tag{52}$$

$$\gamma^{(VI)}_{ijkl} = \sum_{\alpha\beta\gamma\delta}\frac{-V_{-\alpha\beta\gamma\delta}\mu^{(i)}_{\alpha}\mu^{(j)}_{-\beta}\mu^{(k)}_{-\gamma}\mu^{(l)}_{-\delta}S_\alpha S_\beta S_\gamma S_\delta}{(\Omega_\alpha-\omega_1-\omega_2-\omega_3)(\Omega_\beta-\omega_1)(\Omega_\gamma-\omega_2)(\Omega_\delta-\omega_3)}, \tag{53}$$

$$\gamma^{(VII)}_{ijkl} = \sum_{\alpha\beta\gamma}\frac{\mu^{(i)}_{\alpha\beta}\mu^{(k)}_{-\beta\gamma}\mu^{(j)}_{-\alpha}\mu^{(l)}_{-\gamma}S_\alpha S_\beta S_\gamma}{(\Omega_\alpha-\omega_1)(\Omega_\beta-\omega_2-\omega_3)(\Omega_\gamma-\omega_3)}, \tag{54}$$

$$\gamma_{ijkl}^{(VIII)} = \sum_{\alpha\beta\gamma\delta} \frac{-\mu_{\alpha\beta}^{(i)} V_{-\beta\gamma\delta} \mu_{-\alpha}^{(j)} \mu_{-\gamma}^{(k)} \mu_{-\delta}^{(l)} S_\alpha S_\beta S_\gamma S_\delta}{(\Omega_\alpha - \omega_1)(\Omega_\beta - \omega_2 - \omega_3)(\Omega_\gamma - \omega_2)(\Omega_\delta - \omega_3)}. \quad (55)$$

Here $S_\alpha = sign(\alpha)$, indices $s = i, j, k, l$ label the spatial directions (x, y, and z), indices $\nu = \alpha, \beta, \gamma, \delta, \eta = -M, \ldots, M$ run over the excited states, and Ω_ν are excitation energies obtained from the linear response theory by diagonalization of the Liouville operator, which eigenvectors (transition densities ξ_ν) come in conjugated pairs.[171,248] We assume that Ω_ν is positive (negative) for all $\nu > 0$ ($\nu < 0$) according to the convention $\Omega_{-\nu} = -\Omega_\nu$. The line-broadening can be accounted for by replacing the excitation energies Ω_ν with $\Omega_\nu - i\Gamma_\nu$, Γ_ν being the damping factor of excited state ν. Similar to Eq. (40), this gives rise to the Lorentzian lineshapes of the resonances. The other variables[182]

$$\mu_\alpha^{(s)} = Tr(\boldsymbol{\mu}^{(s)} \xi_\alpha), \quad (56)$$

$$\mu_{\alpha\beta}^{(s)} = \sum_{\alpha\beta}^{perm} Tr(\boldsymbol{\mu}^{(s)} (\mathbf{I} - 2\bar{\boldsymbol{\rho}}) \xi_\alpha \xi_\beta), \quad (57)$$

$$\mu_{\alpha\beta\gamma}^{(s)} = -\frac{1}{3} \sum_{\alpha\beta\gamma}^{perm} Tr(\boldsymbol{\mu}^{(s)} \xi_\alpha \xi_\beta \xi_\gamma), \quad (58)$$

$$V_{\alpha\beta\gamma} = \frac{1}{2} \sum_{\alpha\beta\gamma}^{perm} Tr((\mathbf{I} - 2\bar{\boldsymbol{\rho}}) \xi_\alpha \xi_\beta \tilde{\mathbf{V}}(\xi_\gamma)), \quad (59)$$

$$V_{\alpha\beta\gamma\delta} = \frac{1}{12} \sum_{\alpha\beta\gamma\delta}^{perm} Tr((\mathbf{I} - 2\bar{\boldsymbol{\rho}}) \xi_\alpha \xi_\beta \tilde{\mathbf{V}}((\mathbf{I} - 2\bar{\boldsymbol{\rho}}) \xi_\gamma \xi_\delta)) - \frac{1}{12} \sum_{\alpha\beta\gamma\delta}^{perm} Tr(\xi_\alpha \xi_\beta \xi_\gamma \tilde{\mathbf{V}}(\xi_\delta)), \quad (60)$$

are tensors symmetrized with respect to all permutations of their indices $(\alpha, \beta, \gamma, \delta, \eta)$. Here $\boldsymbol{\mu}^{(s)}$ is the dipole matrix for s-spatial direction, $\bar{\boldsymbol{\rho}}$ is the ground-state density matrix, and $\mathbf{I}$ is a unit matrix. ξ_α is a transition density matrix describing a transition from the ground state to α excited state. ξ_α quantities are routinely obtained from the linear response theory as eigenvectors of the corresponding RPA operator.[171,182,248] The terms that depend on the third- and forth-order functional derivatives of $E^{xc}[n]$[182] have been neglected in Eqs. (59) and (60) because the appropriate functional derivatives are not yet available in the widespread computational packages. We believe these quantities may have only a minor impact on polarizability magnitudes.[192] The Coulomb-exchange-correlation operator $\tilde{\mathbf{V}}$ is defined as

$$\tilde{V}_{pq\sigma}(\xi) = \sum_{mn\sigma'} ((pq\sigma|mn\sigma')\xi_{mn\sigma'} - c_x(pm\sigma|qn\sigma)\xi_{mn\sigma}\delta_{\sigma\sigma'}) + \sum_{mn\sigma'} f_{pq\sigma,mn\sigma'}\xi_{mn\sigma'}, \quad (61)$$

where $(pq\sigma|mn\sigma')$ denotes the two-electron integrals (indices p, q, m, n and σ refer to the orbitals spatial and spin indices, respectively). Becke's mixing parameter c_x allows the in-

troduction of Hartree-Fock exchange and the construct of hybrid functionals.[249] $f_{pq\sigma,mn\sigma'}$ is the matrix element of the kernel corresponding to the second functional derivative of an XC functional $E^{xc}[n]$ with respect to the charge density $n(\mathbf{r})$.[170,171]

Expressions (48)-(55) for polarizabilities remind the standard Sum-Over-States equations by Ward and Orr[200,250] for computing resonant polarizabilities (e.g., the expansion for $\boldsymbol{\gamma}$ is given by Eq. (40)) since they include the summation over the contributions from the individual excited electronic states, however, there are significant differences. Eqs. (48)-(55) do not include the dipole moments between the excited states. Instead, the coupling among the electronic states enters indirectly through dipolar $\boldsymbol{\mu}$ and Coulomb-exchange-correlation terms $\mathbf{V}$ defined by Eqs. (56)-(60), where μ_α is the transition dipole between ground and $|\alpha\rangle$ excited states and the other terms describe couplings between two (or more) states.

The SOS expression can be interpreted as the summation over the Liouville space paths.[198,217,218] Panel A of Fig. 2 show paths corresponding to $\mu_{gm}\mu_{mg}$ dipole combinations in the SOS expression for linear response Eq. (39) (here we use the shorthand notation $\mu_{nm} = \langle m|\mu|n\rangle$). Figure 2 B illustrates the dominating term from the third order SOS expression (40) contributing to the TPA response of quadrupolar molecules in the 3-level scheme (Eq. (43)). Similar interpretation can be applied to Eqs. (46)-(55) using the effective oscillator system[248] introduced for TD-DFT in.[181,182] Using our notation, we define that for $\alpha > 0$ μ_α with Ω_α ($\mu_{-\alpha}$ with $\Omega_{-\alpha} = -\Omega_\alpha$) corresponds to a transition from the ground state to the $|\alpha\rangle$ excited state (from the $|\alpha\rangle$ excited state to the ground state) to interpret positive and negative indices. For example, Figure 2C shows the paths for the linear response corresponding to Eq. (46). The third order term corresponding to Eq. (47) is displayed in Fig. 2D. We further notice that $\mu_{-\alpha\beta}$ ($\alpha, \beta > 0$) is partially related to the dipole moment between α and β excited states, namely part derived from the so-called unrelaxed transition density matrix.[175,251] The second contribution stemming from the relaxed part of the interstate transition density matrix enters implicitly through the combination of other dipolar $\boldsymbol{\mu}$ and Coulomb terms $\mathbf{V}$ defined by Eqs. (56)-(60). Particularly terms like $\mu_{\alpha\beta}$ ($\alpha, \beta > 0$) show the contributions from the doubly excited effective oscillators, which appear beyond the linear response theory.[182] Alternatively, such terms can be calculated variationally using the analytic gradient technique for the TD-DFT developed in[175,251] or residue response theory.[179,180]

In our implementation of this methodology[102,192] we used the Gaussian 98 and Gaussian 03 packages[252,253] to calculate the linear response in the adiabatic TD-DFT, and to print out the excitation energies Ω_ν, transition densities ξ_ν, dipole matrices $\boldsymbol{\mu}^{(s)}$, and relevant Coulomb-exchange-correlation matrices $\tilde{\mathbf{V}}(\xi_\nu)$ and $\tilde{\mathbf{V}}(\frac{1}{2}[[\xi_\beta, \bar{\boldsymbol{\rho}}], \xi_\alpha])$ defined by Eq. (61). To calculate the third-order response (Eq. (47)) we utilize the Collective Electronic Oscillator (CEO) program.[248] Minor code modifications were required to interface the CEO with TD-DFT data printout, since both TD-HF and TD-DFT methods share the same mathematical description for the excited-state electronic structure.[182] Computation of TPA cross sections follows from insertion of the appropriate components of $\gamma_{ijkl}(-\omega;\omega,\omega,-\omega)$ derived from (47) in expression (38).

3.5 Dependence on the number of states, basis set and functional

When applying described above TD-DFT approach for calculations of nonlinear polarizabilities, it is important to realize several practical constraints and methodological aspects. First of all, summation in Eqs. (48-55) have to be truncated to some reasonable number of excited states, which is also the case of usual SOS applications. Modern computational codes use direct Krylov sub-space methods to calculate excited states. Typically, in such approaches computational cost and memory requirements scale, respectively, linearly and quadratically with the number of states requested. The final result is also a function of the density functional and a quality of the basis set used. Finally, out of 8 contributions (Eqs. (48-55)) to the response, terms involving multi-dimensional tensors such as $V_{\alpha\beta\gamma\delta}$ bear the majority of the computational expense. Identifying dominant contributions into the total response allows one to formulate truncated approaches to calculate NLO responses of large and complex molecular systems at different levels of accuracy.

We illustrate these dependencies (a detailed analysis was reported in[193]) by considering two examples: donor-donor substituted case of para,para'-bis(dimethylamino)bistyryl and donor-acceptor substituted case of para-dimethylamino,para'-nitrobistyryl shown in Fig. 3 inserts. Substituted bistyryl derivatives were reported to have significant NLO response and experimental NLO data of similar compounds are available.[89,90,254] We start our calculations with geometry optimization of both molecules (insets in Fig. 3) at HF/6-31G level with planarity constraint, and then compute up to 26 singlet electronic states

for each molecule using TD-DFT coupled with different functionals listed in Table 1: adiabatic local density approximation (ALDA, also known as Slater exchange), gradient-corrected functional (BLYP), and hybrid functionals (B3LYP, PBE1PBE, MPW1PW91, and BHandH), which contain an increasing portion of exact HF exchange. Calculations using TD-HF approach coupled with *ab initio* (HF) and semiempirical INDO/S Hamiltonians (HF/S) were conducted as well to explore the limiting case with 100% of HF exchange. The calculations of the static and resonant third-order nonlinear optical polarizabilities were then performed using the procedure described in subsection 3.4. The static polarizabilities ($\boldsymbol{\gamma}_0 = Re(\boldsymbol{\gamma}(0;0,0,0))$ are of interest to a variety of nonlinear applications (i.e., optical switches). We also focus on the resonant response $\boldsymbol{\gamma}(-\omega;\omega,\omega,-\omega)$ responsible for TPA properties. Only a dominant component of the polarizability tensor γ_{zzzz} along the molecular axis was included in the average over all orientations (see Sec. 3.1).

Fig. 3 illustrates the relationships between the first-order properties of our molecules and the third-order static and resonant polarizabilities. The variation of the transition dipole moments between the ground and the first excited states is shown in the Fig. 3(a-a'). For donor-donor molecule, the value of the transition dipoles varies only within 7.25% (from 11.45 D for TD-HF to 12.28 D for TD-PBE1PBE). For donor-acceptor molecule, on the other hand, this value changes considerably (from 7.95 D for TD-BLYP to 11.6 D for TD-HF). This difference reflects electronic delocalization of the excited states: the first excitation in the donor-acceptor compound corresponds to the charge transfer between the two molecular termini, while in the donor-donor molecule it corresponds to the charge transfer from the termini to the central ring.[89, 90, 192] The HF exchange is known to have a strong effect on the description of the long range interactions, and, therefore, it significantly affects donor-acceptor molecule. Fig. 3(b-b') shows the relevant excitation energies. Due to symmetry, the first excited state of donor-donor molecule with frequency Ω_1 is inactive in the TPA process (see Sec. 3.1). However, the two higher-lying states (with frequencies Ω_2 and Ω_n, respectively) show up in the nonlinear spectra.[193] In contrast, the first excited state manifests itself as the first TPA maximum in the the donor-acceptor molecule. Higher-lying state (with frequency Ω_n) is showing in the calculated TPA spectra as well.[193] The excited states of both molecules exhibit large blue shifts with increase of HF exchange fraction in the functional. This fact is due to the nonlocal nature of the HF

exchange, which destabilizes the excited states. Fig. 3(c-c') shows the magnitudes of the third-order polarizabilities at the maxima denoted as γ_1 and γ_2. We observe the gradual decrease of the amplitude for the first maximum, and an increase of the amplitude for the second one upon reduction of the amount of the HF exchange. Static response data are shown in Fig. 3(d-d'). As one can see in Fig. 3d-d', the less HF-exchange is present in the functional, the higher values the static polarizabilities acquire. This is in agreement with highly polarizable free electron gas model, inherent to ALDA functional. We also point out that in all different methods the third-order static polarizablility of the donor-acceptor molecule exceeds that of the donor-donor molecule approximately by a factor of four.

Fig. 4 shows the third-order resonant and static polarizabilities as a function of the number of excited states M used in summations (47)-(55). In most cases, the asymptotic limit is reached with eleven excited states for resonant polarizabilities. However, this is not true for the methods with $c_x \geq 0.25$ for both γ_1 and γ_2 maxima (Fig. 4(a-a') and (b-b')). The absolute values of the third-order polarizability in these cases are very low (see Fig. 4(c-c'),(d-d')) and, thus, the accuracy of calculations is not sufficient. More states are needed also in the case of the third-order static polarizability (Fig. 4(c-c')) where many Liouville space paths contribute to the off-resonant responses.

To study the effect of the basis set size we calculated both molecules at B3LYP/6-31G* and B3LYP/6-31+G levels. In agreement with results reported previously,[192] the basis set size increase changes the polarizability magnitudes by 10 to 20%. The reason for the relatively weak dependence on the basis set lies in the nature of the molecules studied. The third-order response properties are dominated by a delocalized π-electron system, and atomic polarization becomes relatively unimportant. Consequently, addition of the polarization and diffuse functions to the basis set does not change the results substantially.

Finally, Fig. 5 displays the contributions from the different components into the total third-order polarizability for different methods. We observe that the general trends for both molecules are very similar for resonant and static polarizabilities (with the exception of the TD-HF method). In most cases, the major contribution comes from $\gamma^{(I)}$ and $\gamma^{(VII)}$ terms. In fact, $\gamma^{(I)}$ and $\gamma^{(VII)}$ depend only on the dipole couplings (Eqs. (56) and (57)) and are the only terms that give significant contribution into the resonant polarizabilities if HF-exchange is not present in the functional.

$\gamma^{(III)}$ always gives negative contribution to the third-order static polarizability. This term contains dipole coupling between three excited states (Eq. (58)). None of $\gamma^{(I)}$, $\gamma^{(VII)}$ and $\gamma^{(III)}$ terms contains Coulomb operators. For the resonant polarizability, the second major contribution comes from $\gamma^{(II)}$ and $\gamma^{(VIII)}$ terms, but these contributions amount for less than 8.3% each for the functionals with $c_x \leq 0.25$ in the case of the first maximum. However, these terms contribute significantly to TD-BHandH and TD-HF results. Both $\gamma^{(II)}$ and $\gamma^{(VIII)}$ terms contain Coulomb operators coupling three states (Eq. (59)) and dipole couplings (Eq. (57)). The next (usually negative) contribution comes from $\gamma^{(VI)}$. This term is very small in case of resonant polarizability (except for TD-HF method at the first maximum). For static polarizability, $\gamma^{(VI)}$ term has considerable contribution only in the case of TD-BHandH and pure TD-HF methods. This term (Eq. (60)) depends on the Coulomb operator which couples four excited states and, therefore, $\gamma^{(VI)}$ contains most of the computational expense for the third-order polarizability. Thus several approximations can be readily applied to significantly reduce the numerical cost of the third-order polarizability calculations depending on the level of accuracy required.

3.6 Accounting for solvent effects

As presented in subsection 2.4, solvent effect on molecular properties can be accounted for in two steps, the first consisting in evaluation of so-called solute properties, the second in the evaluation of local-field corrections in order to retrieve so-called effective properties. We illustrate the amount of such effects by considering three examples: a donor-acceptor substituted stilbene chromophore ($\mathsf{d_1}$, Fig. 6), the structurally related octupolar derivative obtained by gathering three dipolar units ($\mathsf{3d_1}$, Fig. 6) and a donor-donor functionalized dinonylfluorene chromophore ($\mathsf{q_1}$, Fig. 7). Their TPA properties are discussed in details in section 5. Corresponding computational details can be found in subsection 3.7.

3.6.1 Solute versus gas-phase polarizabilities

Different models for the calculation of solute second-order hyperpolarizabilities have been explored, as illustrated in Fig. 8. To evaluate solvent-induced trends, we used the polarizable continuum model (PCM) as implemented in Gaussian 03.[253] We chose a low polarity solvent, toluene, for our investigations, as most of the available experimental spectra we present here are obtained in this solvent. In particular, three different calculations

were performed: all in vacuum (*vac-vac*); geometry-optimization in vacuum, property-calculations through PCM (*vac-tol*); geometry-optimization and property-calculations in the solvent through PCM (*tol-tol*). As shown in Fig. 8, PCM calculations strongly affect the third-order nonlinear response: a systematic red-shift of the electronic transitions and an increase of the TPA band is observed when going from *vac-vac* to *vac-tol*. On the other hand, changes obtained by geometry optimization in solvent (*tol-tol* versus *vac-tol*) are negligible.

Experimental trends, such as peak position and intensities, are well reproduced by calculations, both for the linear (Table 2) and two-photon (Table 3) properties. However, the quantitative agreement depends on the specific chromophore. In particular, results for the dipolar derivative d_1 show the worst agreement with experimental data for TPA peak position and amplitude. Considering the good agreement of the transition dipole moment to the first excited state (Table 2), expression q_1 obtained within the two-state model suggests that the variation between ground- and excited-state dipole moments is largely overestimated by B3LYP calculations. On the other hand, for the quadrupolar (q_1) and the octupolar ($\mathsf{3d}_1$) compounds a much better agreement is obtained for the TPA cross section. The main reason for such an inconsistent behavior can be found in intrinsic overestimation of charge-transfer in B3LYP calculations, which becomes particularly pronounced for the dipolar molecules.[176, 230]

An interesting question is then investigation of the solvent effects aiming to obtain a better agreement with experimental data. Even if in principle *tol-tol* or *vac-tol* calculations should perform better than calculations with no solvent (*vac-vac*), actual results depend on the specific molecule and on the property of interest (see Table 2 and Table 3). A quite general result is that calculations in solvent overestimate transition dipole moments and, hence, TPA cross sections. Calculations with the B3LYP functional in vacuum slightly overestimate charge-transfer phenomena (this subject is briefly discussed in subsection 3.7), and this effect is magnified in the presence of solvent.

3.6.2 Local-field corrections

Local-field effects on the TPA bands have been investigated on the same set of chromophores: d_1, q_1 and $\mathsf{3d}_1$, in the framework of the three types of calculations (*vac-vac*, *vac-tol* and *tol-tol*). In order to estimate local-field factors, the choice and definition of

the cavity is fundamental. Here we adopt the following approach: we estimate the cavity volume through the PCM method in Gaussian 03; the cavity is then approximated by an ellipsoid; the ratio between the lengths of the semiaxes of the ellipsoid are estimated through Molekel[255] (computing the "fast-surface" and drawing the box around that surface); the semiaxes are rescaled in order to have the same volume as estimated before through the PCM calculations.

Results are reported in Table 3 and exemplified in Fig. 9 for the *tol-tol* case. Accounting for the local field systematically increases the amplitude of the first TPA maxima. But taking into account the refractive-index effect (see Eq. (38)) leads to a global decrease of the amplitude. Table 3 shows that the global effect of local field and refractive index always helps to obtain a better agreement between experimental and calculated TPA cross sections. In general, TPA peak position and intensities are closer to experiment in case of *vac-vac* calculations. It is however important to note that even for the worst agreement, the calculated spectral positions stay inside the value chosen for the full-width at half-maximum of the bands.

The overall correction to the maximum of the TPA band, including local-field and refractive-index effect, is in general on the order of 0.8. It is interesting to compare this result to other possible, less refined approximations. For example, using a spherical cavity of the same volume, corrections would amount to a factor larger than 2. In a different approximation, the Lorentz formula would lead to a global correction L^4/n^2 of ~ 1.8. This shows that the choice of the cavity shape is very important, so that highly simplified models, e.g., based on spherical cavities or on the Lorentz approximation, are to be excluded if a quantitative agreement is desired. Indeed, a discrepancy larger than 2 is found between the Lorentz or spherical approximation and our best estimates. Our choice for the cavity is still somewhat arbitrary, and the use of cavities having the true molecular shape would be a better choice, as proposed and implemented by Cammi et al.[206] It was shown in this reference, that approximating the cavity to an ellipsoid with the volume equal to that of molecular cavity provides much better results than the spherical approximation. However, the effect of the cavity was only investigated for small molecules in ref.[206] Therefore, the study of similar effects for larger chromophores would be a valuable extension.

In conclusion of this subsection, we found that geometry optimization in a non-polar solvent, such as toluene, is not crucial. Intuitively, the *tol-tol* approach seems to be the most

consistent way to calculate TPA cross sections. However, taking into account approximations introduced by the use of the hybrid B3LYP functional, simple calculations in vacuum (*vac-vac* approach) in general provide better quantitative results. Since *vac-vac* calculations are much less time consuming, we exploit them in the following section to investigate different series of chromophores and compare computed properties to experimental values. Local-field corrections are important and depend on the choice of the cavity shape and approximation scheme.

3.7 Computational details

We employ various quantum-chemical approaches to model all chromophores of interest. Unless explicitly stated, the computational details are as follows. For the sake of simplicity, nonyl, hexyl and butyl solubilizing chains have been replaced by methyl groups. Most of the calculations have been performed in vacuum. Ground-state optimized geometries have been obtained using the Gaussian 98[252] or Gaussian 03[253] packages. For ground-state geometries of extended conjugated chromophores, we previously found that the HF method is superior to the DFT-based approaches by reproducing accurately bond length alternation parameter when compared to experiment.[120,192] This alternation reflects the degree of π-conjugation between the double bonds and constitutes an important parameter characterizing electronic properties in these molecules.[147,148] Thus, all ground-state geometries are obtained at the HF level using the 6-31G basis set.

It is well known that TD-HF approach lacks important electronic correlations, and therefore excited states are systematically and significantly blue-shifted with respect to experiments. In contrast, TD-DFT reproduces excited-state properties of many systems in a much better way.[175] However, pure and gradient-corrected DFT functionals do not provide a correct description of the charge transfer states[176,256–259] and bound exciton states.[258,260,261] This, to some extent, can be cured by implementing hybrid functionals, such as B3LYP, where the HF exchange component somewhat compensates incorrect long-range functional asymptotics. In this review we consistently use B3LYP model, which was found to give a very accurate description of excited states in many molecular systems.[174,175,262] However, this model may still be susceptible to the charge-transfer state failures in large molecules in spite of presence of the orbital exchange fraction of 20%.[176] Replacing B3LYP functional with another DFT model with larger fraction of

orbital exchange (e.g., PBE1PBE or BHandHLYP) downplays the charge transfer phenomena and shift the transition energies to the blue. On the other hand, reduction of the orbital exchange in the functional (e.g., TPSSh, BLYP, etc.) enhances charge transfer processes, shift transition energies to the red and slightly reduce the respective transition dipoles. Asymptotically corrected functionals which appeared recently, have a potential to overcome this problem and describe correctly excitations with a long-range spatial extent.[187,263,264] However, applications to different molecular systems[265,266] have shown a mixed picture compared to standard hybrid models.

We further employ the density matrix formalism for nonlinear optical responses, as described in subsection 3.4, with TD-B3LYP/6-31G level of theory to investigate linear and nonlinear optical properties of organic dyes. Excited-state electronic structure analysis is performed for 20 singlet excited states for dipoles or quadrupoles, and 60 singlet excited states for 3-branched chromophores, if not otherwise noted. All theoretical TPA data presented in this review have been computed following the computation scheme described above.

To simulate the finite linewidths in the resonant spectra, a damping factor Γ is introduced in all calculations by adding an imaginary part ($i\Gamma$) to the transition frequencies Ω_ν in Eqs. (46) and (48)-(55). In many theoretical studies, this bandwidth is fixed to $\Gamma_{lor} = 0.1$ eV for bands of Lorentzian shape.[89,90,192] The choice of this specific value is somewhat arbitrary as it corresponds to the one observed experimentally for the series of chromophores for which it was originally used.[90] The error introduced by an inadequate bandwidth on the two-photon absorption cross section scales approximately as $1/\Gamma$ as can be simply inferred from expressions derived within effective two- (Eq. (42)) and three-state (Eq. (44)) models. For the different chromophores investigated in section 5 (except for chromophores of subsection 5.1.1), the experimental half-bandwidth at half-maximum amounts to $\Gamma_{gaus} = 0.25 \pm 0.02$ eV, with bands of roughly Gaussian shape. Thus the damping factor used in all calculations is fixed to $\Gamma_{lor} = 0.17$ eV,[267] except in subsection 5.1.1 where $\Gamma_{lor} = 0.1$ eV is used.

In some of our previous work,[102,120,192–195] an inconsistency occurred between conventions used in order to define the microscopic polarizability and the macroscopic susceptibility, so that the front factor in the expression used for σ_2 was not consistent with the corresponding hyperpolarizability magnitude. This led to an understimation of σ_2 by a factor

6. Despite the inconsistency, the agreement with experimental absolute cross section magnitudes was reasonable due to error cancellation from several factors, in particular linked to the underestimated band-width and the overestimated local-field corrections.[126] In this review the consistency of all expressions has been checked and results reported are corrected accordingly. With respect to previously published calculated results, other changes have been introduced in order to have more reliable expression for the local-field correction and optimize the comparison with experimental results. This is the reason why the damping factor has been chosen to be consistent with experimental spectra and the Lorentz local-field correction has been substituted by a more realistic evaluation of the local-field effect by the use of a reliable molecular volume and a realistic molecular cavity (see subsection 3.6.2). All these implementations allow to recover a good agreement with respect to experiments for absolute values of TPA cross sections,[126] as will be discussed in section 5.

Finally, to analyze the nature of the excited states involved in the photophysical processes we used natural transition orbital analysis of the excited states[268,269] based on the calculated transition density matrices. This analysis offers the most compact representation of a given transition density in terms of an expansion into single-particle transitions. We also note that wavefunctions for degenerate states in the octupolar specimens are defined by implementation of Davidson diagonalization in Gaussian[252] and differ from the "canonical" eigenfunctions $1/\sqrt{6}(2\phi_1-\phi_2-\phi_3)$ and $1/\sqrt{2}(\phi_2-\phi_3)$.[113] Figures visualizing molecular geometries and transition orbitals are obtained with XCrySDen.[270]

4 Experimental methodology

4.1 Techniques: concepts, assets and drawbacks

Although TPA was first predicted more than 70 years ago and first observed more than 40 years ago, reliable measurements of the absolute TPA cross sections are still challenging. Two methods are prominent for this kind of measurements: the Z-scan technique and the two-photon excited fluorescence (TPEF) technique.

The Z-scan method is based on the measurement of the nonlinear transmittance of a sample. In the so-called open-aperture condition, the transmittance is measured as a function of the intensity as the sample is scanned through the focal plane of a tightly

focused Gaussian laser beam (Z-position). In nonresonant conditions, a TPA process is characterized by a decrease in the transmittance which is used to extract the magnitude of the nonlinear process.[271]

The TPEF technique measures the fluorescence signal induced by two-photon absorption and derive the TPEF action cross section ($\sigma_2(\omega)\phi$) by comparison to a reference compound or to the one-photon excited fluorescence of the same compound (here ϕ is the fluorescence quantum yield). Assuming no stimulated emission and self-quenching, the number of fluorescence photons collected per unit time in TPEF experiment is proportional to the total number of photons absorbed per unit time and the fluorescence quantum efficiency of the molecule. If excited states are created through a two-photon excitation process, the number of fluorescence photons is then proportional to the two-photon absorption cross section of the molecule and to the square of the incident intensity.[62]

Both Z-scan and TPEF techniques have a number of advantages and drawbacks. In general, high laser intensities are required for TPA measurements, and this can bring some side-effects such as the concomitant occurrence of other nonlinear phenomena (Raman scattering, stimulated emission, etc.). This particularly affects the Z-scan technique, because laser intensities required by this method are usually higher than those used for the TPEF technique. High laser intensities are also responsible for strong background signals in the Z-scans, making the interpretation of data somewhat challenging. On the other side, the TPEF technique is free from these background problems. Moreover, due to the high sensitivity of modern detectors, possible side-effects can be strongly reduced using low excitation intensities. The Z-scan method being intrinsically less sensitive, also calls for highly concentrated samples (typically 10^{-2} M), i.e., 2-3 orders of magnitude higher compared to that for TPEF. High concentrations ask for enhanced solubility of the compound in the solvent of interest and can also lead to aggregation phenomena, hindering the analysis of true molecular properties. The main drawback of the TPEF technique is the requirement that chromophores must be at least slightly fluorescent in the solvent of interest. This narrows the choice of molecules (and solvents) that can be investigated using TPEF. Nevertheless, the sensitivity of this technique allows for quite low fluorescence quantum yields to enable analysis of molecules with moderate-high TPA cross sections (e.g., quantum yield amounting to a few percent for molecules with $\sigma_2 \geq \sim 100$ GM). It should however be stressed that for a correct estimate of the absolute

TPA cross section, a reliable ϕ value is also needed. This becomes challenging if ϕ is very low.

We should mention one of the main problems affecting measurements of the TPA cross section whatever the experimental technique: the duration of the excitation pulse. Indeed, if the pulse duration is long enough, molecules excited by a two-photon absorption process can further absorb a photon from the same pulse, giving rise to an excited-state absorption. Any excitation is followed by a rapid internal conversion towards the first excited state, so that a fluorescence photon is emitted from that state quite independently of which path the excitation followed before the radiative emission. The excited-state absorption, being a one photon process, is usually much more efficient than the TPA process. This phenomenon is indeed important in the nanosecond range for optical limiting applications aiming for a low-transmitting medium at high laser intensities. However, if not disentangled from the nonlinear effect, excited-state absorption leads to severe overestimation of the actual molecular TPA cross sections as clearly demonstrated in the literature.[272, 273] For example, artificially enhanced effective TPA cross sections were reported with nano- or picosecond excitations.[274] Consequently, a pulse duration in the nanosecond range (which is comparable to typical excited-state lifetimes) is too long to provide reliable measurements of TPA properties. It has been demonstrated and commonly accepted that only pulses in the femtosecond regime assure accurate σ_2 estimates.[62]

It is worthwhile to stress here that high TPA activity can be attained by having a one-photon resonance midway in energy between the ground and the TPA-state. However, in this case measurement of pure TPA cross sections is precluded by the onset of one-photon absorption. Nevetheless, the presence of a one-photon resonance in between the ground and the TPA-state, when not perfectly resonating with the incident photons, increases the TPA cross section thanks to pre-resonance effects (a one-photon denominator becomes almost resonant).[156] While this is an interesting way to obtain high cross sections, the one-photon resonance must fulfill strict requirements. In fact the detuning between the midway energy and the one-photon state must be larger than the bandwidth in order to prevent the one-photon absorption process to obscure TPA. So for small detuning energies the measurement is possible only if the one-photon absorption edge is sharp (as for example in the case of squaraines[240]). It should be also stressed that even if giant TPA responses can be obtained when a single-photon absorption process is concomitant

with the TPA process, several of the specific advantages offered by TPA, such as 3D resolution and linear transparency, are lost.

A significant difference between the two principal methods for measuring the TPA cross section is also apparent with respect to the possibility of estimating absolute cross sections through a comparison with reference compounds. The Z-scan technique does not need any reference, but laser mode and pulse parameters must be accurately measured, i.e., the spatial beam profile and the temporal pulsewidth. Any error in the measurement of these parameters lead to errors in the determination of the cross section.[275] Similarly, the TPEF can be reference-free, if the efficiency of one- and two-photon excitation fluorescence are compared, as first proposed by M. D. Galanin and Z. A. Chizhikova.[276] In this case several set-up parameters are also needed, including pulse duration and shape, average intensity of the excitation light and repetition rate of the laser pulses. On the other hand, the TPEF measurement of a given sample can be compared to the response of a reference compound whose TPA cross section is known, so that an absolute value can be derived through a relative measurement. This is actually the most widely adopted TPEF technique for estimating TPA cross sections. This calls for the need of reference compounds. Xu and Webb measured the absolute TPA cross section of several commercial molecular fluorophores in the spectral range between 690 and 1050 nm,[62] so that these compounds are commonly used as a reference for the TPA cross section measurements in the red-NIR spectral region using the TPEF technique. For the visible spectral range, from 540 to 700 nm, bis-MSB is usually used as a reference, thanks to the absolute measurement of its TPA cross section reported by Lytle.[277] We note that the cross section values reported there must be divided by a factor of 10 due to a typographical error, as stated in Ref.[278] Absolute TPA cross sections measured deeper in the NIR spectral region are scanty. We mention the results of Drobizhev et al. for a series of tetrapyrrolic compounds between 1100 and 1500 nm.[279]

Finally, we stress that complete information on the TPA efficiency can be obtained only by measuring an appropriate spectral range, which allows to explore the extent of the TPA band and to possibly access the TPA maximum. This is particularly important when comparing the absolute two-photon efficiency of different compounds. Measurements carried out at a single wavelength are of course not suitable for such comparisons because an apparent decrease or increase of TPA cross section could simply be due to a shift of

the TPA band. Comparisons between single-wavelength cross sections can however be of major interest in the case of specific applications where the TPA response at a precise wavelength is sought (such as those of nontunable lasers).

4.2 TPA cross section from TPEF measurements

Experimental TPA cross section we present in this review have been derived by the TPEF technique using reference materials. Here we outline the derivation of σ_2 from TPEF measurements and the pitfalls to avoid in order to retrieve reliable values. The fluorescence signal (F) induced by TP excitation is proportional to σ_2, fluorescence quantum yield (ϕ), concentration (c) of the active species, and the squared excitation power (P). When the TPEF of a sample of interest and a reference are measured as a function of the excitation power, the ratio of the slopes F/P^2 is related to the ratio of their TPEF action cross sections ($\sigma_2\phi$):

$$\frac{F}{P^2}\left(\frac{F}{P^2}\right)_R^{-1} = \frac{(\sigma_2\phi)}{(\sigma_2\phi)_R}\frac{K}{K_R}\frac{c}{c_R}\left[\frac{n}{n_R}\right], \tag{62}$$

where the index R labels quantities relevant to the reference. The refractive index correction in the square brackets accounts for focusing efficiency of the excitation light as a function of media refractivity. This correction must be inserted only when the excitation light is focused on a sample through an objective. The setup we use in our measurements calls for this correction, but this is not always the case. For example, the collimated beam setup does not require this correction. K is the detection efficiency, which is proportional to the correction factor (f), taking into account the wavelength dispersion of the response function, and to the inverse square of the refractive index of the medium. The TPEF action cross section of the molecule of interest is thus given by

$$\sigma_2\phi = \frac{f_R}{f}\frac{n^2}{n_R^2}\frac{c_R}{c}\frac{F}{P^2}\left(\frac{F}{P^2}\right)_R^{-1}\left[\frac{n_R}{n}\right](\sigma_2\phi)_R. \tag{63}$$

This expression allows evaluation of the TPEF action cross section of a sample using the TPEF action cross section of the reference compound, concentration of the solutions, correction factors, refractive indexes and, of course, the slopes F/P^2, which are the direct outputs of the measurement. This expression makes it clear that the two experimental slopes must be constant as a function of P, i.e., the fluorescence signals must have a quadratic dependence on the incident power. Indeed, the quadratic dependence of the

TPEF signal on the excitation intensity must always be checked in order to rule out the occurrence of photodegradation or saturation phenomena.

Fluorescence light emitted after two-photon excitation can be detected in different directions. In general, two possible collection geometries are used: the epifluorescence geometry (detection in the backward direction with respect to excitation) or the 90° geometry. In both cases, care has to be taken to avoid reabsorption of the emitted light by the sample itself. Indeed, long passage of the emitted light through the sample before detection raises possibility of reabsorption of the emitted photons, leading to errors in the determination of the fluorescence intensity. The amount of reabsorbed light increases with the path length inside the sample, with the concentration of the sample and for small Stokes-shifts. In order to minimize these effects (which could be quite strong for the typical 10^{-5} - 10^{-4} M concentration range), the path length of the emitted light inside the sample must be minimized. In the epifluorescence geometry, this means that the excitation beam must be focused inside the sample near the first cell window perpendicular to the incident direction. For the 90° geometry, the incident beam must be focused inside the sample near the cell window perpendicular to the detection direction. This also means that in the case of a collimated (not focused) incident beam, only the 90° geometry can be adopted (with beam passing near the cell window perpendicular to the detection direction), because TPEF is induced all along the beam path inside the sample.

From Eq. (63), the importance of accurate data on the TPEF action cross sections of reference compounds is apparent. Indeed errors in the reference values directly affect the evaluation of $\sigma_2\phi$ of the sample. The most widely used reference compound for measurements between 700 and 1000 nm is fluorescein in water at pH = 13, whose absolute TPEF action cross section has been measured by Xu and Webb.[62] We found that the use of this reference systematically leads to unreliable results in the short wavelength limit ($\leq$ 715 nm). This problem was recently confirmed by comparison of results obtained using both fluorescein and bis-MSB as references in the spectral region of overlap between the two absolute standards, i.e., around 700 nm.[126] The TPEF action cross section of fluorescein was then measured with respect to BDPAS (4,4'-bis-(diphenylamino)stilbene) in CH_2Cl_2, whose absolute TPA cross section has been determined by Drobizhev et al.[141] This measurement allowed to refine the TPEF cross section of fluorescein by adjusting two data points at 700 and 710 nm in the original set of the reference values.[126]

4.3 Experimental details

Optical absorption and emission spectroscopy. The experimental measurements of all photophysical properties have been performed with freshly-prepared solutions of the chromophores in air-equilibrated toluene at room temperature (298 K). UV/Vis absorption spectra were recorded on a Jasco V-570 spectrophotometer. Steady-state and time-resolved fluorescence measurements were performed on dilute solutions (ca. 10.6 M, optical density <0.1) contained in standard 1 cm quartz cuvettes using an Edinburgh Instruments (FLS920) spectrometer in photon-counting mode. Emission spectra were obtained, for each compound, under excitation at the wavelength of the absorption maximum. Fluorescence quantum yields were measured according to literature procedures using fluorescein in 0.1 N NaOH as a standard ($\phi = 0.90$).[280, 281]

Two-photon excitation. Unless explicitly stated otherwise, the TPA data presented in this review have been collected with the TPEF technique as described by Xu and Webb,[62] with the appropriate solvent-related refractive index corrections[282] and using excitation pulses in the femtosecond regime (subsection 4.2). TPEF cross sections of 10^{-4} M solutions in toluene were measured relative to known reference compounds (bis-MSB in cyclohexane for 560-700 nm,[277, 278] and fluorescein in 0.01M aqueous NaOH for 700-980 nm[62, 283]). The quadratic dependence of the fluorescence intensity on the excitation intensity was verified for each wavelength and each sample.

For further information on experimental measurements, we refer the reader to the cited original papers. We further underline some differences between TPA data that can be found here and original data in the cited papers. Here we uniformly adjusted all our experimental data to have the same refractive-index correction[282] (see Eq. (63)), and corrected all data points between 700 and 715 nm according to Ref.[126]

5 Applications to NLO chromophores

Given emerging multifarious applications exploiting the TPA phenomenon, in recent years a considerable effort has been devoted to design of a diverse variety of chromophores with large TPA cross sections. Depending on the applications sought, the two-photon chromophores have to satisfy additional requirements besides enhanced TPA. For instance, biological multiphotonic imaging calls for fluorophores combining a high fluorescence quan-

tum yield with a TPA cross section in the spectral range of interest (i.e., 700-1200 nm), several orders of magnitude larger than that of endogenous chromophores. As another example is optical power limitation. Here, high solubility and photostability, combined with superb linear transparency and multiphoton absorptivities (including excited-state absorption) are needed.

Typical NLO-phores are π-conjugated chromophores with strong electron-donor (D) and acceptor (A) groups. In fact, presence of the charge-transfer degrees of freedom is responsible for their intense linear and nonlinear absorption features, with effects depending on the strength and number of D and A groups. A careful choice of D/A groups, π-conjugated connectors and branching symmetry allows for a fine tuning of the optical properties. In this section we review experimental and theoretical results on examples of NLO-phores typical for TPA applications. In particular, we examine dipolar, quadrupolar, octupolar and more extended branched structures aiming to demonstrate consequences of specific structural features on the TPA properties. These chromophores of increasing size also offer a solid testing playground for different computational methods.

5.1 Quadrupolar chromophores

Quadrupolar compounds, which are symmetric conjugated molecules bearing two electron-releasing (D) or electron-withdrawing (A) end-groups, offer a rich platform for designing novel chromophores with large TPA responses. A large body of experimental data is available for many families of quadrupolar systems.[3, 33, 36, 57, 58, 63, 76, 78, 81, 85, 86, 89–107] Their nonlinear response is a non-trivial function of terminal donor and acceptor strength, π-conjugated bridge length and type, nature of the conjugated core, torsional disorder, symmetry and topology.[58] In this subsection we exemplify some of these relationships using two different families of quadrupoles to derive general trends in terms of TPA cross sections and peak positions.

5.1.1 Scaling with donor/acceptor strength and bridge length

We illustrate the dependencies of nonlinear properties on the donor/acceptor strength and on the bridge length using representative series of quadrupolar arylidenepiperidone chromophores q_2-q_{10} shown in Fig. 7. We refer interested readers to a detailed theoretical study of their linear and two-photon absorption spectra published previously.[194]

Optimized geometrical parameters (HF/6-31G level) are in a good agreement with the available experimental X-ray diffraction data.[284] The first 12 singlet excited states are taken into account in every calculation of resonant polarizabilities at 6-31G/B3LYP level of theory. Increase in the number of excited states in TD-DFT calculation gives a negligible impact on UV-visible absorption spectra and only a small effect (within 10%) on the magnitude of the TPA cross sections (see Sec. 3.5). Calculated linear absorption is dominated by two peaks. Similarly, theory predicts two strong TPA absorption bands corresponding to the excited states denoted as e and e'. Typically the lowest TPA peak e corresponds to the fourth (S_4) or third (S_3) excited state. The second TPA maximum e' is due to a high-energy excited state varying between S_{11} (small molecules) and S_7 (large cyclohexanones) positions in the TD-DFT calculations.

The trends in the third order polarizabilities related to TPA activities are summarized in Figs. 10 and 11. Energies of the excited state e and e' are both shifted to the red by $\sim$0.5 eV ($\sim$0.25 eV or 60-100nm peak shifts of the respective TPA maxima) with an increase of the terminal donor strength (Fig. 10a). The four-fold enhancement of the TPA cross section with substitution is even more dramatic (Fig. 10b). Changing the terminal group from methyl-amino to a somewhat stronger ethyl-amino donor substituent has a weak effect on the transition energies, but does increase substantially the NLO response cross sections. Figure 11a shows evolution of the TPA transition frequencies with the size of the π bridge. We observe nearly perfect linear scaling of state energies plotted as a function of the inverse number of π-electrons in the molecules. Such near-linear relationship is typical for a band-gap state in many conjugated polymers[285–288] and is not completely unexpected. A remarkable observation is that this scaling law holds for both e and e' peaks corresponding to the higher-lying electronic states in molecules with and without substituents, and the slope of all curves is about the same. Dependence of the polarizabilities amplitudes on the π bridge length shown in Fig. 11b is not so straightforward. Intensities of both e and e' peaks vary dramatically in unsubstituted molecules. Peak e' is particularly sensitive to the elongation of the π bridge. The situation is different for substituted chromophores. We observe a strong enhancement of e, whereas amplitude of e' is not affected by π bridge length.

5.1.2 Scaling with bridge and core type.

The three quadrupolar chromophores q_1, q_{11} and q_{12} investigated are shown in Fig. 7. Their ground-state optimized geometries are more or less planar depending on the nature of the core and the spacer. The biphenyl core (q_{11}, q_{12}) and the phenylene-vinylene spacer (q_1, q_{12}) introduce torsional degrees of freedom that lead to non-planar optimal ground-state geometries, with twist angles of about 43° and 39° for compounds q_{11} and q_{12}, respectively. All quadrupoles, nevertheless, retain nearly centrosymmetric structures. This is also visible from both ground and excited-state dipole moments calculated for the ground-state geometries: they are either vanishing (q_{11}) or rather small (q_1, q_{12}), when compared, for example, to corresponding transition dipole moments.[126] Transition orbitals associated with vertical transitions between the ground state and the lowest excited states are shown for compound q_1 in Fig. 12. Even if quadrupolar chromophores q_1, q_{11} and q_{12} do not have perfect inversion symmetry, their lowest excited state is predominantly one-photon allowed, while the second one is predominantly two-photon allowed (see Fig. 1). Charge redistribution upon photo-excitation from the periphery to the core is observed for both excited states, but this effect is more pronounced in the second excited state associated with strong TPA. The following excited states (third and fourth) are predominantly TPA and OPA allowed, respectively, and correspond to different charge redistribution upon excitation.

All chromophores show an intense absorption band in the near UV- violet region. Replacement of the phenylene-ethylene spacer (q_{11}) by the phenylene-vinylene unit (q_{12}) induces significant red shift of the absorption band. Additional replacement of the biphenyl core by a fluorene core (q_1) causes further red shift due to increased conjugation related to planarization of the core in the ground state.[125,126] The latter substitution allows for a significant increase of the molar extinction coefficients. However, a concomitant slight reduction of the bandwidth leads to a smaller increase of the transition dipole moment.

Experimental TPA spectra of quadrupolar compounds q_1, q_{11} and q_{12} are shown in Fig. 13, top panel. The first TPA maximum of each of the three chromophores is significantly blue shifted with respect to twice the one-photon absorption maximum, and shows up between 690 and 760 nm. This is directly related to the nearly centrosymmetric molecular symmetry of these quadrupoles that brings the first excited electronic state to be almost

TPA forbidden (Fig. 1). But the red shifts observed for the one-photon absorption spectra when going from chromophore q_{11} to q_{12} to q_1, are observed for the respective TPA peaks as well. All three chromophores show two main TPA bands, a first one in the NIR and a second in the green-yellow spectral region. Although these latter bands are closer to the one-photon resonances, it has been verified that these intense TPA band results from true TPA processes originating from the participation of higher-lying excited states.[126] In fact, calculated TPA spectra (Fig. 13, bottom panel) confirm these experimental findings. The TPA maximum in the NIR region can be assigned to the second excited state that undergoes a significant charge transfer from the periphery to the core upon excitation (see Fig. 12). Virtual states involved in the TPA process are mainly the first and the fourth excited state that bear significant oscillator strengths. Higher-lying excited states such as the third one (Fig. 12) are responsible for significant TPA activity in the visible red region. Large TPA responses at higher energy (i.e., in the green spectral region) are also predicted by calculations, and correspond to the excited states lying above the tenth excited state. However, an accurate description of these high-energy contributions would require incorporation of a very large number of excited states into calculations.

Quadrupole q_1, which showed the highest TPA maximum cross section in the red-NIR region, also show the largest TPA cross section in the yellow-green region. Interestingly, the relative ranking in TPA activity in the quadrupolar series q_1, q_{11} and q_{12} is the same in the yellow-green region and in the red-NIR region. However, the differences in TPA responses between chromophores q_1, q_{11} and q_{12} are even more pronounced for the higher-energy band. Indeed chromophore q_1 shows a TPA cross section at 560 nm, about 3 times larger that its maximal TPA cross section in the NIR. In comparison, chromophore q_{11} shows similar maximum TPA activity in the two distinct spectral regions (i.e., yellow-green and red-NIR), while chromophore q_{12} shows a TPA cross section at 560 nm which is about 1.5 times larger than its maximal TPA cross section in the NIR. Quadrupoles q_1 and q_{12} have the same number of π-electrons in the conjugated system as well as the same number of effective electrons according to Ref.[164] This indicates that the geometrical conformation (i.e., planar core), favoring increased conjugation, leads to dramatically higher TPA responses in the green-yellow region. Unsurprisingly, we observe that this increase accompanies an increase of the transition dipole and a decrease of the energy gap between the ground state and the first excited state, in agreement with increased

conjugation. In addition, the enhancement of the intrinsic TPA is much stronger when replacing the vinyl linker by an ethynylene linker than by a biphenyl core, indicating that the lowering of the energy gap is correlated in that case with the intrinsic TPA magnitude. Finally, quadrupole q_1 shows the highest TPA cross sections over the entire investigated spectral range. It is particularly interesting to observe that quadrupole q_1 has also been shown to lead to the strongest optical limiting efficiency in the visible region.[57] This optical limiting efficiency in the green region might indeed be related to enhanced two-photon absorption.

5.1.3 Optimization of quadrupolar chromophores

In summary, the main structural characteristics of linear (quasi-one-dimensional) organic conjugated dyes that significantly affect TPA cross sections and peak positions are the strengths of the donor and acceptor substituents, as well as both the length and the type of the conjugated core. All these features define the degree of the charge transfer in the molecule upon optical excitation. For the series of quadrupolar molecules where TPA spectra are characterized by two major bands at high- and low-energy regions, the intensity of the low-energy peak is extremely sensitive to the variations in the donor and acceptor strengths, and their spatial separation. In contrast, the TPA absorbance at higher frequencies is only slightly affected by the change of substituents, but it can be effectively enhanced by the elongation of the π-bridge. The absorption peak positions can be easily tuned by either extension of the conjugated core or substitution with polar termini. We observe a linear scaling of the absorption energies with the reciprocal number of π-electrons in the conjugated bridge. The type of core and spacer controls the degree of conjugation mainly through the torsional disorder in the system. A more planar molecular geometry in the ground state leads to red-shifts in the absorption frequencies, and an increase in the transition dipole moments, which leads to larger absorption amplitudes. These trends are general for most of the quadrupolar molecules with nearly centrosymmetric structures. Such linear structures create a rich variety of choices for subsequent synthetic manipulations of TPA response by branching dipolar or quadrupolar chains into dendrimeric-like structures. This approach is covered in the next subsection.

5.2 Branching effect

Among the different strategies implemented to obtain improved TPA responses, the branching strategy has received increasing attention over the recent years.[97,102,112,114–116,118–121,123–126,140–14
In multibranched systems, various behaviors of the TPA cross section have been reported: cooperative enhancement,[97,102,109,114,120,121,140–142] additive behavior,[102,112,123,126,143] or weakening.[112] Such features are related to the nature and the strength of the interbranch coupling that will be discussed in this subsection. The characteristics of the coupling are also responsible for the nature of the ground state that can be either localized[123,289–291] or delocalized.[120,121,289,290] However, in all branched fluorophores, fluorescence stems from a single branch.[120,121,123,142,289,290,292–296] This phenomenon of localization of excitation seems to be a general characteristic of branched systems.
In this subsection we review results on the effects of gathering either dipolar or quadrupolar chromophores via a common core. In particular, we focus on three-branch systems obtained by the branching of dipolar and quadrupolar entities in the weak-medium interaction limit. To be able to consistently compare the responses of the three-branch molecules with those of their dipolar or quadrupolar counterparts, we rescaled the TPA response for the number of branches. This analysis yields information on the intrinsic charge-symmetry and branching effect, allowing to distinguish an additive behavior from the cooperative effects.

5.2.1 Branching of dipoles: Triphenylamine derivatives

Here we focus on a dipolar unit composed from an asymmetrically substituted stilbene moiety bearing the electron-withdrawing end-group SO_2CF_3. The dipolar chromophore d_1 and the respective octupolar structure obtained by grafting three dipolar branches to a central triphenylamine core (compound $\mathsf{3d}_1$) are shown in Fig. 6 and has been studied in detail in Refs.[120,121]
Calculated optimal geometries (HF/6-31G) indicate that the triphenylamine moiety adopts a propeller-shape structure, the phenyl rings being twisted by about 45° with respect to the trigonal planar nitrogen. The two phenyl rings of the conjugated stilbenyl branches are substantially twisted ($\sim 40°$). Overall, branches in the multipolar system have ground-state geometries similar to the geometry of the parent dipolar molecule. Ground-state optimized geometries are in good agreement with crystallographic data.[297]

The chromophores show an intense absorption band in the near UV-blue spectral region.[121] Gathering three dipolar $\mathsf{d_1}$ units via a common electron-donating nitrogen within a trigonal branched molecule (three-branched compound $\mathsf{3d_1}$) leads to a slight red-shift of the absorption band (Table 2). This is indicative of sizeable coupling between the dipolar branches that can be tentatively analyzed within the excitonic model (Fig. 1). The nature of the excited states involved in the photophysical processes can be investigated using the natural transition orbitals[268] shown in Fig. 14. The energetic scheme predicted by the excitonic model is adhered, with two lower-energy degenerate excited states and a higher-energy excited state. The first two excited states are one-photon allowed and correspond to electron transfer from the highest occupied transition orbital (HOTO) to the lowest unoccupied transition orbitals (LUTO and LUTO+1). In contrast, the third excited state has vanishing oscillator strength. The experimental energy difference between the first two degenerate excited states of $\mathsf{3d_1}$ and the first excited state of $\mathsf{d_1}$ gives an excitonic coupling constant V of ~ 0.10 eV for the octupolar chromophore. These values are in good agreement with results deduced from TD-B3LYP calculations (Table 2). The position of the third excited state of chromophore $\mathsf{3d_1}$, which is one-photon forbidden but two-photon allowed, is, thus, predicted within the Frenkel excitonic model to appear 0.30 eV above the degenerate excited states (at ~ 780 nm for two-photon absorption).

Experimental TPA spectra normalized for the number of branches (N) of the investigated chromophores are shown in Fig. 15 (top panel). These spectra exhibit a first maximum close to twice the one-photon maximum absorption wavelength, indicating that the lowest energy excited state is both one-photon and two-photon allowed. The first TPA maximum of the three-branched chromophore is red-shifted with respect to that of the dipolar chromophore, as a result of the red-shift of the one-photon absorption band originating from interaction between the branches. The corresponding normalized TPA amplitude is comparable to that of its dipolar counterpart $\mathsf{d_1}$ showing a nearly additive behavior at this wavelength. On the blue side of the spectrum, the TPA cross section of $\mathsf{3d_1}$ displays a second maximum about four times larger than that of compound $\mathsf{d_1}$, corresponding to a large enhancement of the TPA response in that spectral region. Interestingly, this second TPA maximum is blue shifted with respect to the position predicted within the Frenkel exciton model as it shows up at about 740 nm.

Fig. 15 (bottom panel) shows calculated TPA spectra. The overall agreement between

experimental and calculated spectra is good for chromophore $\mathsf{3d_1}$, while the TPA cross section of $\mathsf{d_1}$ is strongly overestimated. As discussed in subsection 3.6, this is probably due to an overestimation of the charge-transfer character for the dipolar compound. Nevertheless, calculations confirm and illustrate the main trends observed in experiments. In particular, the splitting of the first three excited states of $\mathsf{3d_1}$ with respect to the position of the first excited state of $\mathsf{d_1}$ does not obey the excitonic model prediction, $(-V,+2V)$. In addition, calculations also indicate sizeable enhancement of the TPA cross section (per branch) of $\mathsf{3d_1}$ with respect to $\mathsf{d_1}$. This enhancement, even if undestimated, is better reproduced compared to the Frenkel exciton approach, as discussed in Ref.[120] This means that coherent interactions between branches and higher-lying excited states (beyond the Frenkel exciton model)[298–301] are important in order to interpret the TPA enhancement in the branched structure.[113] Interbranch coupling not only induces shifts of the one- and two-photon absorption bands, but also results in strong TPA enhancement in the whole relevant spectral region. Indeed, the coupling of dipolar chromophores within the branched structure is responsible for a mixing of single-branch excited states, with important consequences on the nature of the excited states themselves.

5.2.2 Branching of dipoles: Triphenylbenzene derivatives

In systems obtained by branching two or more arms to a central core, photophysical and TPA properties not only depend on the nature of the branches, but also on the nature of the coupling core moiety. In that perspective, results reported in the previous subsection are compared to those obtained for a series of branched systems where dipolar units are connected via a common triphenylbenzene (**TPB**) core.[123] The ability of the **TPB** core to promote electronic coupling between branches and to possibly lead to enhanced TPA is investigated by comparing the photophysical and TPA properties of the three-branched system (octupolar compounds $\mathsf{3d_2}$, Fig. 6) with that of its dipolar counterpart where the **TPB** core has been replaced by a biphenyl (**BP**) moiety (compound $\mathsf{d_2}$, Fig. 6).

The octupolar three-branched molecules adopt a propeller-shape conformation[123] where the three phenyl substituents on the central phenyl unit are twisted by about 45°. Interestingly, the ground-state optimized geometry of $\mathsf{d_2}$ can be superposed to that of one branch of $\mathsf{3d_2}$ showing identical geometrical parameters except for a small dissymmetry at the terminal phenyl ring of **BP**. This suggests that the three branches behave as nearly

independent sub-chromophores. The nitrogen atom is slightly out of plane and the twist angle between the two phenyl rings of **BP** is about 45°, while the angle between the two phenyl rings on each side of the double bond is closer to 40°. The bond-length alternation (BLA) parameter, defined as the difference between single and double bonds in the vinyl bridge, is 0.15 Å for all chromophores in the ground state. This parameter reflects the low degree of charge transfer in the ground state. This is confirmed by the large value of the ^{1}H-^{1}H coupling constant (16.4 and 16.3 Hz) in the vinylic bond of compound $\mathsf{d_2}$ and $\mathsf{3d_2}$ in solution, indicative of a full double bond character.

The absorption spectra of dipolar and octupolar compounds show an intense absorption band in the near-UV region.[123] The absorption spectrum of $\mathsf{3d_2}$ is slightly red-shifted as compared to that of the dipolar analogue. The slight red-shift (about 0.04-0.05 eV in toluene) indicates that only weak coupling between the branches occurs in **TBP** derivatives. This suggests that the branches behave as nearly independent subchromophores in the ground state, as suggested by the calculated ground-state geometries. Such conclusion was also derived from recent Hyper-Raman studies conducted on other octupolar derivatives built from a **TPB** core.[291] The quasi-proportionality of the molar extinction coefficient with respect to the number of branches further corroborates this analysis.[123] Experimental and calculated TPA cross sections normalized for the number of branches (N) are shown in Fig. 16. These spectra are in a good agreement for absolute and relative intensities, although transition energies are overestimated. This differs much from what has been reported in the triphenylamine case (subsection 5.2.1). Interestingly, for the **TPB** series, the *tol-tol* calculation better reproduces transition energies, but the TPA cross section of $\mathsf{3d_2}$ is overestimated (not shown). The reason for the inconsistent behavior of the two series lies in a markedly different charge-transfer character of the two dipolar branches: $\mathsf{d_1}$ is much more polar ($\mu_{gg} = 11$D) compared to $\mathsf{d_2}$ ($\mu_{gg} = 3$D).

Figure 16 clearly shows that the TPA response is nearly additive with respect to the number of branches. This is a further confirmation of the almost independency of each branch in octupolar compound, corresponding to weak (almost vanishing) electronic couplings. Moreover, TPA spectra are almost superimposable to corresponding rescaled OPA spectra. While this is always the case for dipolar chromophores, where the same excited state is one- and two-photon allowed, the result is more interesting for the octupolar chromophore $\mathsf{3d_2}$. Within the Frenkel excitonic model the first two degenerate excited

states of three-branched molecules are one-photon allowed, while the third excited state is mainly two-photon allowed (see Fig. 1). These states are separated by an energy $3V$, where V is the excitonic coupling between the branches. While a sizeable splitting was observed for compound $\mathsf{3d_1}$ and other branched systems based on a triphenylamine core[113,120] as well as for several other octupolar molecules,[113] this is not the case for the octupolar compound $\mathsf{3d_2}$. Indeed here, the TPA spectra correspond to the rescaled OPA spectra, even for the three-branched compound. This is a further confirmation that the coupling between branches in the ground state is almost vanishing.

Results obtained for the TPA amplitudes are also markedly different from those obtained for structures based on a triphenylamine central core. For the latter, a strong non-additivity is observed in the octupolar branched structure compared to the dipolar branch. So, while triphenylamine is able to promote a sizeable electronic coupling between branches, **TPB** is not able to do so. While in triphenylamine-based branched structures the coupling leads to mixing of single-branch excited states, in **TPB**-based structures each branch is almost unperturbed by other branches, so that their properties are nearly additive. The different behavior of the triphenylamine-based and **TPB**-based series provides important clues on the nature of the coupling between branches. If coupling was only due to electrostatic interactions between the transition dipole moments of the branches (Frenkel-exciton model),[222] the strength of the coupling should have been comparable in the two series. In fact, transition dipole moments are comparable and even somewhat larger for $\mathsf{d_2}$ than for $\mathsf{d_1}$, as their experimental (calculated within *vac-vac*) values amount, respectively, to 9.5D (10.1D) and 9.0 D (9.6 D).[302] However, this is not the case, indicating that other sources of coupling are needed to explain the behavior of the triphenylamine-based series. Indeed, the need of interactions beyond the Frenkel-exciton model was pointed out for the triphenylamine series in subsection 5.2.1 in order to explain the strong enhancement of TPA cross sections as a consequence of branching. As a matter of fact, high-level quantum mechanical calculations based on the TD-DFT formalism described in subsection 3.4 allow to reproduce this enhancement better than a simple excitonic model. This observation suggests that not only dipolar interactions but also coherent interactions mediated by substantial wavefunction overlaps,[299,301] are important in defining the total coupling values and, hence, the spectroscopic properties of branched structures.[120] While triphenylamine center is able to promote this kind of

coupling, the **TPB** core is not able to do so. We stress here that the absence of coherent coupling in the case of the central **TPB** core with respect to the triphenylamine core can not be ascribed to the twist of the benzene rings, since the twist is comparable to that in the triphenylamine series. This effect in the triaryl core is likely due to the meta positions of the three benzene rings, which breaks the conjugation.[163,303–305]

Finally, the solvatochromic behavior of branched systems built from the dipolar arms has been found to be correlated to the TPA amplitudes[123] (not discussed in this review for the sake of conciseness). This is related to the intramolecular charge transfer character of the transitions and suggests that the solvatochromic behavior may provide a qualitative estimate of the TPA performance of such chromophores.

5.2.3 Branching of quadrupoles: a triphenylamine derivative

This subsection aims to explore experimentally and theoretically how TPA properties are modified by changing the nature of the branches. In that perspective we consider a three-branch system built from a triphenylamine core gathering three identical quadrupolar arms instead of dipolar ones as studied in subsection 5.2.1. The quadrupolar arm q_1 and its three-branch analogue $\mathsf{3q}_1$ are shown in Fig. 7. These molecules have been studied in detail in Ref.[126]

The ground-state optimal geometry of chromophore $\mathsf{3q}_1$ shows geometrical parameters for each branch quasi identical to those obtained for chromophore q_1.[126] The triphenylamine central core leads to a propeller like molecular shape where each branch is twisted by 45° with respect to the plane defined by the nitrogen atoms and the three bonded carbon atoms. An almost identical situation has been already observed for $\mathsf{3d}_1$.

Molar extinction coefficient of the branched molecule $\mathsf{3q}_1$ is approximately three times larger than that of compound q_1, which, given the comparable bandwidths, suggests a nearly additive behavior,[126] as confirmed by the oscillator strengths. The absorption band of the three-branched chromophore $\mathsf{3q}_1$ is red-shifted with respect to that of the corresponding quadrupolar branch q_1. Experimentally, a 0.09 eV decrease of the transition energy is observed for the OPA band, while the calculated value is about three times larger. This discrepancy is related to the well-known problem of the wrong asymptotic behavior of the exchange-correlation potential persistent even in hybrid kernels.[174,306] It leads to substantial errors for excited states of molecules with extended π-systems[256,265,307] as well

as for charge transfer states.[176,258,259,265] This is especially evident for large molecules such as compound $\mathsf{3q_1}$. Moreover, it does not correspond to a constant red shift of all excited states but depends on the characteristics of each excited state such as delocalization and charge-transfer features. Keeping this in mind, we use theoretical results obtained for compound $\mathsf{3q_1}$ for qualitative rationalization of observed photophysical trends.

At a first approximation, molecule $\mathsf{3q_1}$ can be thought as an assembly of three quadrupolar monomers $\mathsf{q_1}$ that share a common nitrogen so that the C_3 symmetry can be assumed. The Frenkel exciton model has been successfully used to treat the qualitative (but not always quantitative) behavior of three-branched systems built from the dipolar moieties as shown in subsection 5.2.2 and 5.2.1 and Ref.[120] Let us first investigate the validity of this simple excitonic scheme for the three-branch compound $\mathsf{3q_1}$. Within this scheme (subsection 3.2 and Fig. 1), the first excited state $|1_q\rangle$ of the quadrupolar unit splits into three excited states according to the following scheme: a two-fold degenerate first excited state which is both OPA and TPA allowed is red shifted by -V and a third, TPA-allowed excited state is blue shifted by $+2V$. The same scheme can be applied to the monomer's second excited state $|2_q\rangle$ with a coupling constant V' instead of V (Fig. 1). Examination of the transition orbitals and respective excitation energies of compounds $\mathsf{q_1}$ (Fig. 12) and $\mathsf{3q_1}$ (Fig. 17) reveals a much more complex picture. In a very crude approximation, the three $|1_q\rangle$ states split into ($|1_{3q}\rangle$, $|2_{3q}\rangle$) and $|6_{3q}\rangle$ and the $|2_q\rangle$ states produce into ($|8_{3q}\rangle$, $|9_{3q}\rangle$) and $|12_{3q}\rangle$ in the branched system. Corresponding couplings are estimated to be 0.12 eV and 0.07 eV respectively, but these splittings do not obey the (-V,+$2V$) rule expected with respect to the transition energies of $|1_q\rangle$ or $|2_q\rangle$. Moreover, intermediate excited states are found. In fact, within this simple excitonic picture, state $|12_{3q}\rangle$ should be the sixth excited state. A closer look to the transition orbitals in Fig. 17 clearly shows that the triphenylamine linker breaks the quadrupolar symmetry of each branch. This is especially visible in the plotted hole orbitals, which are either located on one side (i.e., close to the molecule center, see for example state $|1_{3q}\rangle$) or the other side (i.e., on the molecule periphery, see for example state $|3_{3q}\rangle$) of each branch (Fig. 17). The dissymmetry introduced by the branching of three quadrupolar monomers via a shared donating end-group, clearly invalidates the use of the excitonic model for this type of trimer systems because the quadrupolar branches loose their original symmetry in such molecular systems. This effect is not observed when dipolar branches are assembled

in the same way (subsection 5.2.1) due to the absence of an intrinsic symmetry of the monomers.

Experimental and calculated TPA spectra of compounds $\mathsf{3q_1}$ are shown in Fig. 18 and compared to those of their quadrupolar counterparts $\mathsf{q_1}$. As previously, TPA cross sections have been normalized for the number of branches. Chromophore $\mathsf{3q_1}$ reveals a broad band in the NIR region with a TPA maximum significantly blue shifted with respect to twice the one-photon absorption maximum.[126] Surprisingly, one observes a noteworthy correspondence between some states of quadrupole $\mathsf{q_1}$ and branched system $\mathsf{3q_1}$. The OPA state $|1_q\rangle$ and the TPA state $|3_{3q}\rangle$ as well as the TPA states $|2_q\rangle$ and $|12_{3q}\rangle$ have almost the same transition energies (see Figs. 12 and 17). In addition, transition orbitals on each of the three branches associated with the state $|12_{3q}\rangle$ are very similar to that of state $|2_q\rangle$ and show almost no dissymmetry with respect to the center of each branch (see Figs. 12 and 17). Interestingly, chromophore $\mathsf{3q_1}$ shows a TPA maximum in the NIR region located at almost the same position that the lowest-energy TPA maximum of quadrupole $\mathsf{3q_1}$ (Fig. 18). At the same time, a shoulder is observed in the experimental TPA spectrum of the branched compound $\mathsf{3q_1}$ around 800nm, i.e., close to twice the OPA maximum of quadrupolar chromophore $\mathsf{q_1}$. This corresponds to the lowest-energy one-photon allowed but two-photon forbidden excited state in quadrupole $\mathsf{q_1}$, $|1_q\rangle$. This suggests that the breaking of central symmetry of the quadrupolar branch when incorporated in the three-branched geometry, leads to additional two-photon allowed excited states. These correlations are expected within the excitonic model for a small coupling but may or may not be fortuitous. Given the size of the branched chromophore and the huge number of excited states involved, it is difficult to conclude unambiguously. In fact, the poor description of the long-range Coulomb electron-electron interactions already mentioned above leads to significant red shifts of the calculated transition energies, at least for the first two excited states. Moreover, these shifts vary for different excited states. In addition, the finite number of excited states (60) included in the calculation of the optical properties of chromophore $\mathsf{3q_1}$ provides converged TPA amplitudes only for the low-energy part of the spectrum, while the higher-energy peaks are not converged. This might explain the discrepancy between calculated and experimental relative amplitudes for such TPA peaks. It is, however, insightful to examine the contribution of the different excited states to the successive TPA peaks. The calculated TPA maximum near

800 nm lies in a region where all states from $|3_{3q}\rangle$ up to $|7_{3q}\rangle$ can contribute. The largest transition dipole moments with the two degenerate OPA states is calculated for state $|6_{3q}\rangle$. But it is clear that the broad band results from contributions of several excited states. States $|4_{3q}\rangle$ and $|5_{3q}\rangle$ most probably contribute as virtual states as well as states $|1_{3q}\rangle$ and $|2_{3q}\rangle$. Actually, the transition dipole moments between ground state and states $|4_{3q}\rangle$ and $|5_{3q}\rangle$, though smaller than those between ground state and states $|1_{3q}\rangle$ and $|2_{3q}\rangle$, remain substantial.[126] The two next local maxima visible at lower wavelengths can be attributed to states $|12_{3q}\rangle$ and $|15_{3q}\rangle$, respectively.

Finally, comparison of TPA cross sections normalized with respect to the number of branches (Fig. 18) shows a nearly additive behavior at the first TPA maximum and sizeable enhancements on both NIR and visible sides. This enhancement is most probably related to symmetry-breaking considerations. The almost TPA forbidden states of the quadrupolar branches mix into different excited states of dipolar character on the monomer, among which some show significant TPA activity. Even if this enhancement is not as large as that found for dipolar chromophores gathered via the same triphenylamine core (subsection 5.2.1 and Ref.[121]), the branching strategy proves to be efficient. This is especially visible in the green-yellow part of the visible spectrum due to strong TPA activity of even higher-lying excited states. As for quadrupoles, we have carefully checked that this corresponds to a true TPA process. Even though calculations are not able to provide converged TPA amplitudes in this region because of the limited number of excited states, significant TPA is clearly observed near 560 nm in the calculated spectrum. This peak arises from high-lying excited states and confirms experimental observations.

5.2.4 Comparison between branched systems

Figure 19 shows a comparison between TPA and rescaled OPA spectra for branched systems and their corresponding monomeric arms investigated in this subsection. For a qualitative understanding, this plot can be rationalized using the excitonic scheme of Fig. 1 as a guide. For the dipolar chromophores (d_1 and d_2) the only band in the visible region is both one- and two-photon allowed, so that a good correspondance is observed between OPA and TPA spectra. For octupolar chromophores obtained by grafting dipolar units, the excitonic scheme predicts that the one-photon visible band (red-shifted with respect to the monomeric unit) is also partially two-photon allowed, but the dominant

TPA contribution is due to the higher-energy excited state. This is particularly apparent for chromophore $\mathsf{3d_1}$, allowing to estimate a sizeable excitonic coupling, as discussed in subsection 5.2.1. Chromophore $\mathsf{3d_2}$ displays remarkably different behavior. In this case TPA and OPA spectra are almost superimposable, suggesting very small excitonic splitting between the two lower-energy degenerate excited states ($|1_{3d}\rangle$ and $|2_{3d}\rangle$) and the higher-energy excited state ($|3_{3d}\rangle$).

Quadrupolar compounds have often centrosymmetric or nearly centrosymmetric molecular symmetry. The presence of an inversion center imposes that the lower-energy state $|1_q\rangle$ (antisymmetric) is OPA active, while the higher-energy state $|2_q\rangle$ is allowed by TPA.[308] This case is well exemplified by OPA and TPA spectra of $\mathsf{q_1}$ in Fig. 19, where a sizeable shift is observed between OPA and TPA spectra. When branching quadrupolar entities, as in chromophore $\mathsf{3q_1}$, the excitonic scheme predicts a splitting of the states as reported in Fig. 1 (lower part). In particular, the OPA states of the single branches are expected to interact as in the dipolar case (note that excitonic interaction is proportional to the squared transition dipole moment), while the TPA states are expected to have vanishing interaction if only dipolar interactions are considered. If higher-order interactions are accounted for, a finite coupling is expected also for these states (V' in Fig. 1). Fig. 19 suggests that this simple scheme is qualitatively correct, subject to a sizeable red-shift of the OPA band of $\mathsf{3q_1}$ with respect to $\mathsf{q_1}$ (finite V coupling) and an almost coincidence of corresponding TPA spectra (negligible V' coupling). But, as discussed in subsection 5.2.3, a careful analysis of relevant transition orbtitals shows that the nature of excited states contributing to OPA and/or TPA responses is considerably modified by the triphenylamine branching center compared to the parent monomeric quadrupole. New excited states are found in the branched structure with asymmetric charge transfer, which effectively renders unusable the Frenkel exciton model. In summary, the Frenkel excitonic model allows for a qualitative description of such branched systems but not for a quantitative agreement nor for a good understanding of the real nature of participating excited states.

Comparison of the different branched systems reveals a number of remarkable trends concerning branching effects on the TPA activity. While branched dipolar compounds gathered through a triphenylamine core show important TPA enhancement, those built from the **TPB** core as well as branched quadrupoles based on a triphenylamine core

show nearly additive behavior. In fact, branched dipolar systems based on the **TPB** core, have three phenyl rings attached to the meta positions of the central benzene. This is well known to lead to vanishing conjugation and ultimately inhibits interbranch cross-talk. Subsequently, the TPA response of this type of branched systems is additive, and is only modified by inter-branch electrostatic interactions. On the other hand, in octupolar structures built from triphenylamine, the central connector is shared by three branches and feels the electron-attracting (electron-withdrawing) character of the end groups of all three branches instead of only one in the monomeric counterpart. This is comparable to a monomeric unit bearing a stronger acceptor (donor) end group that is well known to induce a larger polarization. Consequently, this increases the 'absolute' TPA magnitude in combination with some inter-branch conjugation and wavefunction overlap. In contrast to the dipolar cases, the central triphenylamine of three-branched quadrupoles introduces a noticeable dissymmetry to the quadrupolar branches. Such dissymmetry reduces the effective TPA response compared to ideal quadrupoles, while the central core still promotes the cross-branch talk. Thus, both effects cancel each other in the case of triphenylamine branched quadrupoles, leading to weak TPA enhancements, as evidenced in the case of chromophore $\mathsf{3q_1}$. Nevertheless, the nature of the excited states is considerably modified compared to parent monomeric quadrupole and leads to significant TPA broadening.

In general, the branching strategy allows for flexible modifications of the TPA response. Over the entire spectral region investigated, the TPA cross sections of n-branched compounds discussed here are higher than n times their monomeric analogues in the cases of sizeable electronic coupling. The TPA modification induced by the branching is obviously strongly dependent on both the nature and the symmetry (dipolar versus quadrupolar) of the monomers as well as the nature of the central core. These characteristics determine the nature and the strength of the interbranch coupling that can be purely electrostatic or contain other contributions such as coherent interactions.[299,300] In addition, TPA broadening can occur from the inherent symmetry breaking of the sub-chromophores and from a larger number of close excited states which give rise to overlap of TPA bands originating from different states.

6 Conclusions and future perspectives

In the quest of superior chromophores for improved and novel technological capabilities based on TPA, the key performance factor, mostly used in the literature, is the TPA amplitude. It is generally quantified by means of the so-called two-photon absorption cross section (usually symbolized σ_2). It should be stressed, however, that comparisons of data reported in the literature, is non-trivial given the numerous conventions and systems of physical units that can be used. In addition, several sources of errors can yield improper experimental or theoretical evaluations of σ_2. This review attempts to clarify these issues. Well understood photophysics of TPA process is a key issue for the rational design of optimized two-photon chromophores aimed for specific applications relying on TPA. Using different series of two-photon chromophores as test molecules, we illustrate how various theoretical approaches combined with experimental data can contribute to the understanding of structure-property relationships that might ultimately guide organic synthesis. In particular, we show that TD-DFT based methodologies can be a very valuable tool, but should be used with some care, because available models of density functionals have pitfalls and limitations. Particular concerns are problems related to the correct description of electronic states having double excitations, charge-transfer states or excited states of molecules with extended π-systems.

Recent progresses toward a multilevel design strategy for optimized organic TPA chromophores have also been highlighted. The branching strategy successfully proved itself as a valuable tool for modification of the TPA responses. These modifications are, however, strongly dependant on both the nature and the symmetry of the molecular building blocks. Their detailed understanding opens new avenues to the next level of molecular engineering for TPA applications. As an example, assembling octupolar or mixed dipolar and quadrupolar based modules into branched structures via joints, allows for coherent coupling and should lead to complex dendritic structures that would benefit both from TPA broadening and TPA enhancement. Exploiting self-organization is an alternative route towards synergic TPA architectures thanks to implicit degree of ordering and inherent modularity.

Last but not least, TPA offers a rich framework for novel multifunctional technologies that are only currently emerging. This is particularly true for applications based on organic

TPA chromophores thanks to the synthetic versatility and modularity offered by organic chemistry. This opens the way toward synthetically challenging strategies for the creation of highly robust smart materials and devices based on either all-organic nanoarchitectures[51,52,309] (in particular for bioimaging or biomedical applications by combination of two-photon absorbers with bioactive molecules such as drugs, proteins, recognition moieties, etc.) or hybrid materials[19,65,310–312] such as metal/organic, semiconductor/metallic, nanoassemblies or functionalized surfaces.

References

[1] M. Göppert-Mayer, *Ann. Phys. Lpz.* **1931**, *9*, 273.

[2] W. Kaiser, C. G. B. Garret, *Phys. Rev. Lett.* **1961**, *7*, 229.

[3] M. Blanchard-Desce, *C. R. Physique* **2002**, *3*, 439.

[4] S. R. Marder, *Chem. Commun.* **2006**, 131.

[5] B. Strehmel, V. Strehmel, *Adv. Photochem.* **2007**, *29*, 111.

[6] P. Cronstrand, Y. Luo, H. Agren, *Adv. Quantum Chem.* **2005**, *50*, 1.

[7] J. D. Bhawalkar, G. S. He, P. N. Prasad, *Rep. Prog. Phys.* **1996**, *59*, 1041.

[8] T. C. Lin, S. J. Chung, K. S. Kim, X. P. Wang, G. S. He, J. Swiatkiewicz, H. E. Pudavar, P. N. Prasad, in *Polymers for Photonics Appl. II*, Springer-Verlag, Berlin, **2003**, 157–193.

[9] F. Helmchen, W. Denk, *Nat. Methods* **2005**, *2*, 932.

[10] R. R. Birge, *Acc. Chem. Res.* **1986**, *19*, 138.

[11] S. Shima, R. Ilagan, N. Gillespie, B. Sommer, R. Hiller, F. Sharples, H. Frank, R. R. Birge, *J. Phys. Chem. A* **2003**, *107*, 8052.

[12] M. P. Joshi, H. E. Pudavar, J. Swiatkiewicz, P. N. Prasad, B. A. Reianhardt, *Appl. Phys. Lett.* **1999**, *74*, 170.

[13] S. Maruo, O. Nakamura, S. Kawata, *Opt. Lett.* **1997**, *22*, 132.

[14] B. H. Cumpston, S. P. Ananthavel, S. Barlow, D. L. Dyer, J. E. Ehrlich, L. L. Erskine, A. A. Heikal, S. M. Kuebler, I. Y. S. Lee, D. McCord-Maughon, J. Q. Qin, H. Rockel, M. Rumi, X. L. Wu, S. R. Marder, J. W. Perry, *Nature* **1999**, *398*, 51.

[15] S. Kawata, H.-B. Sun, T. Tanaka, K. Takada, *Nature* **2001**, *412*, 697.

[16] W. Zhou, S. M. Kuebler, K. L. Braun, T. Yu, J. K. Cammack, C. K. Ober, J. W. Perry, S. R. Marder, *Science* **2002**, *296*, 1106.

[17] W. Denk, J. H. Strickler, W. W. Webb, *Science* **1990**, *248*, 73.

[18] C. Xu, W. Zipfel, J. B. Shear, R. M. Williams, W. W. Webb, *Proc. Natl. Acad. Sci.* **1996**, *93*, 10763.

[19] D. R. Larson, W. R. Zipfel, R. M. Williams, S. W. Clark, M. P. Bruchez, F. W. Wise, W. W. Webb, *Science* **2003**, *300*, 1434.

[20] W. Denk, P. B. Detwiler, *Proc. Natl. Acad. Sci.* **1999**, *96*, 7035.

[21] G. C. Cianci, J. R. Wu, K. M. Berland, *Microsc. Res. Tech.* **2004**, *64*, 135.

[22] G. McConnell, E. Gu, C. Griffin, C. W. Jeon, H. W. Choi, A. M. Gurney, J. M. Girkin, M. D. Dawson, *Design and Nature* **2004**, *6*, 341.

[23] G. M. Palmer, P. J. Keely, T. M. Breslin, N. Ramanujam, *Photochem. Photobiol.* **2003**, *78*, 462.

[24] A. N. Kuzmin, A. V. Kachynski, T. Y. Ohulchanskyy, I. Roy, P. N. Prasad, S. Bruckenstein, *Appl. Phys. Lett.* **2004**, *84*, 2454.

[25] D. A. Parthenopoulos, P. M. Rentzepis, *Science* **1989**, *245*, 843.

[26] J. H. Strickler, W. W. Webb, *Opt. Lett.* **1991**, *16*, 1780.

[27] A. S. Dvornikov, P. M. Rentzepis, *Opt. Commun.* **1995**, *119*, 341.

[28] K. Belfield, K. Schafer, *Chem. Mater.* **2002**, *14*, 3656.

[29] K. Belfield, Y. Liu, R. Negres, M. Fan, G. Pan, D. Hagan, F. Hernandez, *Chem. Mater.* **2002**, *14*, 3663.

[30] Y. Z. Shen, J. Swiatkiewicz, D. Jakubczyk, F. M. Xu, P. N. Prasad, R. A. Vaia, B. A. Reinhardt, *Appl. Opt.* **2001**, *40*, 938.

[31] H. E. Pudavar, M. P. Joshi, P. N. Prasad, B. A. Reinhardt, *Appl. Phys. Lett.* **1999**, *74*, 1338.

[32] S. Kawata, Y. Kawata, *Chem. Rev.* **2000**, *100*, 1777.

[33] G. S. He, G. C. Xu, P. N. Prasad, B. A. Reinhardt, J. C. Bhatt, A. G. Dillard, *Opt. Lett.* **1995**, *20*, 435.

[34] G. S. He, J. D. Bhawalkar, C. F. Zhao, P. N. Prasad, *Appl. Phys. Lett.* **1995**, *67*, 2433.

[35] J. E. Ehrlich, X. L. Wu, L. S. Lee, A. A. Heikal, Z. Y. Hu, H. Roeckel, S. R. Marder, J. W. Perry, *Mater. Res. Soc. Symp. Proc.* **1997**, *479*, 9.

[36] J. E. Ehrlich, X. L. Wu, I. Y. S. Lee, Z. Y. Hu, H. Rockel, S. R. Marder, J. W. Perry, *Opt. Lett.* **1997**, *22*, 1843.

[37] C. W. Spangler, *J. Mater. Chem.* **1999**, *9*, 2013.

[38] J. W. Perry, S. Barlow, J. E. Ehrlich, A. A. Heikal, Z. Y. Hu, I. Y. Lee, K. Mansour, S. R. Marder, H. Röckel, M. Rumi, S. Thayumanavan, X. L. Wu, *Nonlinear Opt.* **1999**, *21*, 225.

[39] C. Bauer, B. Schnabel, E. B. Kley, U. Scherf, H. Giessen, R. F. Mahrt, *Adv. Mater.* **2002**, *14*, 673.

[40] J. D. Bhawalkar, G. S. He, C.-K. Park, C. F. Zhao, G. Ruland, P. N. Prasad, *Opt. Commun.* **1996**, *124*, 33.

[41] A. Abbotto, L. Beverina, R. Bozio, S. Bradamante, C. Ferrante, G. A. Pagani, R. Signorini, *Adv. Mater.* **2000**, *12*, 1963.

[42] G. S. He, R. Signorini, P. N. Prasad, *Appl. Opt.* **1998**, *37*, 5720.

[43] K. Konig, *J. Microscopy* **2000**, *200*, 83.

[44] W. R. Zipfel, R. M. Williams, R. Christie, A. Y. Nikitin, B. T. Hyman, W. W. Webb, *Proc. Nat. Acad. Sci. USA* **2003**, *100*, 7075.

[45] R. H. Kohler, J. Cao, W. R. Zipfel, W. W. Webb, M. R. Hanson, *Science* **1997**, *276*, 2039.

[46] M. J. Miller, S. H. Wei, I. Parker, M. D. Cahalan, *Science* **2002**, *296*, 1869.

[47] A. M. R. Fisher, A. L. Murphree, C. J. Gomer, *Lasers Surg. Med.* **1995**, *17*, 2.

[48] J. D. Bhawalkar, N. D. Kumar, C. F. Zhao, P. N. Prasad, *J.Clin. Laser Med. Surg.* **1997**, *15*, 201.

[49] D. L. Pettit, S. S. H. Wang, K. R. Gee, G. J. Augustine, *Neuron* **1997**, *19*, 465.

[50] S. Kim, T. Ohulchanskyy, H. Pudavar, R. Pandey, P. Prasad, *J. Am. Chem. Soc.* **2007**, *129*, 2669.

[51] E. Nickel, C. W. Spangler, A. Rebane, U.s. pat. appl. publ., **2003**, us2003105070.

[52] W. Dichtel, J. Serin, C. Edder, J. Frechet, M. Matuszewski, L.-S. Tan, T. Ohulchanskyy, P. Prasad, *J. Am. Chem. Soc.* **2004**, *126*, 5380.

[53] P. N. Prasad, *Introduction to Biophotonics*, Wiley Interscience, New York, **2003**.

[54] P. N. Prasad, *Nanophotonics*, Wiley Interscience, New York, **2004**.

[55] N. Izard, C. Menard, D. Riehl, E. Doris, C. Mioskowski, E. Anglaret, *Chem. Phys. Lett.* **2004**, *391*, 124.

[56] C. Li, C. Liu, Q. Li, Q. Gong, *Chem. Phys. Lett.* **2004**, *400*, 569.

[57] M. Charlot, N. Izard, O. Mongin, D. Riehl, M. Blanchard-Desce, *Chem. Phys. Lett.* **2006**, *417*, 297.

[58] O. Mongin, L. Porrès, M. Charlot, C. Katan, M. Blanchard-Desce, *Chem. Eur. J.* **2007**, *13*, 1481.

[59] K. R. Weishaupt, T. J. Dougherty, *Radiation Res.* **1978**, *74*, 586.

[60] T. J. Dougherty, J. E. Kaufman, A. Goldfarb, K. R. Weishaupt, D. Boyle, A. Mittleman, *Cancer Res.* **1978**, *38*, 2628.

[61] T. J. Dougherty, *J. Natl. Cancer Inst.* **1974**, *52*, 1333.

[62] C. Xu, W. W. Webb, *J. Opt. Soc. Am. B* **1996**, *13*, 481.

[63] P. Frederiksen, M. Jorgensen, P. Ogilby, *J. Am. Chem. Soc.* **2001**, *123*, 1215.

[64] K. Ogawa, H. Hasegawa, Y. Inaba, Y. Kobuke, H. Inouye, Y. Kanemitsu, E. Kohno, T. Hirano, S. Ogura, I. Okura, *J. Med. Chem.* **2006**, *49*, 2276.

[65] S. Kim, T. Y. Ohulchanskyy, H. E. Pudavar, R. K. Pandey, P. N. Prasad, *J. Am. Chem. Soc.* **2007**, *129*, 2669.

[66] S. McIlroy, E. Clo, L. Nikolajsen, P. Frederiksen, C. Nielsen, K. Mikkelsen, K. Gothelf, P. Ogilb y, *J. Org. Chem.* **2005**, *70*, 1134.

[67] C. Nielsen, M. Johnsen, J. Arnbjerg, M. Pittelkow, S. McIlroy, P. Ogilby, M. Jorgensen, *J. Org. Chem.* **2005**, *70*, 7065.

[68] D. W. Piston, M. S. Kirby, H. Cheng, W. J. Lederer, W. W. Webb, *Appl. Opt.* **1994**, *33*, 662.

[69] S. Charpak, J. Mertz, E. Beaurepaire, L. Moreaux, K. Delaney, *Proc. Natl. Acad. Sci.* **2001**, *98*, 1230.

[70] M. Wachowiak, W. Denk, R. W. Friedrich, *Proc. Natl. Acad. Sci. USA* **2004**, *101*, 9097.

[71] M. Taki, J. Wolford, T. O'Halloran, *J. Am. Chem. Soc.* **2004**, *126*, 712.

[72] C. Chang, E. Nolan, J. Jaworski, K.-I. Okamoto, Y. Hayashi, M. Sheng, S. Lippard, *Inorg. Chem.* **2004**, *43*, 6774.

[73] Y. Meshalkin, *Kvantovaya Elektron.* **1996**, *23*, 551.

[74] G. F. White, K. L. Litvinenlo, S. R. Meech, D. L. Andrews, A. J. Thomson, *Photochem. Photobiol.* **2004**, *3*, 47.

[75] G. S. He, L. Yuan, N. Cheng, J. D. Bhawalkar, P. N. Prasad, L. L. Brott, S. J. C. larson, B. A. Reinhardt, *J. Opt. Soc. Am. B* **1997**, *14*, 1079.

[76] B. A. Reinhardt, L. L. Brott, S. J. Clarson, A. G. Dillard, J. C. Bhatt, R. Kannan, L. X. Yuan, G. S. He, P. N. Prasad, *Chem. Mater.* **1998**, *10*, 1863.

[77] K. Belfield, D. Hagan, E. Van Stryland, K. Schafer, R. Negres, *Org. Lett.* **1999**, *1*, 1575.

[78] O.-K. Kim, K.-S. Lee, H. Y. Woo, K.-S. Kim, G. S. He, J. Swiatkiewicz, P. N. Prasad, *Chem. Mater.* **2000**, *12*, 284.

[79] K. Belfield, K. Schafer, W. Mourad, B. Reinhardt, *J. Org. Chem.* **2000**, *65*, 4475.

[80] R. Kannan, G. He, L. Yuan, F. Xu, P. Prasad, A. Dombroskie, B. Reinhardt, J. Baur, R. V aia, L.-S. Tan, *Chem. Mater.* **2001**, *13*, 1896.

[81] B. Strehmel, A. M. Sarker, H. Detert, *ChemPhysChem* **2003**, *4*, 249.

[82] L. Antonov, K. Kamada, K. Ohta, F. S. Kamounah, *Phys. Chem. Chem. Phys.* **2003**, *5*, 1193.

[83] P. Audebert, K. Kamada, K. Matsunaga, K. Ohta, *Chem. Phys. Lett.* **2003**, *367*, 62.

[84] Z.-Q. Liu, Q. Fang, D. Wang, D.-X. Cao, G. Xue, W.-T. Yu, H. Lei, *Chem. Eur. J.* **2003**, *9*, 5074.

[85] J. Kawamata, M. Akiba, T. Tani, A. Harada, Y. Inagaki, *Chem. Lett.* **2004**, *33*, 448.

[86] W. Yang, C. Kim, M.-Y. Jeong, S. Lee, M. Piao, S.-J. Jeon, B. Cho, *Chem. Mater.* **2004**, *16*, 2783.

[87] S. Charier, O. Ruel, J.-B. Baudin, D. Alcor, J.-F. Allemand, A. Meglio, L. Jullien, *Angew. Chem. Int. Ed.* **2004**, *43*, 4785.

[88] Y. Wang, O. Y.-H. Tai, C. H. Wang, A. K.-Y. Jen, *J. Chem. Phys.* **2004**, *121*, 7901.

[89] M. Albota, D. Beljonne, J. L. Brédas, J. E. Ehrlich, J. Y. Fu, A. A. Heikal, S. E. Hess, T. Kogej, M. D. Levin, S. R. Marder, D. McCord Maughon, J. W. Perry, H. Rockel, M. Rumi, C. Subramaniam, W. W. Webb, X. L. Wu, C. Xu, *Science* **1998**, *281*, 1653.

[90] M. Rumi, J. E. Ehrlich, A. A. Heikal, J. W. Perry, S. Barlow, Z. Y. Hu, D. McCord-Maughon, T. C. Parker, H. Rockel, S. Thayumanavan, S. R. Marder, D. Beljonne, J. L. Bredas, *J. Am. Chem. Soc.* **2000**, *122*, 9500.

[91] L. Ventelon, M. Blanchard-Desce, L. Moreaux, J. Mertz, *Chem. Commun.* **1999**, 2055.

[92] L. Ventelon, S. Charier, L. Moreaux, J. Mertz, M. Blanchard-Desce, *Angew. Chem. Int. Ed.* **2001**, *40*, 2098.

[93] O. Mongin, L. Porrès, L. Moreaux, J. Mertz, M. Blanchard-Desce, *Org. Lett.* **2002**, *4*, 719.

[94] S. J. K. Pond, M. Rumi, M. D. Levin, T. C. Parker, D. Beljonne, M. W. Day, J. L. Bredas, S. R. Marder, J. W. Perry, *J. Phys. Chem. A* **2002**, *106*, 11470.

[95] A. Abbotto, L. Beverina, R. Bozio, A. Facchetti, C. Ferrante, G. Pagani, D. Pedron, R. Signorini, *Org. Lett.* **2002**, *4*, 1495.

[96] W. J. Yang, D. Y. Kim, M.-Y. Jeong, H. M. Kim, S.-J. Jeon, B. R. Cho, *Chem. Commun.* **2003**, 2618.

[97] J. Yoo, S. Yang, M.-Y. Jeong, H. Ahn, S.-J. Jeon, B. Cho, *Org. Lett.* **2003**, *5*, 645.

[98] M. G. Silly, L. Porrès, O. Mongin, P. A. Chollet, M. Blanchard-Desce, *Chem. Phys. Lett.* **2003**, *379*, 74.

[99] H. Kim, M.-Y. Jeong, H. Ahn, S.-J. Jeon, B. Cho, *J. Org. Chem.* **2004**, *69*, 5749.

[100] S. Pond, O. Tsutsumi, M. Rumi, O. Kwon, E. Zojer, J.-L. Bredas, S. Marder, J. Perry, *J. Am. Chem. Soc.* **2004**, *126*, 9291.

[101] M. H. V. Werts, S. Gmouh, O. Mongin, T. Pons, M. Blanchard-Desce, *J. Am. Chem. Soc.* **2004**, *126*, 16294.

[102] G. P. Bartholomew, M. Rumi, S. J. K. Pond, J. W. Perry, S. Tretiak, G. C. Bazan, *J. Am. Chem. Soc.* **2004**, *126*, 11529.

[103] S. J. Chung, M. Rumi, V. Alain, S. Barlow, J. W. Perry, S. R. Marder, *J. Am. Chem. Soc.* **2005**, *127*, 10844.

[104] H. Woo, J. Hong, B. Liu, A. Mikhailovsky, D. Korystov, G. Bazan, *J. Am. Chem. Soc.* **2005**, *127*, 820.

[105] S. Lee, W. Yang, J. Choi, C. Kim, S.-J. Jeon, B. Cho, *Org. Lett.* **2005**, *7*, 323.

[106] V. Strehmel, A. M. Sarker, P. M. Lahti, F. E. Karasz, M. Heydenreich, H. Wetzel, S. Haebel, B. Strehmel, *ChemPhysChem* **2005**, *6*, 267.

[107] H. Woo, B. Liu, B. Kohler, D. Korystov, A. Mikhailovsky, G. Bazan, *J. Am. Chem. Soc.* **2005**, *127*, 14721.

[108] M. P. Joshi, J. Swiatkiewicz, F. Xu, P. N. Prasad, B. A. Reinhardt, R. Kannan, *Opt. Lett.* **1998**, *23*, 1742.

[109] S.-J. Chung, K.-S. Kim, T.-C. Lin, G. He, J. Swiatkiewicz, P. Prasad, *J. Phys. Chem. B* **1999**, *103*, 10741.

[110] G. He, J. Swiatkiewicz, Y. Jiang, P. Prasad, B. Reinhardt, L.-S. Tan, R. Kannan, *J. Phys. Chem. A* **2000**, *104*, 4805.

[111] B. Cho, K. Son, S. Lee, Y.-S. Song, Y.-K. Lee, S.-J. Jeon, J. Choi, H. Lee, M. Cho, *J. Am. Chem. Soc.* **2001**, *123*, 10039.

[112] S.-J. Chung, T.-C. Lin, K.-S. Kim, G. He, J. Swiatkiewicz, P. Prasad, G. Baker, F. Bright, *Chem. Mater.* **2001**, *13*, 4071.

[113] D. Beljonne, W. Wenseleers, E. Zojer, Z. G. Shuai, H. Vogel, S. J. K. Pond, J. W. Perry, S. R. Marder, J. L. Bredas, *Adv. Func. Mater.* **2002**, *12*, 631.

[114] A. Abbotto, L. Beverina, R. Bozio, A. Facchetti, C. Ferrante, G. A. Pagani, D. Pedron, R. Signorini, *Chem. Commun.* **2003**, 2144.

[115] O. Mongin, J. Brunel, L. Porrès, M. Blanchard-Desce, *Tetrahedron Lett.* **2003**, *44*, 2813.

[116] D. Brousmiche, J. Serin, J. Frechet, G. He, T.-C. Lin, S. Chung, P. Prasad, *J. Am. Chem. Soc.* **2003**, *125*, 1448.

[117] L. Porrès, O. Mongin, C. Katan, M. Charlot, T. Pons, J. Mertz, M. Blanchard-Desce, *Org. Lett.* **2004**, *6*, 47.

[118] L. Porrès, C. Katan, O. Mongin, T. Pons, J. Mertz, M. Blanchard-Desce, *J. Mol. Struct.* **2004**, *704*, 17.

[119] C. L. Droumaguet, O. Mongin, M. H. V. Werts, M. Blanchard-Desce, *Chem. Commun.* **2005**, 2802.

[120] C. Katan, F. Terenziani, O. Mongin, M. H. V. Werts, L. Porrès, T. Pons, J. Mertz, S. Tretiak, M. Blanchard-Desce, *J. Phys. Chem. A* **2005**, *109*, 3024.

[121] C. Katan, F. Terenziani, C. L. Droumaguet, O. Mongin, M. H. V. Werts, S. Tretiak, M. Blanchard-Desce, *SPIE Proc.* **2005**, *5935*, 593503.

[122] A. Bhaskar, G. Ramakrishna, Z. Lu, R. Twieg, J. Hales, D. Hagan, E. VanStryland, T. Goodson, *J. Am. Chem. Soc.* **2006**, *128*, 11840.

[123] F. Terenziani, C. L. Droumaguet, C. Katan, O. Mongin, M. Blanchard-Desce, *ChemPhysChem* **2007**, *8*, 723.

[124] O. Mongin, L. Porrès, C. Katan, T. Pons, J. Mertz, M. Blanchard-Desce, *Tetrahedron Lett.* **2003**, *44*, 8121.

[125] L. Porrès, O. Mongin, C. Katan, M. Charlot, B. K. C. Bhatthula, V. Jouikov, T. Pons, J. Mertz, M. Blanchard-Desce, *J. Nonlin. Opt. Phys. Mater.* **2004**, *13*, 451.

[126] C. Katan, S. Tretiak, M. Werts, A. Bain, R. Marsh, N. Leonczek, N. Nicolaou, E. Badaeva, O. Mongin, M. Blanchard-Desce, *J. Phys. Chem. B* **2007**, *111*, 9468.

[127] F. Terenziani, M. Morone, S. Gmouh, M. Blanchard-Desce, *ChemPhysChem* **2006**, *7*, 685.

[128] M. Drobizhev, A. Karotki, M. Kruk, A. Rebane, *Chem. Phys. Lett.* **2002**, *355*, 175.

[129] M. Drobizhev, A. Karotki, M. Kruk, Y. Dzenis, A. Rebane, F. Meng, E. Nickel, C. W. Spangler, *SPIE Proc.* **2003**, *5211*, 63.

[130] K. Ogawa, A. Ohashi, Y. Kobuke, K. Kamada, K. Ohta, *J. Am. Chem. Soc.* **2003**, *125*, 13356.

[131] M. Drobizhev, Y. Stepanenko, Y. Dzenis, A. Karotki, A. Rebane, P. Taylor, H. Anderson, *J. Am. Chem. Soc.* **2004**, *126*, 15352.

[132] H. Rath, J. Sankar, V. PrabhuRaja, T. Chandrashekar, A. Nag, D. Goswami, *J. Am. Chem. Soc.* **2005**, *127*, 11608.

[133] D. Kim, T. Ahn, J. Kwon, D. Kim, T. Ikeue, N. Aratani, A. Osuka, M. Shigeiwa, S. Maeda, *J. Phys. Chem. A* **2005**, *109*, 2996.

[134] T. Ahn, K. Kim, D. Kim, S. Noh, N. Aratani, C. Ikeda, A. Osuka, D. Kim, *J. Am. Chem. Soc.* **2006**, *128*, 1700.

[135] R. Misra, R. Kumar, T. Chandrashekar, A. Nag, D. Goswami, *Org. Lett.* **2006**, *8*, 629.

[136] M. Drobizhev, Y. Stepanenko, A. Rebane, C. Wilson, T. Screen, H. Anderson, *J. Am. Chem. Soc.* **2006**, *128*, 12432.

[137] Y. Morel, A. Irimia, P. Najechalski, Y. Kervella, O. Stephan, P. L. Baldeck, C. Andraud, *J. Chem. Phys.* **2001**, *114*, 5391.

[138] R. Anemian, J.-C. Mulatier, C. Andraud, O. Stephan, J.-C. Vial, *Chem. Commun.* **2002**, 1608.

[139] K. Belfield, A. Morales, J. Hales, D. Hagan, E. VanStryland, V. Chapela, J. Percino, *Chem. Mater.* **2004**, *16*, 2267.

[140] M. Drobizhev, A. Karotki, A. Rebane, C. W. Spangler, *Opt. Lett.* **2001**, *26*, 1081.

[141] M. Drobizhev, A. Karotki, Y. Dzenis, A. Rebane, Z. Y. Suo, C. W. Spangler, *J. Phys. Chem. B* **2003**, *107*, 7540.

[142] O. Varnavski, X. Yan, O. Mongin, M. Blanchard-Desce, T. Goodson, *J. Phys. Chem. C* **2007**, *111*, 149.

[143] A. Adronov, J. Frechet, G. He, K.-S. Kim, S.-J. Chung, J. Swiatkiewicz, P. Prasad, *Chem. Mater.* **2000**, *12*, 2838.

[144] O. Mongin, T. R. Krishna, M. H. V. Werts, A.-M. Caminade, J.-P. Majoral, M. Blanchard-Desce, *Chem. Commun.* **2006**, 915.

[145] O. Mongin, A. Pla-Quintana, F. Terenziani, D. Drouin, C. L. Droumaguet, A.-M. Caminade, J.-P. Majoral, M. Blanchard-Desce, *New J. Chem.* **2007**, *31*, 1354.

[146] D. Jacquemin, B. Champagne, E. A. Perpete, J. M. Luis, B. Kirtman, *J. Phys. Chem. A* **2001**, *105*, 9748.

[147] C. B. Gorman, S. R. Marder, *Proc. Nat. Acad. Sci. USA* **1993**, *90*, 11297.

[148] S. R. Marder, C. B. Gorman, F. Meyers, J. W. Perry, G. Bourhill, J. L. Brédas, B. M. Pierce, *Science* **1994**, *265*, 632.

[149] M. Nakano, R. Kishi, S. Ohta, H. Takahashi, T. Kubo, K. Kamada, K. Ohta, E. Botek, B. Champagne, *Phys. Rev. Lett.* **2007**, *99*, 033001 .

[150] M. Barzoukas, C. Runser, A. Fort, M. Blanchard-Desce, *Chem. Phys. Lett.* **1996**, *257*, 531.

[151] A. Painelli, *Chem. Phys. Lett.* **1998**, *285*, 352.

[152] F. Terenziani, A. Painelli, *Phys. Rev. B* **2003**, *68*, 165405.

[153] V. Chernyak, S. Tretiak, S. Mukamel, *Chem. Phys. Lett.* **2000**, *319*, 261.

[154] S. Hahn, D. Kim, M. Cho, *J. Phys. Chem. B* **1999**, *103*, 8221.

[155] M. Barzoukas, M. Blanchard-Desce, *J. Chem. Phys.* **2000**, *113*, 3951.

[156] J. M. Hales, D. J. Hagan, E. W. Van Stryland, K. J. Schafer, A. R. Morales, K. D. Belfield, P. Pacher, O. Kwon, E. Zojer, J. L. Bredas, *J. Chem. Phys.* **2004**, *121*, 3152.

[157] B. Strehmel, S. Amthor, J. Schelter, C. Lambert, *ChemPhysChem* **2005**, *6*, 893.

[158] F. Terenziani, A. Painelli, C. Katan, M. Charlot, M. Blanchard-Desce, *J. Am. Chem. Soc.* **2006**, *128*, 15742.

[159] W.-H. Lee, H. Lee, J.-A. Kim, J.-H. Choi, M. Cho, S.-J. Jeon, B. Cho, *J. Am. Chem. Soc.* **2001**, *123*, 10658.

[160] F. Terenziani, G. D'Avino, A. Painelli, *ChemPhysChem* **2007**, *8*, 2433.

[161] V. Chernyak, E. Y. Poliakov, S. Tretiak, S. Mukamel, *J. Chem. Phys.* **1999**, *111*, 4158.

[162] E. Y. Poliakov, V. Chernyak, S. Tretiak, S. Mukamel, *J. Chem. Phys.* **1999**, *110*, 8161.

[163] S. Tretiak, V. Chernyak, S. Mukamel, *J. Phys. Chem. B* **1998**, *102*, 3310.

[164] M. G. Kuzyk, *J. Chem. Phys.* **2003**, *119*, 8327.

[165] J. F. Stanton, *J. Chem. Phys.* **2001**, *115*, 10382.

[166] A. Szabo, N. S. Ostlund, *Modern Quantum Chemistry: Introduction to Advanced Electronic Structure Theory*, McGraw-Hill, New York, **1989**.

[167] M. J. S. Dewar, E. G. Zoebisch, E. F. Healy, J. J. P. Stewart, *J. Am. Chem. Soc.* **1985**, *107*, 3902.

[168] J. Ridley, M. C. Zerner, *Theor. Chim. Acta* **1973**, *32*, 111.

[169] B. G. Janesko, D. Yaron, *J. Chem. Phys.* **2004**, *121*, 5635.

[170] E. Runge, E. K. U. Gross, *Phys. Rev. Lett.* **1984**, *52*, 997.

[171] M. E. Casida, *Recent Advances in Density-Functional Methods*, vol. 3 of *Part I*, World Scientific, Singapore, **1995**.

[172] S. Grimme, *Rev. Comput. Chem.* **2004**, *20*, 153.

[173] A. Dreuw, M. Head-Gordon, *Chem. Rev.* **2005**, *105*, 4009.

[174] M. E. Casida, C. Jamorski, K. C. Casida, D. R. Salahub, *J. Chem. Phys.* **1998**, *108*, 4439.

[175] F. Furche, R. Ahlrichs, *J. Chem. Phys.* **2002**, *117*, 7433.

[176] R. J. Magyar, S. Tretiak, *J. Chem. Theory Comput.* **2007**, *3*, 976.

[177] B. Champagne, M. Guillaume, F. Zutterman, *Chem. Phys. Lett.* **2006**, *425*, 105.

[178] M. Miura, Y. Aoki, B. Champagne, *J. Chem. Phys.* **2007**, *127*, 084103 .

[179] P. Salek, O. Vahtras, J. D. Guo, Y. Luo, T. Helgaker, H. Agren, *Chem. Phys. Lett.* **2003**, *374*, 446.

[180] B. Jansik, P. Salek, D. Jonsson, O. Vahtras, H. Agren, *J. Chem. Phys.* **2005**, *122*, 54107.

[181] O. Berman, S. Mukamel, *Phys. Rev. A* **2003**, *67*, 42503.

[182] S. Tretiak, V. Chernyak, *J. Chem. Phys.* **2003**, *119*, 8809.

[183] P. Salek, O. Vahtras, T. Helgaker, H. Agren, *J. Chem. Phys.* **2002**, *117*, 9630.

[184] L. Frediani, Z. Rinkevicius, H. Agren, *J. Chem. Phys.* **2005**, *122*, 244104.

[185] P. Salek, T. Helgaker, O. Vahtras, H. Agren, D. Jonsson, J. Gauss, *Mol. Phys.* **2005**, *103*, 439.

[186] P. Cronstrand, B. Jansik, D. Jonsson, Y. Luo, H. Agren, *J. Chem. Phys.* **2004**, *121*, 9239.

[187] E. Rudberg, P. Salek, T. Helgaker, H. Agren, *J. Chem. Phys.* **2005**, *123*, 184108.

[188] P. Salek, H. Agren, A. Baev, P. N. Prasad, *J. Phys. Chem. A* **2005**, *109*, 11037.

[189] P. N. Day, K. A. Nguyen, R. Pachter, *J. Chem. Phys.* **2006**, *125*, 094103.

[190] L. Ferrighi, L. Frediani, E. Fossgaard, K. Ruud, *J. Chem. Phys.* **2007**, *127*, 244103.

[191] B. Champagne, F. A. Bulat, W. T. Yang, S. Bonness, B. Kirtman, *J. Chem. Phys.* **2006**, *125*, 194114.

[192] A. M. Masunov, S. Tretiak, *J. Phys. Chem. B* **2004**, *108*, 899.

[193] N. Kobko, A. Masunov, S. Tretiak, *Chem. Phys. Lett.* **2004**, *392*, 444.

[194] E. A. Badaeva, T. V. Timofeeva, A. M. Masunov, S. Tretiak, *J. Phys. Chem. A* **2005**, *109*, 7276.

[195] J. F. Kauffman, J. M. Turner, I. V. Alabugin, B. Breiner, S. V. Kovalenko, E. A. Badaeva, A. Masunov, S. Tretiak, *J. Phys. Chem. A* **2006**, *110*, 241.

[196] C. Wu, S. Tretiak, V. Y. Chernyak, *Chem. Phys. Lett.* **2007**, *433*, 305.

[197] A. E. Clark, *J. Phys. Chem. A* **2006**, *110*, 3790.

[198] S. Mukamel, *Principles of Nonlinear Optical Spectroscopy*, Oxford University Press, New York, **1995**.

[199] P. N. Butcher, D. Cotter, *The Elements of Nonlinear Optics*, Cambridge University Press, Cambridge, **1990**.

[200] B. J. Orr, J. F. Ward, *Mol. Phys.* **1971**, *20*, 513.

[201] The reader is encouraged to derive the expression for $\mathbf{P}^{(n)}_{\omega_\sigma}$ directly from previous equations for specific cases such as ($n = 2$,$\omega_\sigma = 2\omega$) or ($n = 3$,$\omega_\sigma = \omega$).

[202] A. Willetts, J. E. Rice, D. M. Burland, D. P. Shelton, *J. Chem. Phys.* **1992**, *97*, 7590.

[203] B. Dick, R. M. Hochstrasser, H. P. Trommsdorff, in *Nonlinear Properties of Organic Molecules and Crystals* (Eds. D. S. Chemla, J. Zyss), Academic Press Inc., London, **1987**, 167–170.

[204] R. L. Sutherland, *Handbook of nonlinear optics*, Dekker, New York, **1996**.

[205] J. Burris, T. J. McIlrath, *J. Opt. Soc. Am. B* **1985**, *2*, 1313.

[206] R. Cammi, B. Mennucci, J. Tomasi, *J. Phys. Chem. A* **1998**, *102*, 870.

[207] S. J. Cyvin, J. E. Rauch, J. C. Decius, *J. Chem. Phys.* **1965**, *43*, 4083.

[208] R. Cammi, B. Mennucci, J. Tomasi, *J. Phys. Chem. A* **2000**, *104*, 4690.

[209] J. Tomasi, R. Cammi, B. Mennucci, C. Cappelli, S. Corni, *Phys. Chem. Chem. Phys.* **2002**, *4*, 5697.

[210] W. Barford, R. J. Bursill, D. Yaron, *Phys. Rev. B* **2004**, *69*, 155203 .

[211] A. Klamt, G. Schuurmann, *J. Chem. Soc. - Perkin Trans. 2* **1993**, *5*, 799.

[212] A. Klamt, *J. Phys. Chem.* **1995**, *99*, 2224.

[213] R. Wortmann, D. M. Bishop, *J. Chem. Phys.* **1998**, *108*, 1001.

[214] L. Onsager, *J. Am. Chem. Soc.* **1936**, *58*, 1486.

[215] C. J. F. Bottcher, *Theory of Electric Polarization*, Elsevier, Amsterdam, **1973**.

[216] M. G. Kuzyk, in *Characterization Techniques and Tabulations for Organic Nonlinear Materials* (Eds. M. G. Kuzyk, C. W. Dirk), Marcel Dekker, New York, **1998**, 111–220.

[217] D. R. Kanis, M. A. Ratner, T. J. Marks, *Chem. Rev.* **1994**, *94*, 195.

[218] J. L. Brédas, C. Adant, P. Tackx, A. Persoons, B. M. Pierce, *Chem. Rev.* **1994**, *94*, 243.

[219] A. Painelli, F. Terenziani, *Chem. Phys. Lett.* **1999**, *312*, 211.

[220] G. D. Scholes, G. Rumbles, *Nature Mater.* **2006**, *5*, 683.

[221] A. M. Moran, A. M. Kelley, S. Tretiak, *Chem. Phys. Lett.* **2003**, *367*, 293.

[222] A. S. Davydov, *Theory of molecular excitons*, Plenum Press, New York-London, **1971**.

[223] M. Pope, C. E. Swenberg, *Electronic Processes in Organic Crystals*, Clarendon Press, Oxford University Press, Oxford, New York, **1982**.

[224] T. Förster, *Naturwissenschaften* **1946**, *33*, 166.

[225] V. M. Agranovich, M. D. Galanin, *Electronic excitation energy transfer in condensed matter*, North-Holland, Amsterdam, **1982**.

[226] D. J. Heijs, V. A. Malyshev, J. Knoester, *Phys. Rev. Lett.* **2005**, *95*, 1.

[227] M. Bednarz, V. A. Malyshev, J. Knoester, *J. Chem. Phys.* **2004**, *120*, 3827.

[228] M. Bednarz, V. A. Malyshev, J. Knoester, *Phys. Rev. Lett.* **2003**, *91*, 217401.

[229] P. Yang, E. R. Batista, S. Tretiak, A. Saxena, R. L. Martin, D. L. Smith, *Phys. Rev. B* **2007**, *76*, 241201.

[230] A. Masunov, S. Tretiak, J. W. Hong, B. Liu, G. C. Bazan, *J. Chem. Phys.* **2005**, *122*, 1 .

[231] L. T. Liu, D. Yaron, M. I. Sluch, M. A. Berg, *J. Phys. Chem. B* **2006**, *110*, 18844.

[232] G. L. Silva, V. Ediz, D. Yaron, B. A. Armitage, *J. Am. Chem. Soc.* **2007**, *129*, 5710 .

[233] F. C. Spano, *Annu. Rev. Phys. Chem.* **2006**, *57*, 217.

[234] J. Clark, C. Silva, R. H. Friend, F. C. Spano, *Phys. Rev. Lett.* **2007**, *98*.

[235] F. C. Spano, *Chem. Phys. Lett.* **2000**, *331*, 7.

[236] D. B. Cook, *Handbook of Computational Quantum Chemistry*, Oxford University Press, New York, **1998**.

[237] G. P. Das, A. T. Yeates, D. S. Dudis, *Chem. Phys. Lett.* **2002**, *361*, 71.

[238] K. Ohta, K. Kamada, *J. Chem. Phys.* **2006**, *124*, 124303.

[239] K. Ohta, L. Antonov, S. Yamada, K. Kamada, *J. Chem. Phys.* **2007**, *127*, 084504.

[240] S.-J. Chung, S. Zheng, T. Odani, L. Beverina, J. Fu, L. A. Padilha, A. Biesso, J. M. Hales, X. Zhan, K. Schmidt, A. Ye, E. Zojer, S. Barlow, D. J. Hagan, E. W. V. Stryland, Y. Yi, Z. Shuai, G. A. Pagani, J.-L. Brdas, J. W. Perry, S. R. Marder, *J. Am. Chem. Soc.* **2006**, *128*, 14444.

[241] J. Fu, L. A. Padilha, D. J. Hagan, E. W. V. Stryland, O. V. Przhonska, M. V. Bondar, Y. L. Slominsky, A. D. Kachkovski, *J. Opt. Soc. Am. B* **2007**, *24*, 67.

[242] J. R. Heflin, K. Y. Wong, O. Zamanikhamiri, A. F. Garito, *Phys. Rev. B* **1988**, *38*, 1573.

[243] M. van Faassen, P. L. de Boeij, R. van Leeuwen, J. A. Berger, J. G. Snijders, *Phys. Rev. Lett.* **2002**, *88*, 186401.

[244] L. Reining, V. Olevano, A. Rubio, G. Onida, *Phys. Rev. Lett.* **2002**, *88*, 066404.

[245] D. Rappoport, F. Furche, *J. Chem. Phys.* **2007**, *126*, 201104.

[246] F. Furche, J. P. Perdew, *J. Chem. Phys.* **2006**, *124*, 44103.

[247] M. J. Paterson, O. Christiansen, F. P. owski, P. J. rgensen, C. Hättig, T. Helgaker, P. S. ek, *J. Chem. Phys.* **2006**, *124*, 054322.

[248] S. Tretiak, S. Mukamel, *Chem. Rev.* **2002**, *102*, 3171.

[249] A. D. Becke, *J. Chem. Phys.* **1993**, *98*, 5648.

[250] J. F. Ward, *Rev. Mod. Phys.* **1965**, *37*, 1.

[251] F. Furche, *J. Chem. Phys.* **2001**, *114*, 5982.

[252] M. J. Frisch, G. W. Trucks, H. B. Schlegel, G. E. Scuseria, M. A. Robb, J. R. Cheeseman, V. G. Zakrzewski, J. A. Montgomery, Jr., R. E. Stratmann, J. C. Burant, S. Dapprich, J. M. Millam, A. D. Daniels, K. N. Kudin, M. C. Strain, O. Farkas, J. Tomasi, V. Barone, M. Cossi, R. Cammi, B. Mennucci, C. Pomelli, C. Adamo, S. Clifford, J. Ochterski, G. A. Petersson, P. Y. Ayala, Q. Cui, K. Morokuma, D. K. Malick, A. D. Rabuck, K. Raghavachari, J. B. Foresman, J. Cioslowski, J. V. Ortiz, A. G. Baboul, B. B. Stefanov, G. Liu, A. Liashenko, P. Piskorz, I. Komaromi, R. Gomperts, R. L. Martin, D. J. Fox, T. Keith, M. A. Al-Laham, C. Y. Peng, A. Nanayakkara, M. Challacombe, P. M. W. Gill, B. Johnson, W. Chen, M. W. Wong, J. L. Andres, C. Gonzalez, M. Head-Gordon, E. S. Replogle, J. A. Pople, *Gaussian 98 (Revision A.11)*, Gaussian, Inc., Pittsburgh PA, **2002**.

[253] M. J. Frisch, G. W. Trucks, H. B. Schlegel, G. E. Scuseria, M. A. Robb, J. R. Cheeseman, J. A. Montgomery, Jr., T. Vreven, K. N. Kudin, J. C. Burant, J. M. Millam, S. S. Iyengar, J. Tomasi, V. Barone, B. Mennucci, M. Cossi, G. Scalmani,

N. Rega, G. A. Petersson, H. Nakatsuji, M. Hada, M. Ehara, K. Toyota, R. Fukuda, J. Hasegawa, M. Ishida, T. Nakajima, Y. Honda, O. Kitao, H. Nakai, M. Klene, X. Li, J. E. Knox, H. P. Hratchian, J. B. Cross, V. Bakken, C. Adamo, J. Jaramillo, R. Gomperts, R. E. Stratmann, O. Yazyev, A. J. Austin, R. Cammi, C. Pomelli, J. W. Ochterski, P. Y. Ayala, K. Morokuma, G. A. Voth, P. Salvador, J. J. Dannenberg, V. G. Zakrzewski, S. Dapprich, A. D. Daniels, M. C. Strain, O. Farkas, D. K. Malick, A. D. Rabuck, K. Raghavachari, J. B. Foresman, J. V. Ortiz, Q. Cui, A. G. Baboul, S. Clifford, J. Cioslowski, B. B. Stefanov, G. Liu, A. Liashenko, P. Piskorz, I. Komaromi, R. L. Martin, D. J. Fox, T. Keith, M. A. Al-Laham, C. Y. Peng, A. Nanayakkara, M. Challacombe, P. M., Gaussian 03, Revision D.02, Gaussian, Inc., Wallingford, CT, 2004.

[254] V. Alain, S. Redoglia, M. Blanchard-Desce, S. Lebus, K. Lukaszuk, R. Wortmann, U. Gubler, C. Bosshard, P. Gunter, *Chem. Phys.* **1999**, *245*, 51.

[255] P. Flükiger, H. P. Lüthi, S. Portmann, J. Weber, *MOLEKEL 4.0*, Swiss Center for Scientific Computing, Manno (Switzerland), **2000**.

[256] S. Grimme, M. Parac, *ChemPhysChem* **2003**, *4*, 292.

[257] A. Pogantsch, G. Heimel, E. Zojer, *J. Chem. Phys.* **2002**, *117*, 5921.

[258] A. Dreuw, J. L. Weisman, M. Head-Gordon, *J. Chem. Phys.* **2003**, *119*, 2943.

[259] A. Dreuw, M. Head-Gordon, *J. Am. Chem. Soc.* **2004**, *126*, 4007.

[260] S. Tretiak, K. Igumenshchev, V. Chernyak, *Phys. Rev. B* **2005**, *71*, 33201.

[261] K. I. Igumenshchev, S. Tretiak, V. Y. Chernyak, *J. Chem. Phys.* **2007**, *127*, 1 .

[262] G. Onida, L. Reining, A. Rubio, *Rev. Mod. Phys.* **2002**, *74*, 601.

[263] M. Chiba, T. Tsuneda, K. Hirao, *J. Chem. Phys.* **2006**, *124*, 144106.

[264] M. J. G. Peach, T. Helgaker, P. Salek, T. W. Keal, O. B. Lutnaes, D. J. Tozer, N. C. Handy, *Phys. Chem. Chem. Phys.* **2006**, *8*, 558.

[265] D. Jacquemin, E. A. Perpete, G. Scalmani, M. J. Frisch, R. Kobayashi, C. Adamo, *J. Chem. Phys.* **2007**, *126*, 144105.

[266] D. Jacquemin, E. A. Perpete, M. Medved', G. Scalmani, M. J. Frisch, R. Kobayashi, C. Adamo, *J. Chem. Phys.* **2007**, *126*, 191108.

[267] The half-width at half-maximum (HWHM) of a Lorentzian band having the same height of a Gaussian of HWHM = Γ_{gaus} is given by: $\Gamma_{lor} = \frac{\Gamma_{gaus}}{\sqrt{\pi \ln 2}}$.

[268] R. L. Martin, *J. Chem. Phys.* **2003**, *118*, 4775.

[269] I. Franco, S. Tretiak, *J. Am. Chem. Soc.* **2004**, *126*, 12130.

[270] A. Kokalj, *J. Mol. Graph. Model.* **1999**, *17*, 176.

[271] M. Sheik-Bahae, A. A. Said, T.-H. Wei, D. J. Hagan, E. W. Van Stryland, *IEEE J. Quantum Electronics* **1990**, *26*, 760.

[272] J. Swiatkiewicz, P. N. Prasad, B. A. Reinhardt, *Opt. Commun.* **1998**, *157*, 135.

[273] O. K. Kim, K. S. Lee, H. Y. Woo, K. S. Kim, G. S. He, J. Swiatkiewicz, P. N. Prasad, *Chem. Mater.* **2000**, *12*, 284.

[274] A. Fischer, C. Cremer, E. H. K. Stelzer, *Appl. Opt.* **1995**, *34*, 1989.

[275] E. W. V. Strylandn, M. Sheik-Bahae, in *Characterization Techniques and Tabulations for Organic Nonlinear Materials* (Eds. M. G. Kuzyk, C. W. Dirk), Marcel Dekker, New York, **1998**, 655–692.

[276] M. D. Galanin, Z. A. Chizhikova, *JETP Lett* **1966**, *4*, 27.

[277] S. M. Kennedy, F. E. Lytle, *Anal. Chem.* **1986**, *58*, 2643.

[278] K. S. Overway, F. E. Lytle, *Appl. Spectrosc.* **1998**, *52*, 298.

[279] A. Karotki, M. Drobizhev, M. Kruk, C. Spangler, E. Nickel, N. Mamardashvili, A. Rebane, *J. Opt. Soc. Am. B* **2003**, *20*, 321.

[280] J. N. Demas, G. A. Crosby, *J. Phys. Chem.* **1971**, *75*, 991.

[281] D. F. Deaton, *Pure Appl. Chem.* **1988**, *60*, 1107.

[282] M. H. V. Werts, N. Nerambourg, D. Pelegry, Y. L. Grand, M. Blanchard-Desce, *Photochem. Photobiol. Sci.* **2005**, *4*, 531.

[283] M. A. Albota, C. Xu, W. W. Webb, *Appl. Opt.* **1998**, *37*, 7352.

[284] V. N. Nesterov, T. V. Timofeeva, S. S. Sarkisov, A. Leyderman, C. Y. Lee, M. Y. Antipin, *Acta Crystallogr. C: Cryst. Struct. Commun.* **2003**, *59*, o605.

[285] H. S. Woo, O. Lhost, S. C. Graham, D. D. C. Bradley, R. H. Friend, C. Quattrocchi, J. L. Bredas, R. Schenk, K. Mullen, *Synth. Met.* **1993**, *59*, 13.

[286] S. Tretiak, V. Chernyak, S. Mukamel, *Phys. Rev. Lett.* **1996**, *77*, 4656.

[287] M. Schulz, S. Tretiak, V. Chernyak, S. Mukamel, *J. Am. Chem. Soc.* **2000**, *122*, 452.

[288] G. R. Hutchison, Y. J. Zhao, B. Delley, A. J. Freeman, M. A. Ratner, T. J. Marks, *Phys. Rev. B* **2003**, *68*, 035204.

[289] T. G. Goodson, *Annu. Rev. Phys. Chem.* **2005**, *56*, 581.

[290] T. G. Goodson, *Acc. Chem. Res.* **2005**, *38*, 99.

[291] A. M. Kelley, L. C. T. Shoute, M. Blanchard-Desce, G. P. Bartholomew, G. C. Bazan, *Mol. Phys.* **2006**, *104*, 1239.

[292] O. Varnavski, J. Ostrowski, L. Sukhomlinova, R. Twieg, G. Bazan, T. Goodson, *J. Am. Chem. Soc.* **2002**, *124*, 1736.

[293] W. Verbouwe, L. Viaene, M. Van der Auweraer, F. De Schryver, H. Masuhara, R. Pansu, J. Faure, *J. Phys. Chem. A* **1997**, *101*, 8157.

[294] W. Verbouwe, M. Van der Auweraer, F. De Schryver, J. Piet, J. Warman, *J. Am. Chem. Soc.* **1998**, *120*, 1319.

[295] S. A. Lahankar, R. West, O. Varnavski, X. Xie, T. G. III, L. Sukhomlinova, R. Twieg, *J. Chem. Phys.* **2004**, *120*, 337.

[296] Y. Wang, G. He, P. Prasad, T. Goodson, *J. Am. Chem. Soc.* **2005**, *127*, 10128.

[297] A. N. Sobolev, V. K. Belsky, I. P. Romm, N. Y. Chernikova, E. N. Guryanova, *Acta Crystallogr. Sect. C* **1985**, *41*, 967.

[298] S. A. Lahankar, R. West, O. Varnavski, X. B. Xie, T. Goodson, L. Sukhomlinova, R. Twieg, *J. Chem. Phys.* **2004**, *120*, 337.

[299] G. D. Scholes, K. P. Ghiggino, A. M. Oliver, M. N. Paddonrow, *J. Am. Chem. Soc.* **1993**, *115*, 4345.

[300] S. Tretiak, W. M. Zhang, V. Chernyak, S. Mukamel, *Proc. Nat. Acad. Sci. USA* **1999**, *96*, 13003.

[301] A. E. Clark, C. Y. Qin, A. D. Q. Li, *J. Am. Chem. Soc.* **2007**, *129*, 7586 .

[302] In order to compare calculated and experimental transition dipole moments, corrections relative to solvent effects have to be accounted for. As the local field correction involves the polarizability $\alpha(-\omega;\omega)$, experimental values can not be easily transformed to gas phase properties. Here, the *effective* transition dipole moments correspond to the experimental values corrected for the refractive index n as given by $(\mu_{01}^{exp})_{eff} = A\sqrt{3kn\int_{1stband}\epsilon(\nu)d\nu}$ with $k = 4.32.10^{-9}$ L^{-1} mol. cm and $A = 0.266$ while the calculated values are corrected for the local field effects.

[303] A. L. Thompson, K. M. Gaab, J. J. Xu, C. J. Bardeen, T. J. Martinez, *J. Phys. Chem. A* **2004**, *108*, 671.

[304] C. Wu, S. V. Malinin, S. Tretiak, V. Y. Chernyak, *Nature Phys.* **2006**, *2*, 631.

[305] R. J. Magyar, S. Tretiak, Y. Gao, H. L. Wang, A. P. Shreve, *Chem. Phys. Lett.* **2005**, *401*, 149.

[306] D. J. Tozer, N. C. Handy, *J. Chem. Phys.* **1998**, *109*, 10180.

[307] Z.-L. Cai, K. Sendt, J. R. Reimers, *J. Chem. Phys.* **2002**, *117*, 5543.

[308] For centrosymmetric molecules, TPA to the $|1_q\rangle$ state and OPA to the $|2_q\rangle$ can only be allowed through vibronic activation.

[309] T. R. Krishna, M. Parent, M. H. V. Werts, L. Moreaux, S. Gmouh, S. Charpak, A.-M. Caminade, J.-P. Majoral, M. Blanchard-Desce, *Angew. Chem. Int. Ed.* **2006**, *45*, 4645.

[310] M. Lal, L. Levy, K. Kim, G. He, X. Wang, Y. Min, S. Pakatchi, P. Prasad, *Chem. Mater.* **2000**, *12*, 2632.

[311] L. Levy, Y. Sahoo, K.-S. Kim, E. Bergey, P. Prasad, *Chem. Mater.* **2002**, *14*, 3715.

[312] D. Bharali, D. Lucey, H. Jayakumar, H. Pudavar, P. Prasad, *J. Am. Chem. Soc.* **2005**, *127*, 11364.

[313] An NTO eigenvalue shows a relative contribution of a given pair of orbitals into correlated excited state in question.[268]

Table 1: DFT methods. The results are obtained using Gaussian 98[252] and Gaussian 03[253] implementation of all functionals.

Functional	c_x (HF-exchange)	Gradient-correction	LDA component
HF	1	no	no
HF/S	1	no	no
BHandH	0.5	yes	yes
MPW1PW91	0.25	yes	yes
PBE1PBE	0.25	yes	yes
B3LYP	0.2	yes	yes
BLYP	0	yes	yes
ALDA (Xalpha)	0	no	yes

Table 2: Experimental and calculated transition energies ω_{01} and effective transition dipole moments $(\mu_{01})_{eff}$[302] to the first excited state of dipolar ($\mathsf{d_1}$), quadrupolar ($\mathsf{q_1}$) and octupolar ($\mathsf{3d_1}$) chromophores. Experimental values are measured in toluene. Calculated results are reported for three different schemes: *vac-vac*, *vac-tol* and *tol-tol* (see main text).

compound	$(\mu_{01}^{exp})_{eff}$ [D]	$(\mu_{01}^{vac-vac})_{eff}$ [D]	$(\mu_{01}^{vac-tol})_{eff}$ [D]	$(\mu_{01}^{tol-tol})_{eff}$ [D]	ω_{01}^{exp} [eV]	$\omega_{01}^{vac-vac}$ [eV]	$\omega_{01}^{vac-tol}$ [eV]	$\omega_{01}^{tol-tol}$ [eV]
$\mathsf{d_1}$	9.0±0.2	9.6	10.5	10.6	2.99	2.84	2.67	2.66
$\mathsf{q_1}$	14.5±0.5	14.2	15.1	15.3	3.10	3.06	2.95	2.93
$\mathsf{3d_1}$	9.6±0.2	10.6	11.4	11.7	2.88	2.75	2.61	2.59

Table 3: Experimental and calculated TPA cross sections σ_2 at the first TPA maximum and corresponding peak positions ω_{TPA} of dipolar ($\mathsf{d_1}$), quadrupolar ($\mathsf{q_1}$) octupolar ($\mathsf{3d_1}$) chromophores. Experimental values in toluene. TPA cross sections in italic include local-field and refractive-index corrections according to expression (38).

compound	σ_2^{exp} [GM]	$\sigma_2^{vac-vac}$ [GM]	$\sigma_2^{vac-tol}$ [GM]	$\sigma_2^{tol-tol}$ [GM]	ω_{TPA}^{exp} [eV]	$\omega_{TPA}^{vac-vac}$ [eV]	$\omega_{TPA}^{vac-tol}$ [eV]	$\omega_{TPA}^{tol-tol}$ [eV]
$\mathsf{d_1}$	100	360	500	480	2.99	2.84	2.67	2.66
		320	*490*	*470*				
$\mathsf{q_1}$	1100	1730	2160	2110	3.35	3.41	3.34	3.30
		1330	*1770*	*1740*				
$\mathsf{3d_1}$	1200	1680	2570	2300	3.35	3.10	2.92	2.92
		1400	*2270*	*2090*				

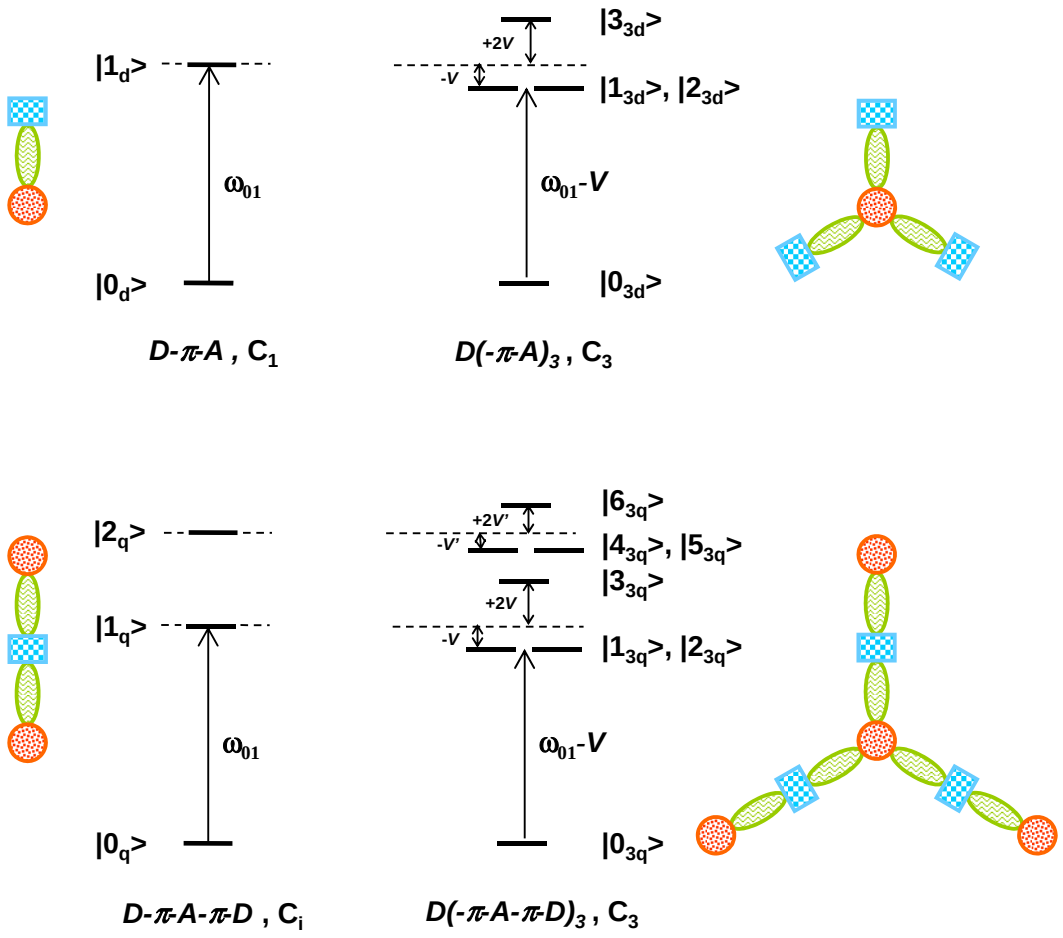

Figure 1: Schematic electronic level diagrams within the excitonic model for a dipole (D-π-A, top left), an octupolar system made up from three dipolar branches (D(-π-A)$_3$, C_3 symmetry, top right), a quadrupole (D-π-A, C_i symmetry, bottom left) and a branched structure obtained by grafting three quadrupoles (D(-π-A-π-D)$_3$, C_3 symmetry, bottom right). $|0_j\rangle$ denotes the ground state and $|n_j\rangle$ the n^{th} excited state where $j = d, 3d, q, 3q$ respectively for dipolar, 3-branched from dipoles, quadrupolar, 3-branched from quadrupoles structures. V (V') denotes the interbranch coupling for the first (second) excited state. Adapted from[121] and.[126]

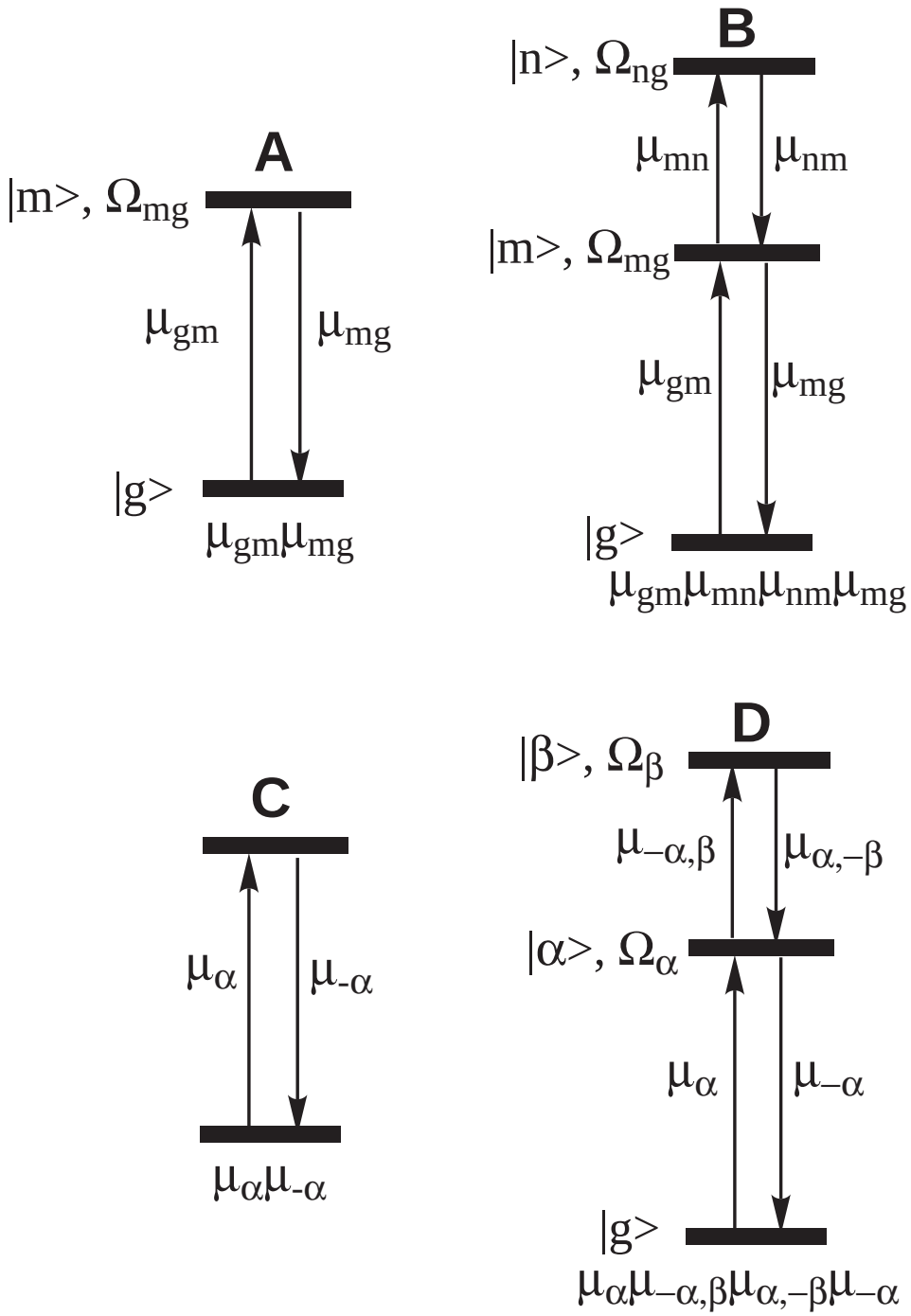

Figure 2: (A) and (B) show the representation of the SOS for the first and third order responses (Eq. (39 and 40)) in terms of Liouville space pathways. (C) and (D) illustrate similar interpretation of TD-DFT response expressions (Eq. (46) and (47)). Adapted from.[182]

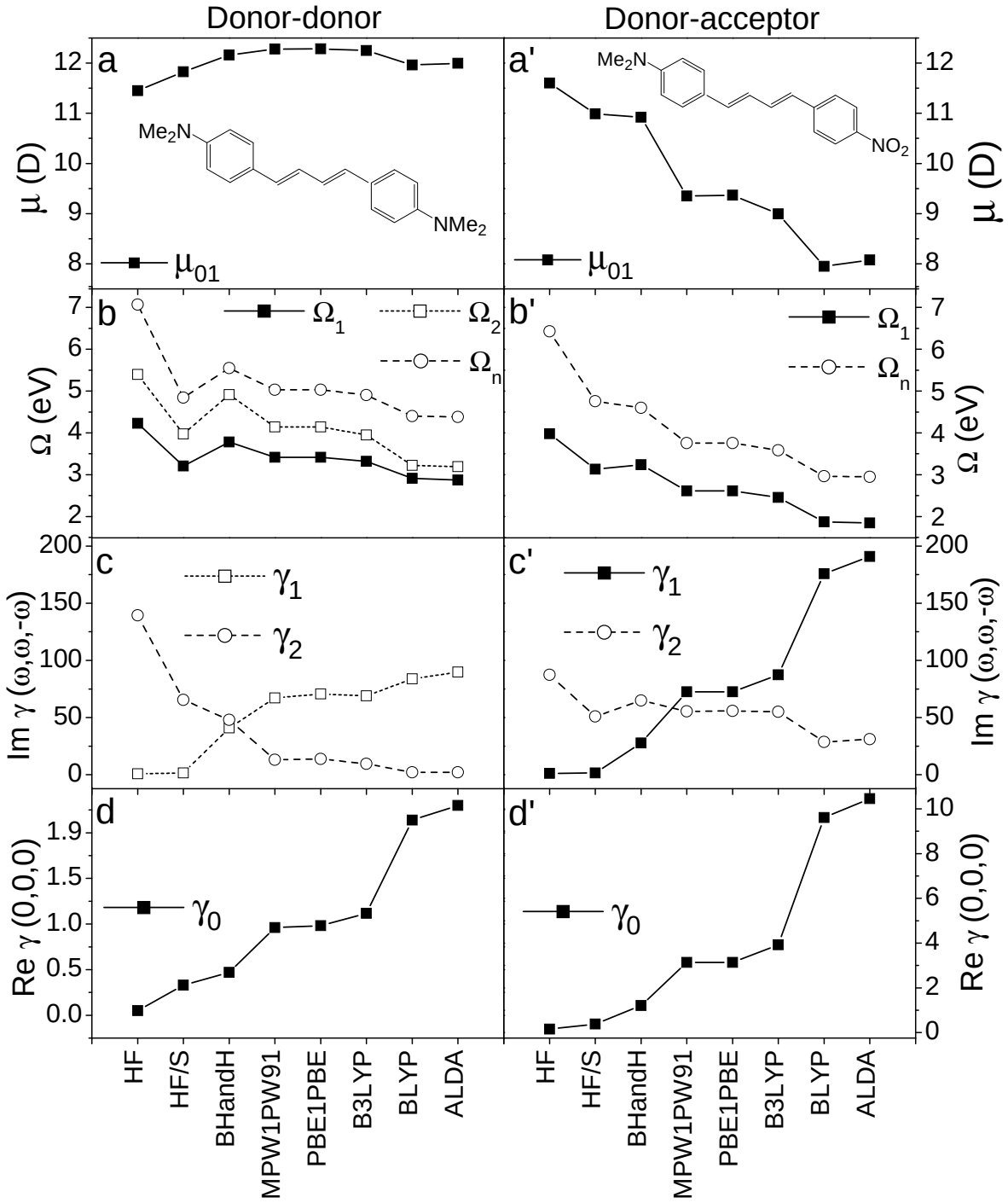

Figure 3: Transition dipoles between the ground and first excited states (*a* and *a'*), transition energies between the ground and excited states contributing to NLO response (*b* and *b'*), resonant (*c* and *c'*) and static (*d* and *d'*) third-order polarizabilities (all γ are given in $10^{-33} esu$) as a function of DFT model used for calculations. Adapted from.[193]

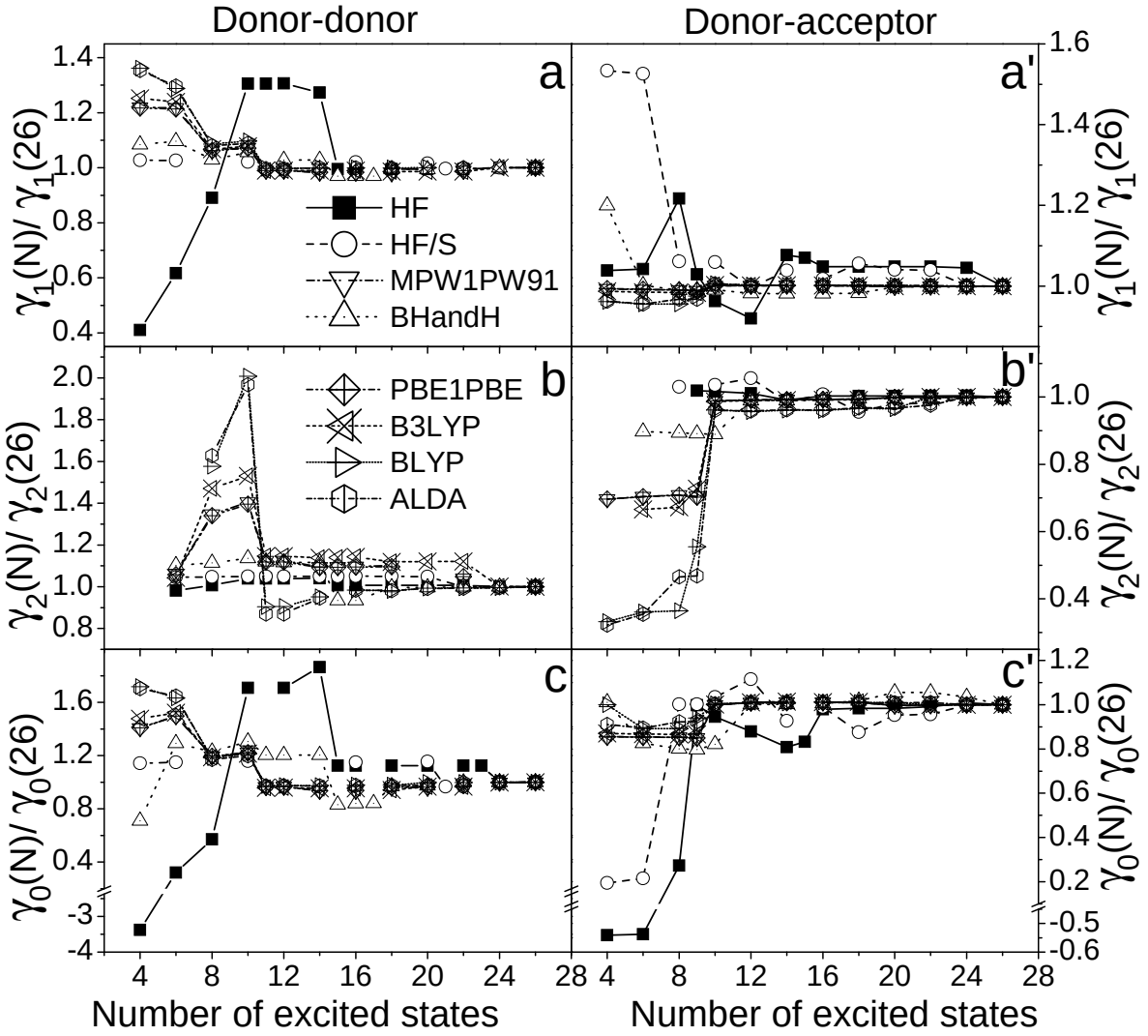

Figure 4: Variation of magnitudes of resonant polarizabilities at the first (a and a') and second (b and b') TPA maxima, and static polarizability (c and c') with the number of excited states used for calculations. Adapted from.[193]

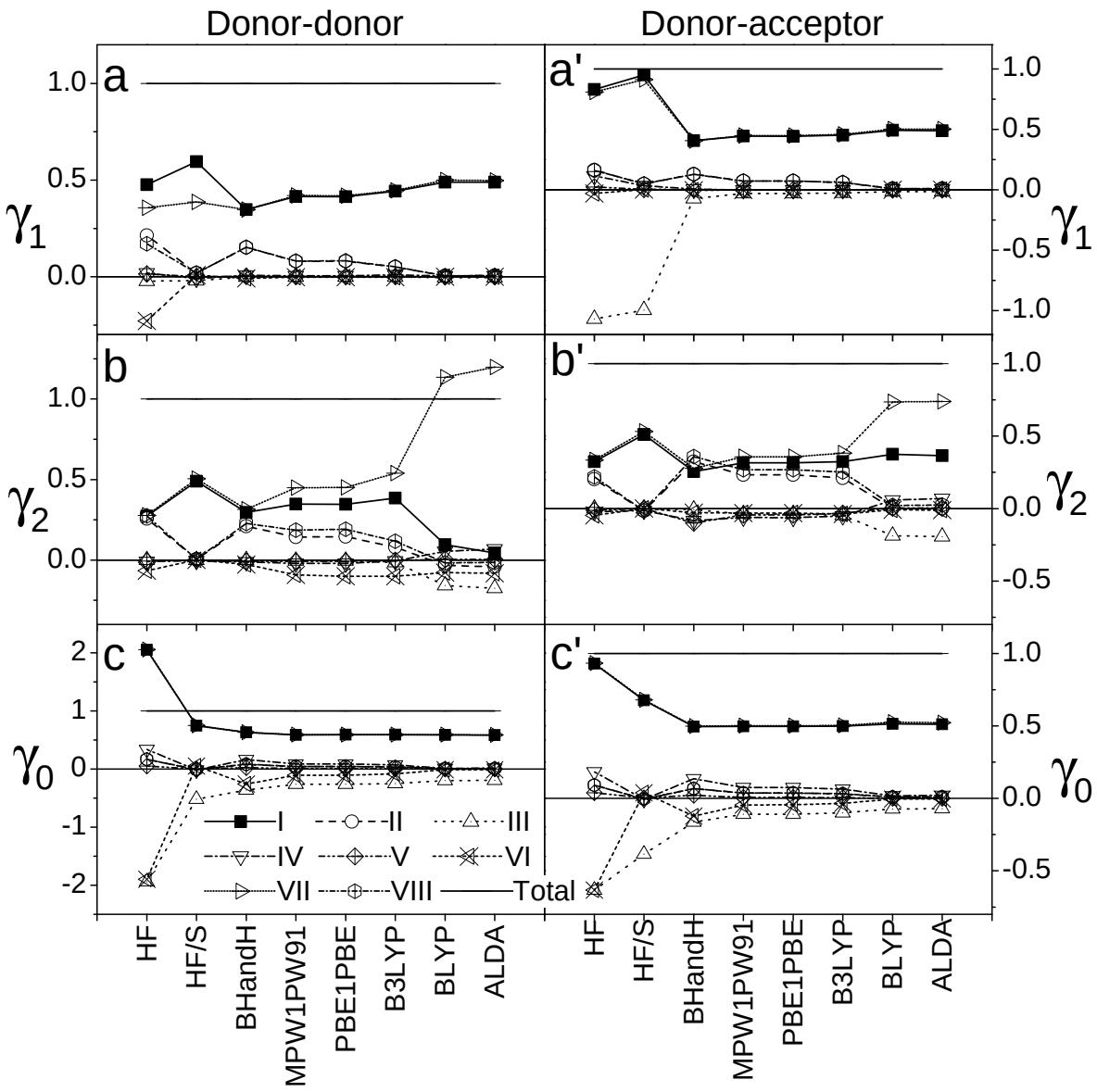

Figure 5: Relative contributions from different terms in expansion (47) to resonant (*a*, *a'* and *b*, *b'*) and static (*c* and *c'*) NLO responses as a function of DFT model. Adapted from.[193]

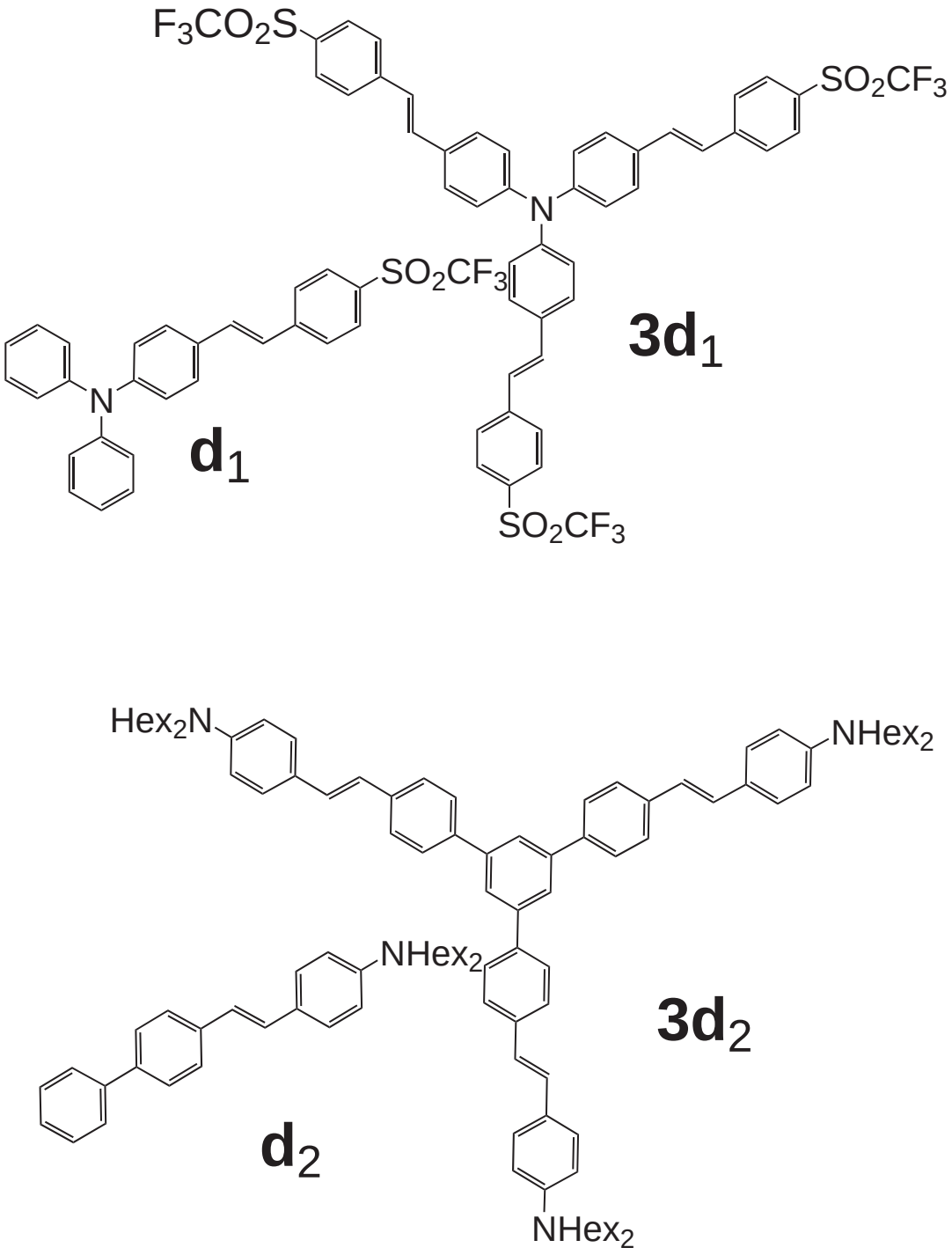

Figure 6: Molecular structures of dipolar chromophores d_1 and d_2, and three-branched octupolar compounds $\mathsf{3d}_1$ and $\mathsf{3d}_2$.

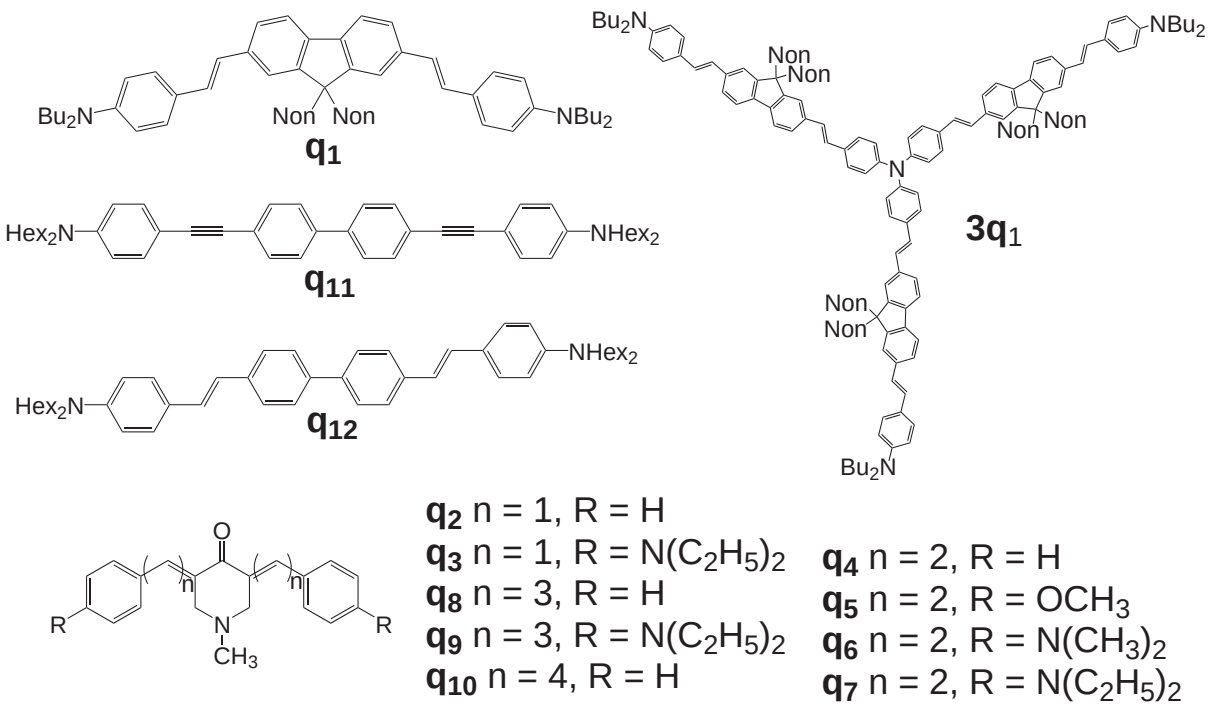

Figure 7: Molecular structure of quadrupolar compounds $\mathtt{q}_1$-$\mathtt{q}_{12}$ and branched chromophore $3\mathtt{q}_1$. Index n denotes the number of vinyl units (i.e., the number of double bonds in the conjugated bridge) for the arylidenecyclohexanone chromophores $\mathtt{q}_2$-$\mathtt{q}_{10}$.

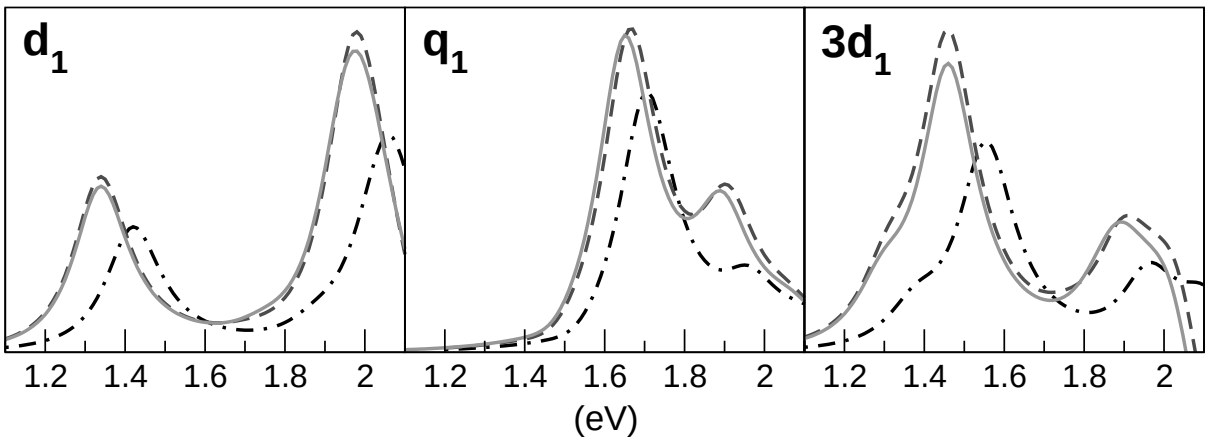

Figure 8: TPA cross sections (arbitrary units) of dipolar (d_1), quadrupolar (q_1) and 3-branched octupolar ($\mathsf{3d}_1$) chromophores obtained with different models for the second-order hyperpolarizability (γ^{sol}): *vac-vac* (dashed-dotted line), *vac-tol* (dashed line) and *tol-tol* (continuous line) (see main text).

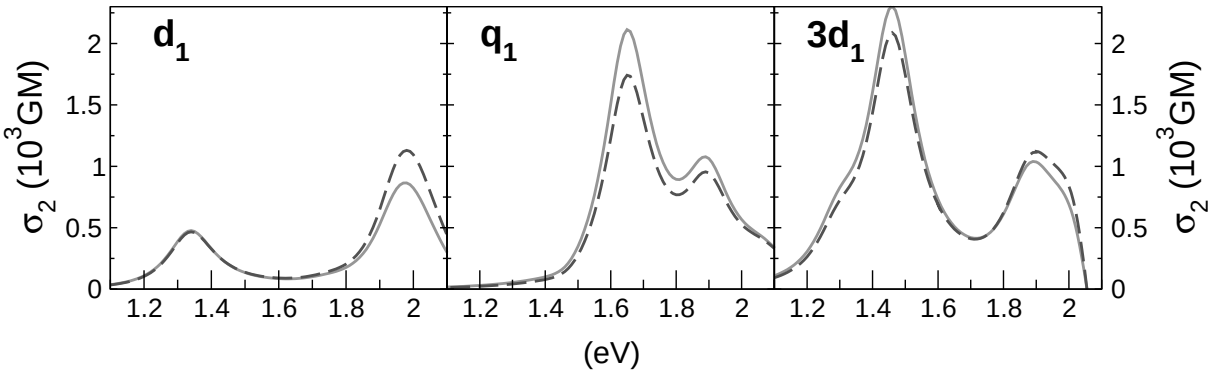

Figure 9: Effect of local-field and refractive-index corrections on TPA cross sections of dipolar (d_1), quadrupolar (q_1) and 3-branched octupolar ($\mathsf{3d}_1$) chromophores obtained using the *tol-tol* ("single point - optimization level") model to calculate second-order hyperpolarizability (γ^{sol}): no local-field correction (continuous line), local-field correction according to expression (38) (dashed line).

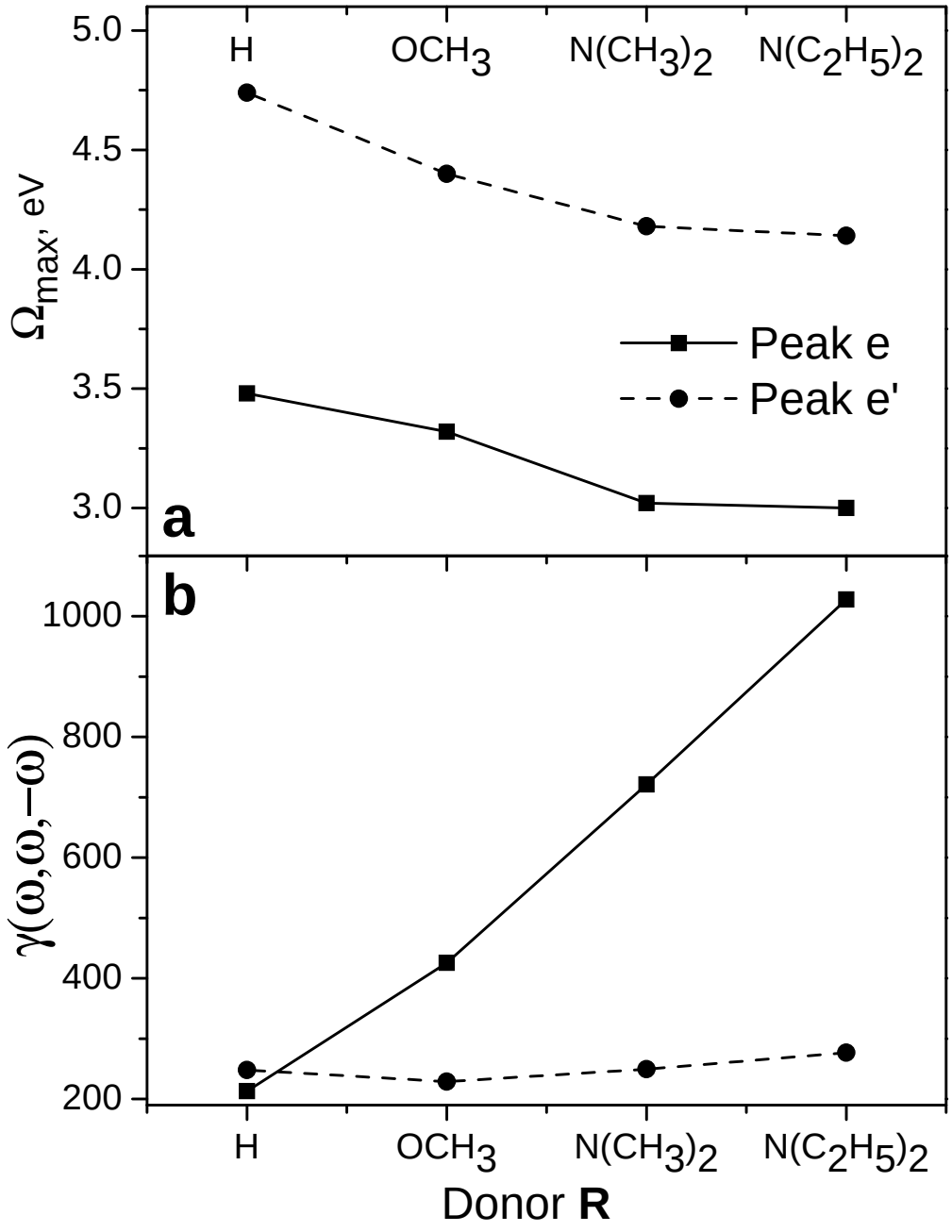

Figure 10: Variation of third-order polarizabilities (all γ are given in $10^{-32}esu$) with the strength of the terminal donor groups for compounds q_4-q_7 in Fig. 7. The lines connecting the points serve as a visual guide. Adapted from.[194]

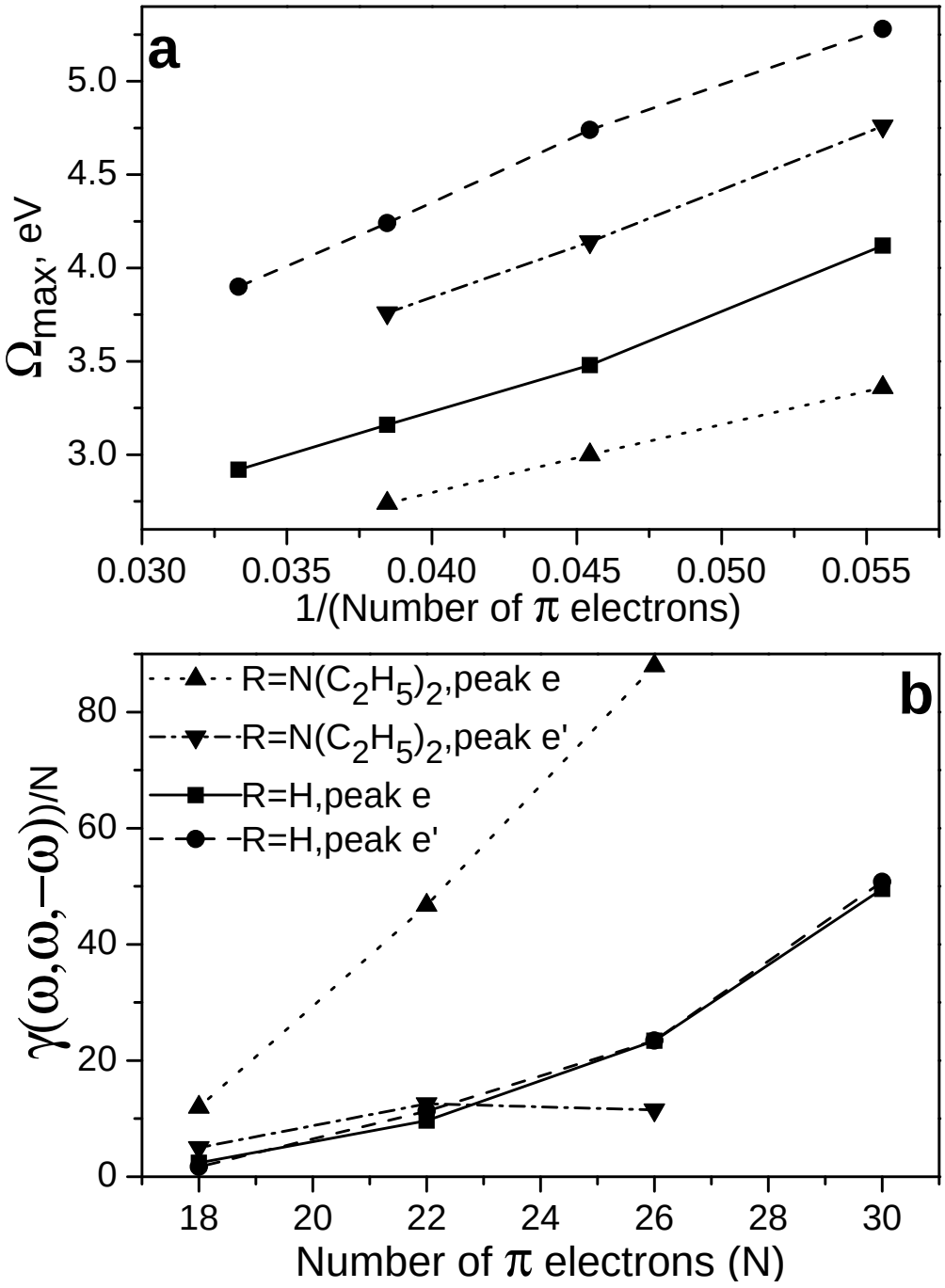

Figure 11: Variation of third-order polarizabilities (all γ are given in $10^{-32}esu$) with the number of π electrons roughly representing the length of the π-bridge for compounds $\mathsf{q}_2, \mathsf{q}_4, \mathsf{q}_8, \mathsf{q}_{10}$ ($\mathbf{R}$= H) and $\mathsf{q}_3, \mathsf{q}_7, \mathsf{q}_9$($\mathbf{R}$= $N(C_2H_5)_2$) in Fig. 7. The lines connecting the points serve as a visual guide. Adapted from.[194]

OPA	*hole*	*electron*
$\|1_q\rangle$ **w=.99 3.06 eV**	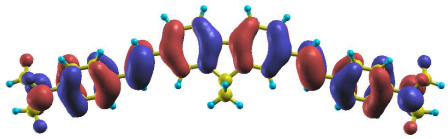	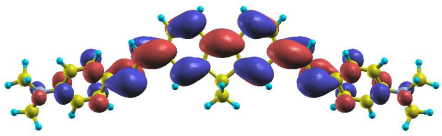
$\|4_q\rangle$ **w=.53 4.08 eV**	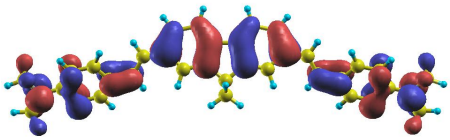	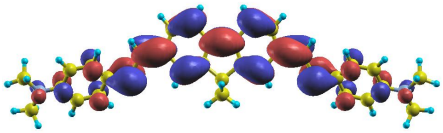
$\|4_q\rangle$ **w=.42 4.08 eV**	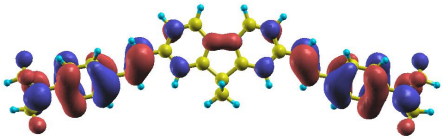	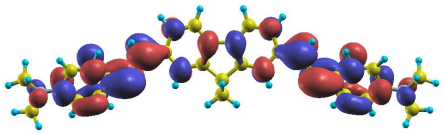
TPA	***hole***	***electron***
$\|2_q\rangle$ **w=.95 3.41 eV**	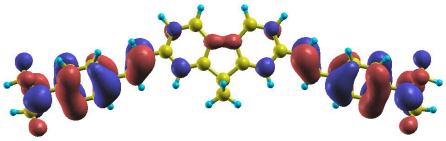	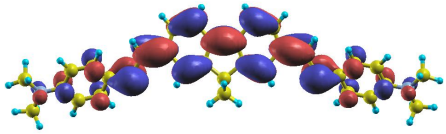
$\|3_q\rangle$ **w=.95 3.9 eV**	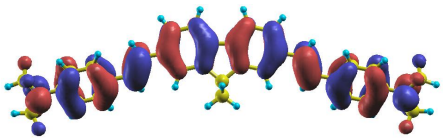	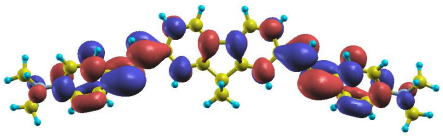

Figure 12: Natural transition orbitals[268] of chromophore q_1. Left panels quote in sequence excited state number, associated NTO eigenvalues[313] and transition energies. Adapted from.[126]

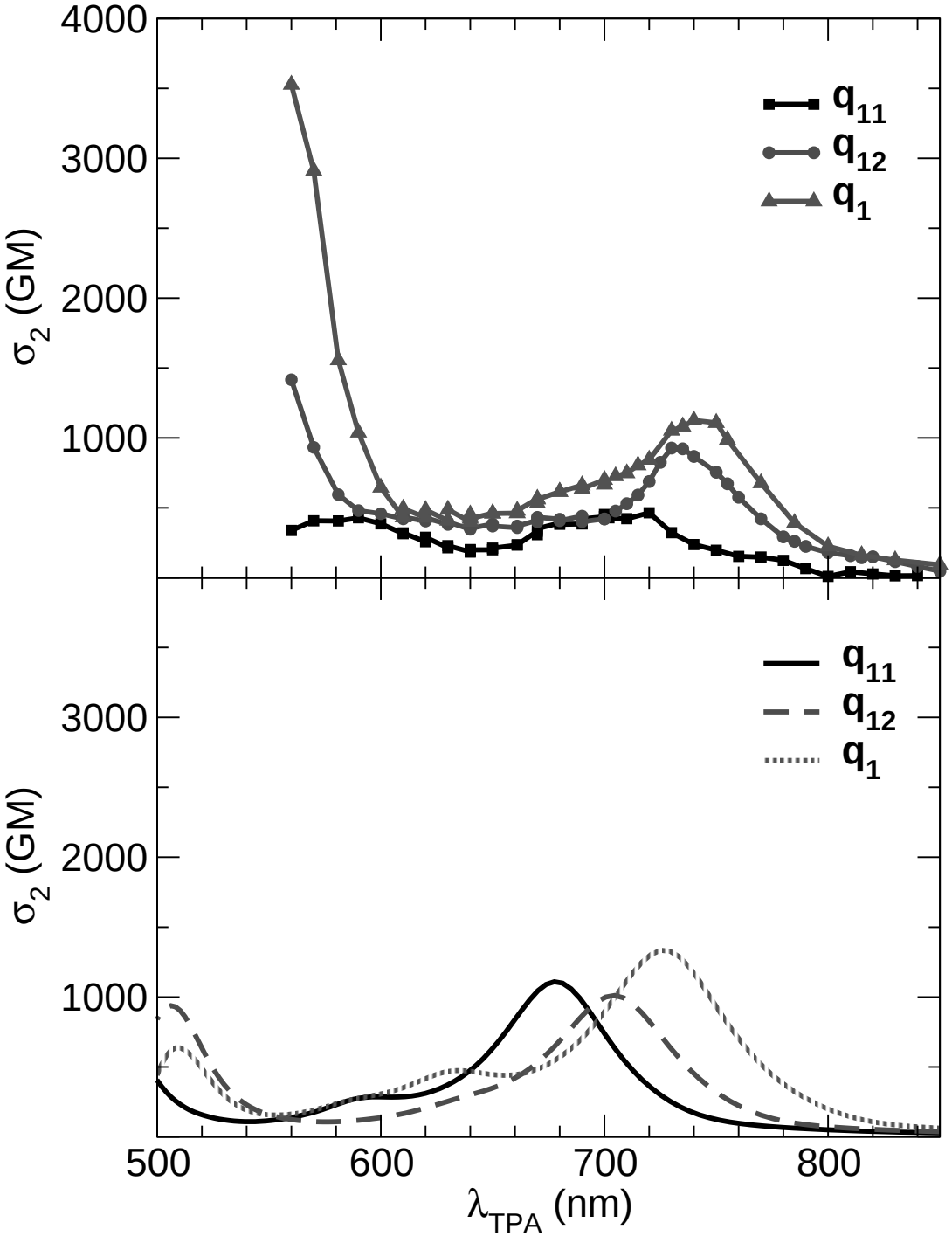

Figure 13: TPA cross section of chromophores q_1, q_{11} and q_{12}. Top panel: experimental data in toluene; Bottom panel: calculated cross section in vacuum, but corrected for local field and refractive index. Adapted from.[126]

<table>
<tr><th colspan="3">d_1</th></tr>
<tr><th>OPA/TPA</th><th>hole</th><th>electron</th></tr>
<tr><td>$|1_d>$
w=1.00
2.84 eV</td><td> 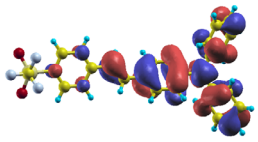 </td><td> 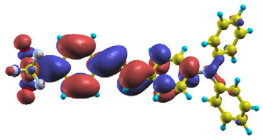 </td></tr>
<tr><th colspan="3">$3d_1$</th></tr>
<tr><th>OPA</th><th>hole</th><th>electron</th></tr>
<tr><td>$|1_{3d}>$
w=.99
2.75 eV</td><td> 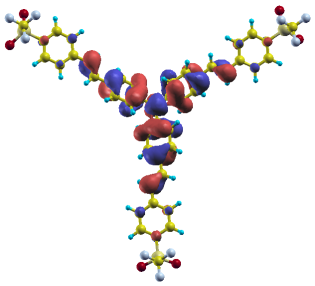 </td><td> 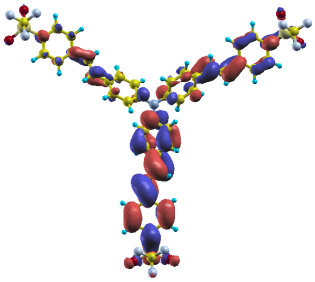 </td></tr>
<tr><td>$|2_{3d}>$
w=.99
2.75 eV</td><td> 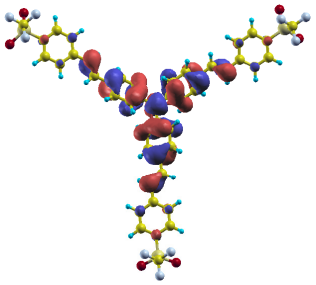 </td><td> 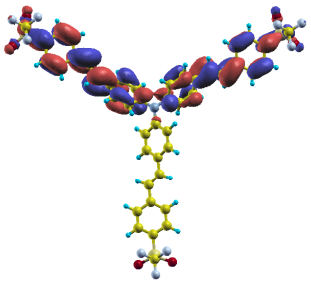 </td></tr>
<tr><th>TPA</th><th>hole</th><th>electron</th></tr>
<tr><td>$|3_{3d}>$
w=.98
3.10 eV</td><td> 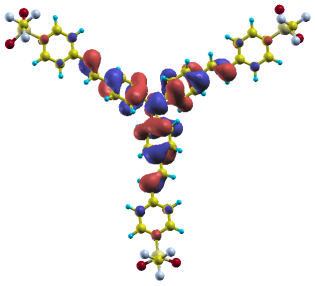 </td><td> 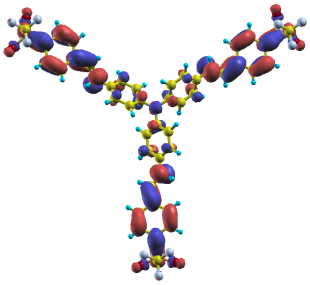 </td></tr>
</table>

Figure 14: Natural transition orbitals[268] of chromophores d_1 and $3d_1$. Left panels quote in sequence excited state number, associated NTO eigenvalues[313] and transition energies. Adapted from.[121]

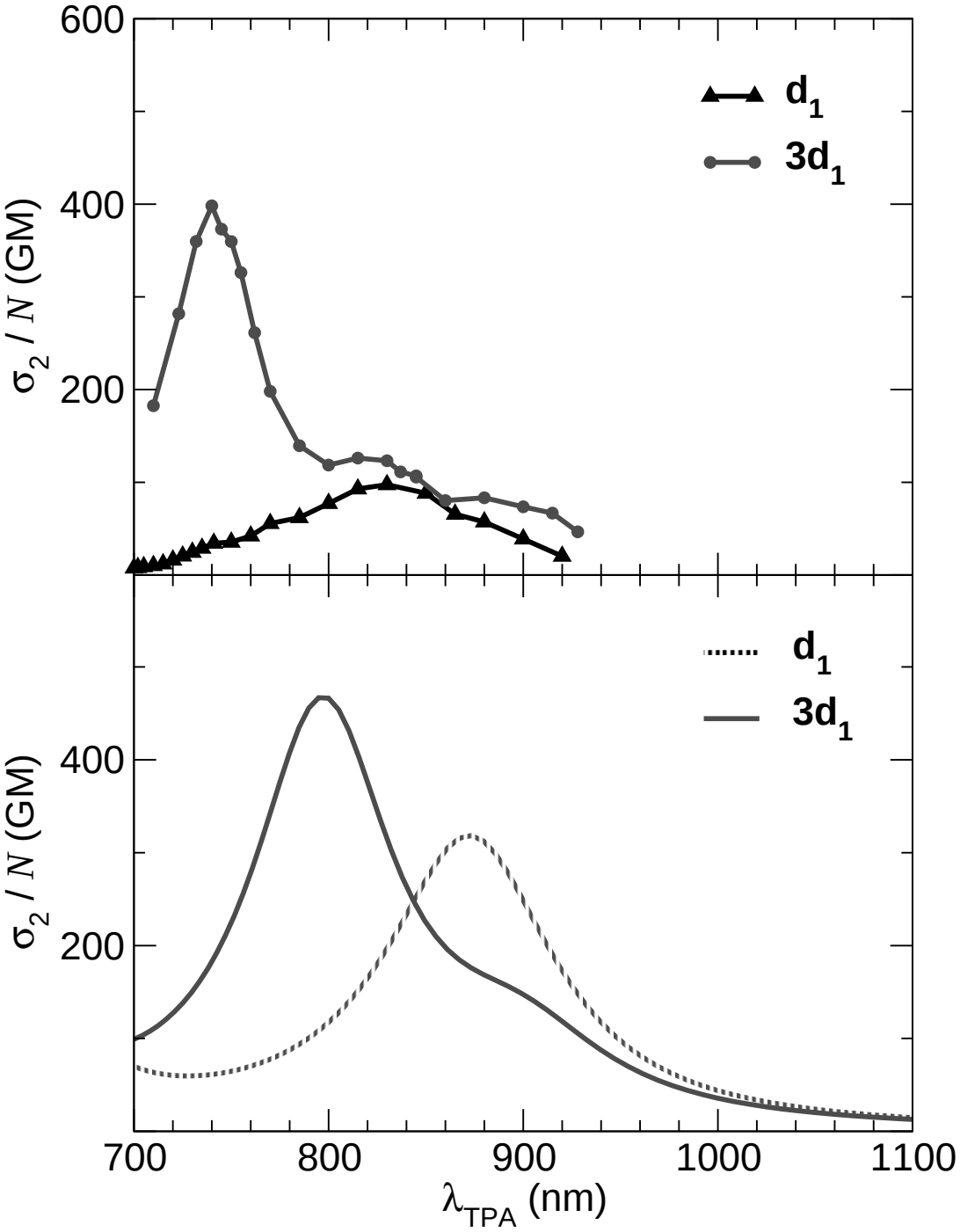

Figure 15: TPA cross section of chromophores d_1 and $\mathsf{3d}_1$ normalized for the number of branches (N). Top panel: experimental data in toluene; Bottom panel: calculated cross section in vacuum, but corrected for local field and refractive index. Adapted from.[121]

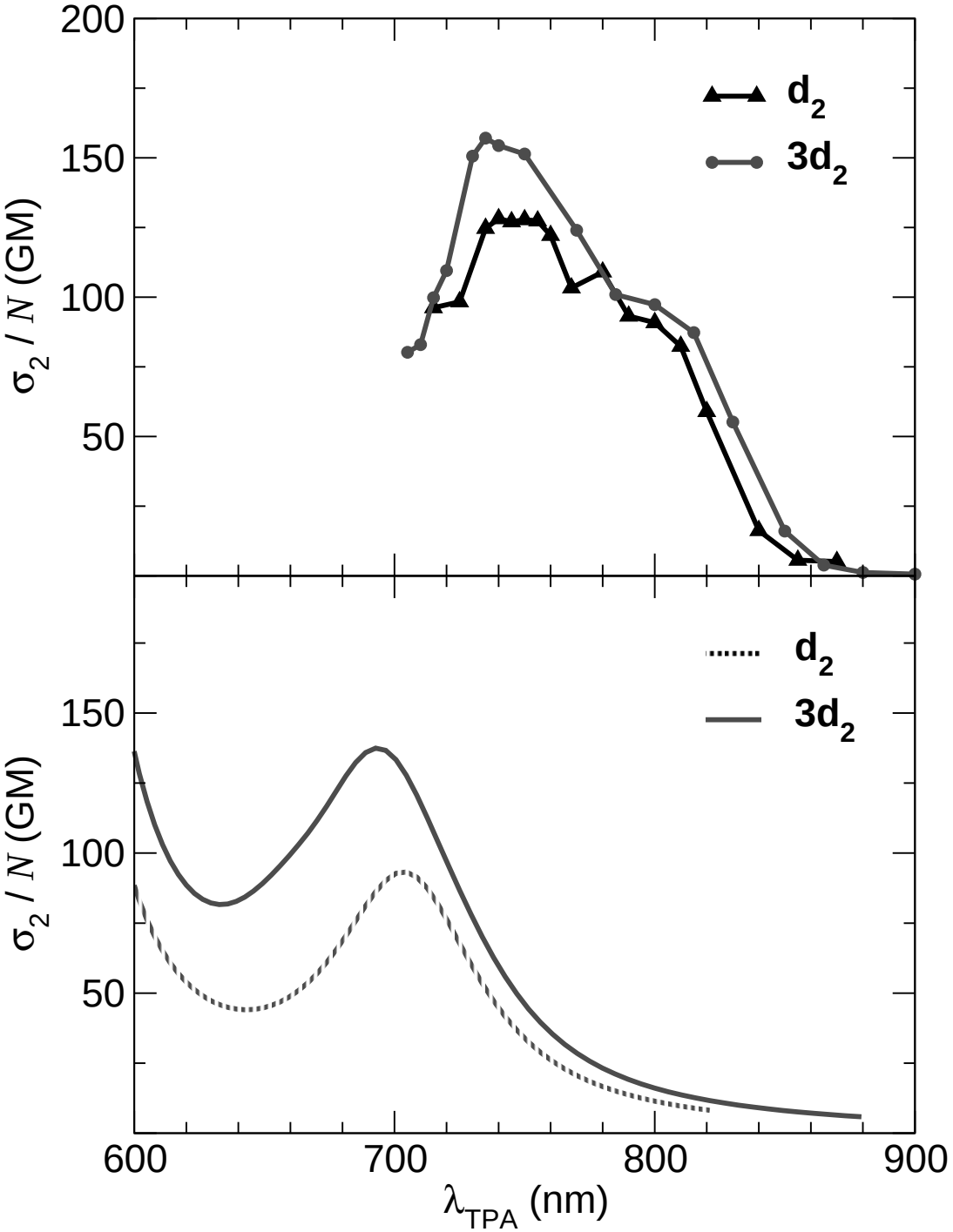

Figure 16: TPA cross section of chromophores d_2 and $\mathsf{3d}_2$ normalized for the number of branches (N). Top panel: experimental data in toluene; Bottom panel: calculated cross section in vacuum, but corrected for local field and refractive index. Adapted from.[123]

OPA/TPA	*hole*	*electron*
$\|1_{3q}\rangle$ w=.92 2.78 eV	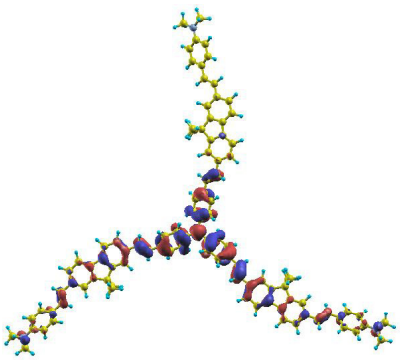	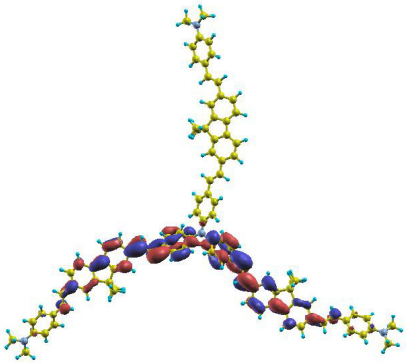
$\|2_{3q}\rangle$ w=.92 2.78 eV	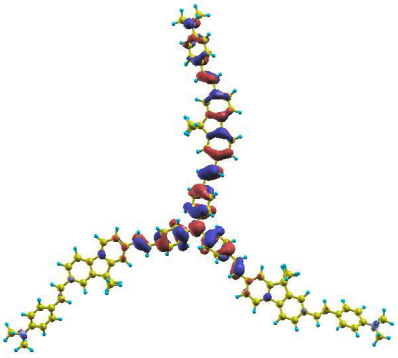	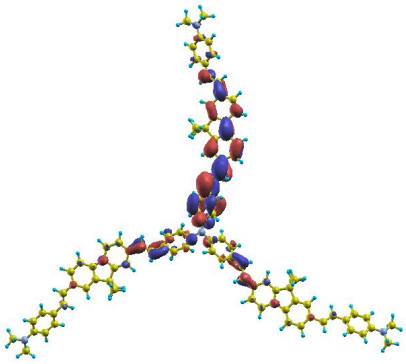
$\|8_{3q}\rangle$ w=.96 3.21 eV	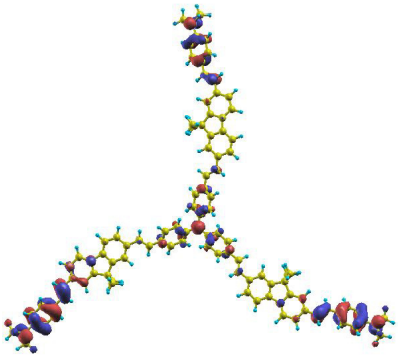	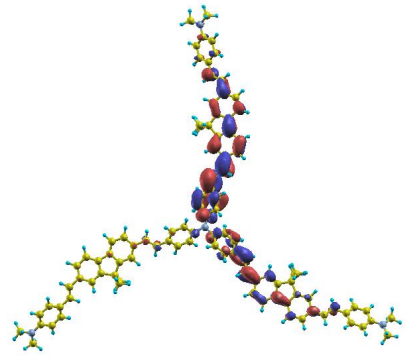
$\|9_{3q}\rangle$ w=.96 3.21 eV	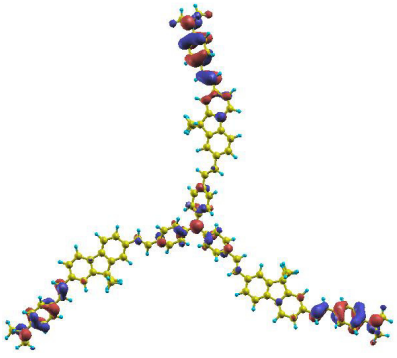	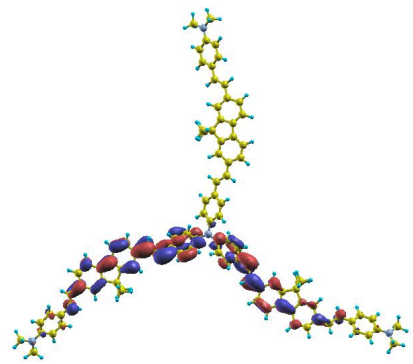

TPA	*hole*	*electron*
$\|3_{3q}\rangle$ **w=.46 3.05 eV**	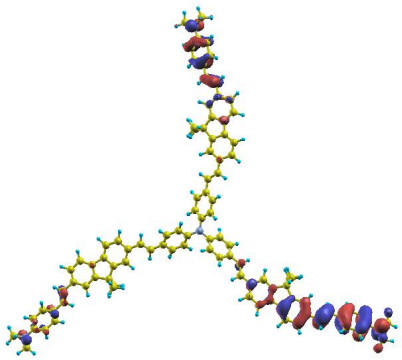	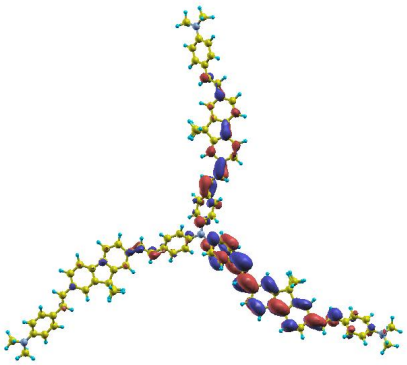
$\|3_{3q}\rangle$ **w=.46 3.05 eV**	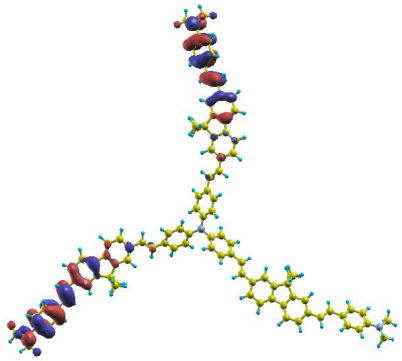	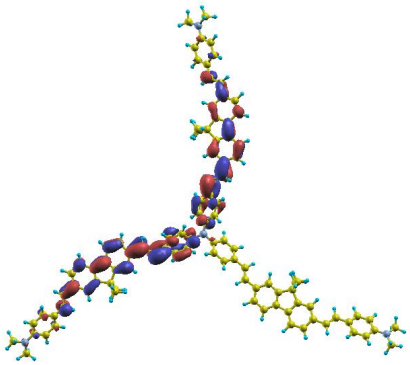
$\|6_{3q}\rangle$ **w=.93 3.13 eV**	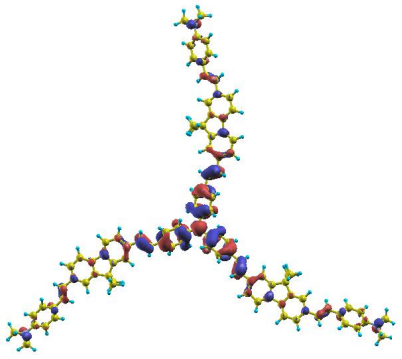	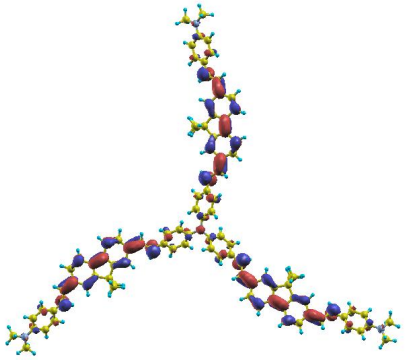
$\|12_{3q}\rangle$ **w=0.95 3.42 eV**	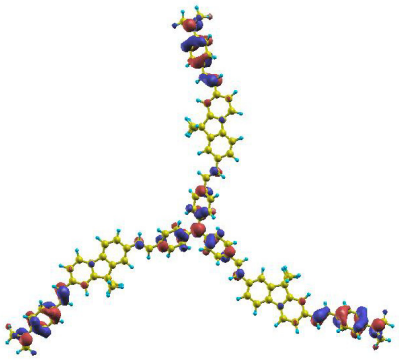	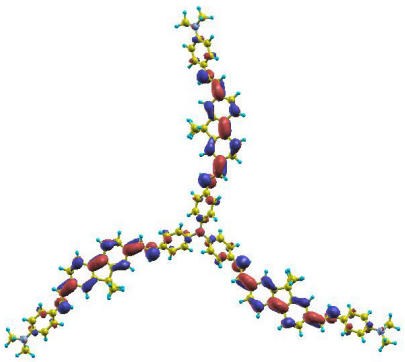

Figure 17: Natural transition orbitals[268] of chromophore $3q_1$. Left panels quote in sequence excited state number, associated NTO eigenvalues[313] and transition energies. Adapted from.[126]

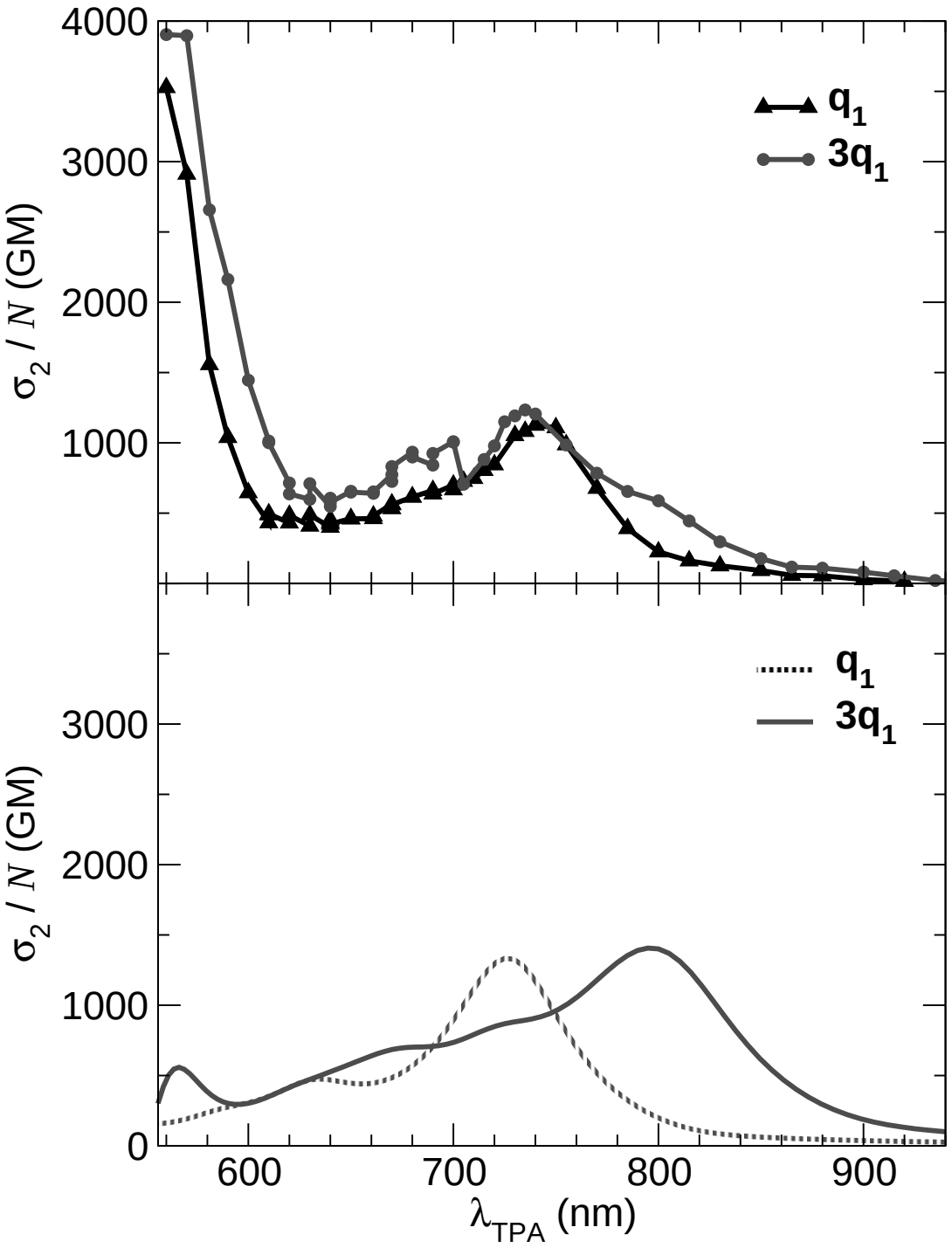

Figure 18: TPA cross section of chromophores $3q_1$ and q_1 normalized for the number of branches (N). Top panel: experimental data in toluene; Bottom panel: calculated cross section in vacuum, but corrected for local field and refractive index. Adapted from.[126]

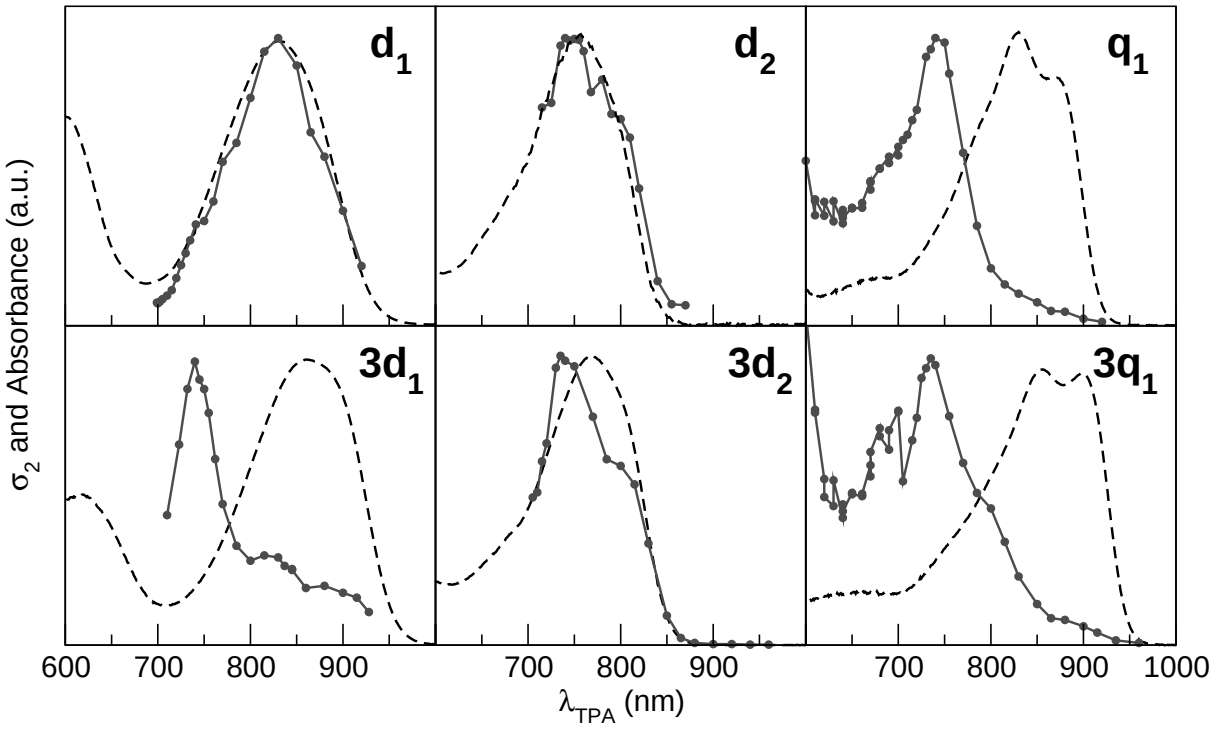

Figure 19: Experimental TPA (circles and lines) and rescaled OPA (dashed lines) spectra for monomeric compounds d_1, d_2 and q_1, and their corresponding branched systems $3\mathsf{d}_1$, $3\mathsf{d}_2$ and $3\mathsf{q}_1$ in toluene.

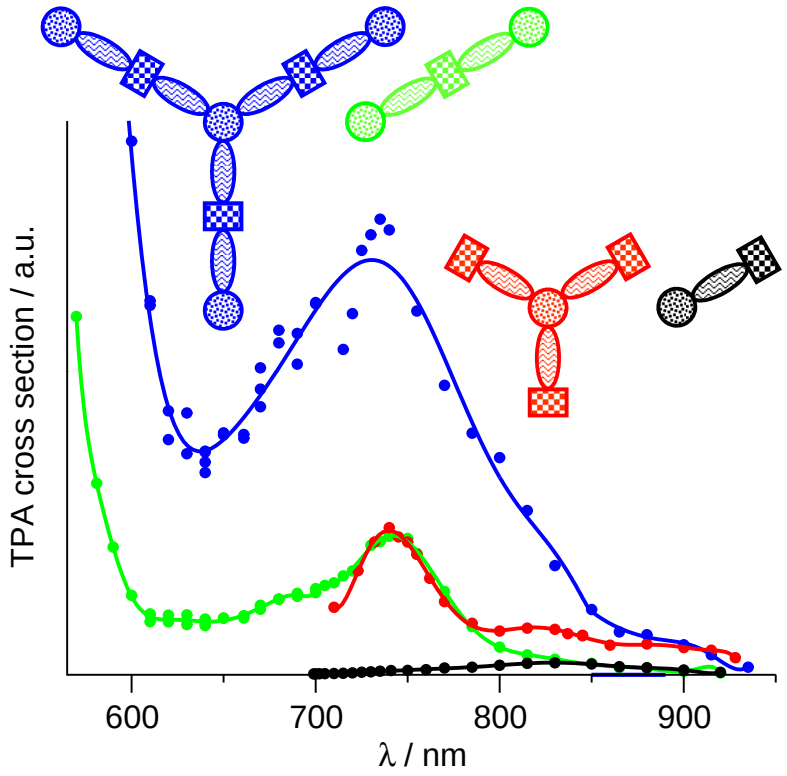

TOC-abstract:

Two-photon absorption (TPA) offers a rich playground for development of novel optical multifunctional technologies. Related experimental and theoretical methodologies are reviewed with special attention on sources of errors that yield improper evaluation of TPA cross sections. Trends leading to large TPA responses are illustrated and thoroughly analyzed through a set of typical organic TPA-fluorophores including branched systems.

TOC-Keyword: Nonlinear Optics

By *Francesca Terenziani, Claudine Katan*, Ekaterina Badaeva, Sergei Tretiak** and *Mireille Blanchard-Desce*

Enhanced two-photon absorption of organic chromophores: theoretical and experimental assessments